ADDIS ABABA UNIVERSITY FACULTY OF
TECHNOLOGY SCHOOL OF GRADUATE STUDIS
MECHANICAL ENGINEERING DEPARTMENT

COMPUTER-AIDED AERODYNAMIC AND STRUCTURAL DESIGN OF HORIZONTAL-AXIS WIND TURBINE BLADES

By: Mulugeta Biadgo Asress

Advisor: Dr. –Ing. Tamrat Tesfaye

A THESIS SUBMITTED IN PARTIAL FULFILMENT OF THE REQUIREMENTS OF MASTER'S OF SCIENCE DEGREE IN MECHANICAL ENGINEERING.

June 2009

ADDIS ABABA UNIVERSITY

SCHOOL OF GRADUATE STUDIS

FACULTY OF TECHNOLOGY

DEPARTMENT OF MECHANICAL ENGINEERING

COMPUTER-AIDED AERODYNAMIC AND STRACTURAL DESIGN OF HORIZONTAL-AXIS WIND TURBINE BLADES

By:

Mulugeta Biadgo Asress

Approved By Board of Examiners:

1	**Hamsasew Moges**		
	Chairman, ME Department	Signature	Date
2	Dr.-Ing. Tamrat Tesfaye		
	Advisor	Signature	Date
4	Dr. -Ing. Abebayehu Assefa		
	Internal Examiner	Signature	Date

ABSTRACT

Designing horizontal-axis wind turbine (HAWT) blades to achieve satisfactory levels of performance starts with knowledge of the aerodynamic forces acting on the blades. In this thesis, HAWT blade design is studied first from the aspect of aerodynamic view and the basic principles of the aerodynamic behaviors of HAWTs are investigated. Second the structural design which consists of the blade material selection and the determination of structural cross section, FEM analysis is done using CATIA V5 R16 and ANSYS 10. The displacement, Von Mises and Principal stress results are determined, these results shows that ANSYS is more conservative than CATIA in FEM analysis.

Blade-element momentum theory (BEM) known as also strip theory, which is the current mainstay of aerodynamic design and analysis of HAWT blades, is used for HAWT blade design in this thesis.

BLADE DESIGN PROGRAM which is a user-interface computer program for HAWT blade design is written. It gives blade geometry parameters (chord-length and twist distributions) and design conditions (design tip-speed ratio, design power coefficient and rotor diameter) for the following inputs; power required from a turbine, number of blades, design wind velocity and blade profile type (airfoil type). The program can be used by anyone who may not be intimately concerned with the concepts of blade design procedure and the results taken from the program can be used for further studies.

To My Mother

ACKNOWLEDGEMENT

I would like to express my deepest gratitude and appreciation to my Advisor, Dr.-Ing. Tamirat Tesfaye, for his invaluable guidance and encouragement throughout this study. I especially thank my Advisor for his patience and trust during the study. I also would like to thank my colleagues for their supports.

Also I would like to thank Ato Demeke Kuchu, who take care of me when I was stressed and upset by circumstances that faced me during my study and for his continuous support and encouragement throughout time since I have known him.

Finally I want to take this opportunity to thank all my families specially my brother Ato Alachew Biadgo, whose advice and sacrifice made me strong through all the hindrances during my study.

TABLE OF CONTENTS

LIST OF FIGURES

LIST OF TABLES

TABLES

NOMENCLATURE

C_p : Power coefficient of wind turbine rotor

$C_{p,\max}$: Maximum rotor power coefficient

C_T : Thrust coefficient of wind turbine rotor

P : power output from wind turbine rotor

$\dot{m}$: Air mass flow rate through rotor plane

U_∞ : Free stream velocity of wind

U_{rel} : Relative wind velocity

U_R : Uniform wind velocity at rotor plane

U_w : Uniform wind velocity at far wake

u : Axial wind velocity at rotor plane

v : Radial wind velocity at rotor plane

w : Angular wind velocity at rotor plane

w' : Induced angular velocity due to bound vorticity of rotor blades

u_w : Axial wind velocity at far wake

v_w : Radial wind velocity at far wake

w_w : Angular wind velocity at far wake

A : Area of wind turbine rotor

R : Radius of wind turbine rotor

r : Radial coordinate at rotor plane

r_w : Radial coordinates at far wake

r_h : Rotor radius at hub of the blade

r_i : Blade radius for the r^{th} blade element

p_o : Pressure of undisturbed air

p : Upwind pressure of rotor

dp : Downwind pressure of rotor

p' : Pressure drop across rotor plane

p_w : Pressure at far wake

Ho : Bernoulli's constant between free-stream and inflow

H_1 : Bernoulli's constant between outflow and far wake

T : Rotor thrust

Q : Rotor torque

F_D : Drag force on an annular blade element

F_L : Lift force on an annular blade element

L : Force on an annular element tangential to the circle swept by the rotor

C_D : Drag coefficient of an airfoil

C_L : Lift coefficient of an airfoil

$C_{L,design}$: Design lift coefficient of an airfoil

F : Tip-loss factor

F_i : Tip-loss factor for the ith blade element

N : Number of blade elements

B : Number of blades of a rotor

a : Axial induction factor at rotor plane

b : Axial induction factor at far wake

a' : Angular induction factor

l : Tip-speed ratio of rotor

l_d : Design tip-speed ratio

l_r : Local tip-speed ratio

$l_{r,i}$: Local tip-speed ratio for the ith blade element

l_h : Local tip-speed ratio at the hub

a_1 : Corresponding axial induction factor at $l_r = l_h$

a_2 : Corresponding axial induction factor at $l_h = l$

c : Blade chord length

c_i : Blade chord length for the ith blade element

r : Air density

Ω : Angular velocity of wind turbine rotor

a : Angle of attack

a_{design} : Design angle of attack

q : Pitch angle (blade setting angle)

q_i : Pitch angle for the i^{th} blade element

j : Angle of relative wind velocity with rotor plane

j_{opt} : Optimum relative wind angle

$j_{opt,i}$: Optimum relative wind angle for the i_{th} blade element

s : Solidity ratio

n : Kinematic viscosity of air

g : Glide ratio

Γ : Circulation along a blade length

$d\Gamma$: Incremental circulation along a blade length

Re : Reynolds number

HAWT : Horizontal-axis wind turbine

VAWT : Vertical-axis wind turbine

BEM : Blade element-momentum theory

TSR : Tip-speed ratio

CHAPTER 1

INTRODUCTION

1.1 OBJECTIVE AND SCOPE OF THE THESIS

The objective of this study is to develop a user-interface computer program on VISUALBASIC for HAWT blade design and power performance prediction using the Blade Element Momentum (BEM) theory. The program is well established and can be readily used for the purpose of designing horizontal-axis wind turbine blades. It takes power required from a wind turbine rotor, number of blades to be used on the rotor, the average wind speed, an airfoil type which can be selected from the airfoil database in the program as input and gives the following as output; blade geometry parameters (twist and chord-length) for the designed blade considering the ease of fabrication, the elemental trust and tangential forces and the approximate rotor diameter to be constructed for the specified power. The program shows the results with figures for making the design decision more clear. It also gives the three dimensional views and solid models of the designed blade for visualization after exported to AutoCAD.

The scope of the thesis is restricted to horizontal-axis wind turbines within two general configurations of wind turbines; namely horizontal-axis and vertical-axis wind turbines. The following sections of this chapter, however, gives an introductory remarks about wind turbine; its origin, development in history, some innovative types of wind turbines, the exploration of major advantages of horizontal-axis wind turbines over all other wind turbines, technological development and use of horizontal-axis wind turbines around the world.

In 'Chapter 2', the detail information on horizontal-axis wind turbines are given. The concepts and some innovative types of horizontal-axis wind turbines are mentioned. Then today's modern horizontal-axis wind turbines are introduced giving the common configurations and explanations of their sub-components. Also nomenclatures used in horizontal-axis wind turbines with their definitions are included. The control strategies from the aspect of aerodynamic view are examined and major performance parameters are introduced. Finally, classification of horizontal-axis wind turbines and criteria in horizontal-

axis wind turbine design regarding all their sub-components apart from the rotor which is the main scope of this thesis are given.

In 'Chapter 3', the aerodynamic behaviors of horizontal-axis wind turbines are dealt with in detail. All theories on aerodynamic of horizontal-axis wind turbines are examined under separate subtitles for each. The assumptions made for each theory are emphasized and their physical meanings are explained for the purpose of making the understanding of each theory easier.

In 'Chapter 4', HAWT blade design procedure is given based on the BEM theory. Equations obtained from BEM theory in chapter 3 are modified considering various corrections including tip-losses and thrust coefficient modifications. It is mentioned about the airfoil selection criteria in HAWT blade design. How airfoil characteristics affect the performance of a blade is discussed as well. Design procedure is then studied for a designed blade and the validity of an approximation used for determining the optimum relative wind angle for a certain local tip-speed ratio is explained. At the end of this chapter results are given with illustrative figures.

In 'Chapter 5', the computer programs namely XFOIL used for airfoil analysis and the user-interface program on HAWT blade design; BLADE DESIGN PROGRAM developed on VISUALBASIC are introduced. An example of blade design performed on the mentioned program is given.

In 'Chapter 6', the structural analysis was then carried out using a cantilever beam analysis, with the help of CATIA V5 R16 and ANSYS. To simplify the design of wind mill structures, it is well to understand the loads which try to break apart these machines are considered during analysis. These loads are trust force and gravity. The blade geometry parameters (model) are take form the outputs of BALADE DESIGN PROGRAM for structural analysis. The displacement, Von Mises and principal stress results are compared.

Finally in 'Chapter 7', conclusion and possible future works are discussed.

1.2 HISTORICAL DEVELOPMENT OF WINDMILLS

Even though today's modern technology has firmly and rightly established the definition of wind turbine as the prime mover of a wind machine capable of being harnessed for a number of different applications, none of which are concerned with the milling of grain or other substances (at least industrialized countries), the term windmill was used for the whole system up to recent time, whatever its duty, be it generating electricity, pumping water, sawing wood. Since here the historical development of wind machine is considered it is convenient and has certain logic in it to retain its term, windmill in its historic sense [1].

The windmill has had a singular history among prime movers. Its existence as a provider of useful mechanical power has been known for the last thousands years. The earliest mentions of the use of wind power come from the East India, Tibet, Persia and Afghanistan. It is also mentioned that the wind power was used to play the organ instrument in •skenderiye about two thousands years ago. Nearly all stories and the records we have about windmill from between the first and twelfth centuries come from the Near East and Central Asia and those regions of the world are generally considered to be the birthplace of the windmill.

The first record of the use of the windmill is seen in the tenth century in Persia. Inhabitants who lived in Eastern Persia, which bordered on Afghanistan today, utilized the windmill, which were vertical-axis and drag type of windmill as illustrated in Figure 1.1. The invention of the vertical-axis windmills subsequently spread in the twelfth century throughout Islam and beyond to the Far East. The basic definition of the primitive vertical-axis windmills were imported in the later centuries such as placing the sails above millstones , elevating the driver to a more open exposure which improved the output by exposing the rotor to higher wind speeds and using of reeds instead of cloth to provide the working surface [1].

Figure 1.1 Early Persian windmill [2]

However, it lies in the fact that the vertical-axis Persian windmills never came into use in Europe. At the end of the twelfth century, there was an efflorescence of a completely different type, the horizontal-axis windmill. This development present second enigma in the technical development of the wind turbine that occurred some thousands years after the enigma left by Persian vertical-axis windmills [1].

Before European countries, horizontal-axis windmills were designed by Ebul•z (1153) from Artuk Turks and used in the region of Diyarbakir in 1200's. However, Northwest Europe, particularly France, Germany, Great Britain, Iberia and the Low Countries are considered to be the first region that developed the most effective type of windmill, one in which the shaft carrying the sails was oriented horizontally rather than vertically as in the Persian mill. In a relatively short time, tens of thousands of what it is called horizontal-axis European windmills were in use for nearly all mechanical task, including water pumping, grinding grain, sawing wood and powering tools. The familiar cruciform pattern of their sails prevailed for almost 800 years, from the twelfth to the twentieth century [1].

The horizontal-axis windmill was a considerably more complex mechanism than the Persian vertical-axis windmill since it presented several engineering problems three major of which were transmission of power from a horizontal rotor shaft to a vertical shaft, on which the grindstones were set, turning the mill into the wind and stopping the rotor when necessary. But the adoption of horizontal-axis windmill is readily explained by the fact that it was so much more efficient [1].

In the historical development of windmills, it must be required the consideration of very innovative step that warrants somewhat more attention that it has received, the use of

horizontal-axis windmills instead of vertical-axis ones. Although the right angle gear mechanism allowed the rotor axis to be transposed from vertical to horizontal, the action of sails also had to be turned through 90°. This was revolutionary because it meant that the simple, straightforward push of the wind on the face of the sail was replaced by the action of the wind in flowing smoothly around the sail, providing a force normal to the direction of the wind. As a concept, it is indeed a sophisticated one that was not fully developed until the advent of the airplane at the end of the nineteenth century and the engineering science of aerodynamics [1].

The transition from windmills supplying mechanical power to wind turbines producing electrical energy took place during the last dozen years of the nineteenth century. The initial use of wind for electric generation, as opposed to for mechanical power, included the successful commercial development of small wind generators and research and experiments using large turbines. The advent and development of the airplane in the first decades of the twentieth century gave rise to intense analysis and design studies of the propeller that could immediately be applied to the wind turbine [1].

An innovative type of wind turbine rotor, the Savonius rotor, was named after its inventor, Finnish engineer S.J. Savonius. The inventor's interest had been aroused by the Flettner rotor ship with its large, rotating cylindrical sails. .Wind passing over these cylinders created lift by the Magnus effect, which propelled the ship forward. He was intrigued by the possibility of substituting wind power for the external motor power used to rotate these cylinders on the Flettner ship. His experiments resulted in a rotor with an S-shaped cross section which, in its simplest form, could be constructed by cutting a circular cylinder in half longitudinally and rejoining opposite edges along an axle, an illustration of a more modern one is given in Figure 1.2. According to the inventor, the Savonius rotor achieved some popularity in Europe especially in Finland, but it has not prospered commercially as a means for driving an electrical generator. It had advantages having high starting torque and the ability to accept wind from any direction; its drawbacks were low speed and heavy weight [3].

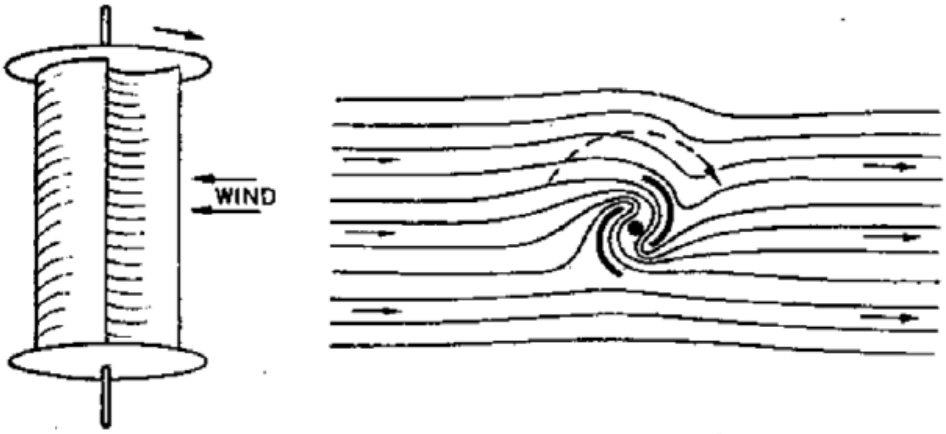

Figure 1.2 The Savonius rotor [3]

Another innovative rotor design introduced in the early 1930s was a type of vertical-axis turbine invented by F.M.Darrieus. The Darrieus rotor, which is illustrated in Figure 1.3, has two or three curved blades attached top and bottom to a central column, accepting the wind from all directions without yawing. This column rotates in upper and lower bearings and transmits torque from the blades to the power train, which is located below the rotor, where the maintenance is easier and weight is not quite so important [4].

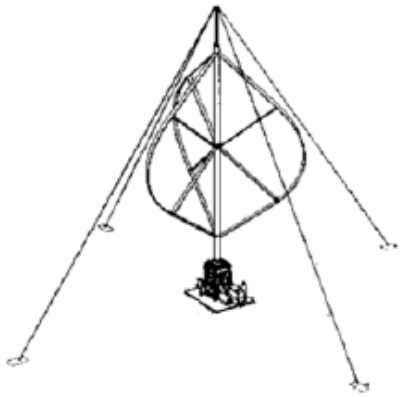

Figure 1.3 Darrieus rotor [4]

The wind continued to be major source of energy in Europe through the period just prior to the Industrial Revolution, but began to recede in importance after that time. The reason that wind energy began to disappear is primarily attributable to its non-dispatch ability and its non-transportability. In addition to that, with the invention of the steam engine, the internal combustion engine and the development of electricity, the use of wind turbines was often neglected and abandoned [1].

Prior to its demise, the European wind turbines had reached a high level of design sophistication. In the latter wind turbines, the majority of the turbine was stationary. Only the top would be moved to face wind. Yaw mechanisms included both manually operate arms and separate yaw rotors. Blades had acquired somewhat of an airfoil shape and included some twist. The power output of some turbines could be adjusted by an automatic control system [1].

The re-emergence of wind energy can be considered to have begun in the late 1960s. Many people became awareness of the environmental consequences of industrial development. Nearly all authorities concerning in energy began arguing that unfettered growth would inevitably lead to either disaster or change. Among the culprits identified were fossil fuels. The potential dangers of nuclear energy also became more public at this time. Discussion of these topics formed the backdrop for an environmental movement which began to advocate cleaner sources of energy [2].

During the 1990s many wind power manufacturers spread all over the Europe, particularly Denmark and Germany. Concerns about global warming and continued apprehensions about nuclear power have resulted in a strong demand for more wind generation there and in other countries as well. Over the last 25 years, the size of the largest commercial wind turbines has increased from approximately 50 kW to 2 MW, with machines up to 5 MW under design. The total installed capacity in the world as of the year 2001 was approximately 20,000 MW, with the majority of installations in Europe. Offshore wind energy systems are also under active development in Europe. Design standards and machine certifications procedures have been established, so that the reliability and performance are far superior to those of the 1970s and 1980s. The cost of energy from wind has dropped to the point that in some sites it is nearly competitive with conventional sources, even without incentives [2].

The cost of utility-scale wind power has come down dramatically in the last two decades due to technological and design advancements in turbine production and installation. In the early 1980s, wind power cost about 30 cents per kWh. In 2006, wind power costs as little as 3 to 5 cents per kWh where wind is especially abundant. The higher the wind speed over time in a given turbine area, the lower the cost of the electricity that turbine produces. On average, the cost of wind power is about 4 to 10 cents per kWh in the United States.

Table 1.1 Energy Costs Comparison

Resource Type	Average Cost (cents per kWh)
Hydroelectric	2-5
Nuclear	3-4
Coal	4-5
Natural gas	4-5
Wind	4-10
Geothermal	5-8
Biomass	8-12
Hydrogen fuel cell	10-15
Solar	15-32

Turkey has enormous wind energy potential as to European countries in that wind energy sources of Turkey are theoretically enough for meeting its electrical energy need. 83000 MW of this wind energy potential can be technically used for electricity production in Turkey. In Table 1.2, the wind energy potential and installed capacity of electrical energy production from the wind energy in some European countries by the year 2008 are given [5]. From this table it is seen that Turkey should utilize the wind energy for electrical energy production much more than its installed capacity now.

Table 1.2 Technical wind energy installed capacities in some European Countries

Countries	Technical Wind Energy Potential(MW)	Installed Capacity (MW)
Germany	42,000	23,902.4
Spain	43,000	16,740.3
Italy	35,000	3,736.9
France	42,000	3,404.0
England	57,000	3,387.9
Denmark	14,000	3,160.0
Sweden	20,000	1,066.9
Greece	22,000	989.7
Turkey	83,0000	333.4

1.3 TECHNOLOGICAL DEVELOPMENTS OF MODERN WIND TURBINES

Wind turbine technology, dormant for many years, awoke at the end of the 20th century to a world of new opportunities. Developments in many other areas of technology were adapted to wind turbines and have helped to hasten re-emergence. A few of the many areas which have contributed to the new generation of wind turbines include material science, computer science, aerodynamics, analytical methods, testing and power electronics. Material science has brought new composites for the blades and alloys for the metal components. Developments in computer science facilitate design, analysis, monitoring and control. Aerodynamics design methods, originally developed for the aerospace industry, have now been adapted to wind turbines. Analytical methods have now developed to the point where it is possible to have much clearer understanding of how a new design should perform than was previously possible. Testing using a vast array of commercially available sensors and data collection and analysis equipment allows designers to better understand how the new turbines actually perform. Power electronics is relatively new area which is just beginning to be used with wind turbines. Power electronic devices can help connect the turbine's generator smoothly to the electrical network; allow the turbine to run at variable speed, producing more energy, reducing fatigue damage and benefiting the utility in the process; facilitate operation in a small, isolated network; and transfer energy to and from storage [2].

The trends of wind turbines have evolved a great deal over the last 25 years. They are more reliable, more cost effective and quieter. It can not be concluded that the evolutionary period is over, however. It should still be possible to reduce the cost of energy at sites with lower wind speeds. Turbines for use in remote communities remain to be made commercially viable. The world of offshore wind energy is just in its infancy. There are tremendous opportunities in offshore locations but many difficulties to be overcome. As wind energy comes to supply an ever larger fraction of the world's electricity, the issues of intermittency transmission and storage must be revisited. There will be continuing pressure for designers to improve the cost effectiveness of wind turbines for all applications. Improved engineering methods for the analysis, design and for mass-produced manufacturing will be required. Opportunities also exist for the development of new materials to increase wind turbine life. Increased consideration will need to be given to the requirements of specialized applications. In all cases, the advancement of the wind industry represents an opportunity and a challenge

for a wide range of disciplines, especially including mechanical, electrical, materials, aeronautical, controls and civil engineering as well as computer science [2].

1.4 THE ETHIOPIAN EXPERIENCE

Ethiopia, a country under a severe drought that relies on hydroelectric plants for the bulk of its power, is now turning to wind energy. In October 9, 2008, The Ethiopian Electric Power Corp. signed a deal with French wind turbine maker Vergnet, which plans to spend €210 million ($286 million) to build a 120-megawatt wind farm, the largest in sub-Saharan Africa. The wind farm, which will consist of 120, 1-megawatt turbines, will increase the Ethiopian utility's generation capacity by 15 percent. This project will help the country to fill the gap of hydrological risks facing Ethiopia with the droughts.

All studies covering wind energy in Ethiopia, so far, were looking at the wind energy potential as a side bar, i.e. "the role of wind energy for rural development" or the like. As such, a thorough and complete coverage of the wind energy prospects in Ethiopia has yet to be undertaken. In addition, when estimating the wind regime, all these studies relied on meteorological data, which is understandable in the absence of other wind data, carried out particularly for wind energy assessments. As is known from other countries and regions, meteorological data are suitable to give a first hint on the seasonal variation of wind speeds (i.e. higher wind speeds during dry season or in summer etc.). However, they are generally completely useless for the determination of the absolute level of available wind energy. This is because meteorological stations have generally been established at the beginning of the 20th century, normally at the outskirts of towns. As is obligatory, the anemometers were installed at towers with a standard measuring height of 10 m. With time, vegetation (trees) grew and buildings were erected in the immediate vicinity of the meteorological station and thus, the measurements were no longer correct.

Mekelle airport has an average annual wind speed of 6.7 m/s at 10m height above ground. This is an excellent value when compared with a typical costal site in Europe which has about 6 m/s at 10 m. Apart from Mekelle rather large areas of Ethiopia have similar good wind regimes: practically the whole Eastern part of the country, as well as larger areas of the North and the Central part of Ethiopia.

Wind energy is one of the resources which is virtually unexploited in Ethiopia. Only sporadic attempts were made by a few organizations to harness this free and inexhaustible source of energy.

According to Adams, "the Rift Valley and the Eastern lowlands have a moderate wind regime well suited for medium machines... the Western provinces (all around the Sudanese

border) are generally poor in wind energy. The rest of the country (mainly the Central highlands) are suitable for low or medium running machines, especially if careful site selection is used.

"Wolde-Ghiorgis" has made a wind energy survey using wind data collected by the National Meteorological Services Agency (NAMSA) and showed that mean winds speeds grater than 2.8 m/s are found extensively in Ethiopia [6].

Munoz studied 18 drought stricken sites and concluded that wind energy was the most economical and expeditious natural resource to be used for pumping applications in those areas [6].

Ethiopian Water Resources Authority (EWRA):-A few commercial windmills - multi-bladed Australian Southern-Cross windpumps - were imported and installed by the then EWRA, notably in the Rift Valley basin. Most of these machines were either blown down by severe storms or were damaged for lack of proper maintenance [6].

American Presbyterian Mission at Omo:- In 1973, the "Food from Wind Project" had used a series of locally manufactured Cretan Sail windmills for irrigating small plots of land on the banks of the Omo River [6].

Addis Ababa University (AAU):- During the "Development through Cooperation Campaign", three types of vertical-axis and two types of horizontal-axis rotors were manufactured and tested by the Mechanical Engineering Department, Faculty of Technology of the AAU. Experimentation on the above wind turbines was discontinued when the Campaign ended in 1976 [6].

Lay Volunteers International Association (LVIA):-The other main organization that is engaged in wind pumping technology is LVIA. It is based in Meki and engaged in partially manufacturing multi-bladed windpumps with rotor diameters of 5 and 6 meters locally. Some components of these units are produced in Addis Ababa, others are fabricated in Meki and a few components are imported from Italy. The density of installation of these water abstraction devices is highest in the Rift Valley basin [6].

The Experience of the Research and Development Services (RADS) of the Ethiopian Water Works Construction Authority (EWWCA):- An extensive research work was undertaken by RADS on windpumps using different construction materials, over-speed control mechanisms and various types of pumps. RADS had designed, manufactured and tested 7 types of windpump prototypes ranging in diameter from 3 to 10 meters. Only one of these

prototypes was a vertical-axis windpump, known as the Filippini Rotor. From the scanty information available the 10 meter diameter windpump (Fig.1.4) is believed to be the largest ever built in Africa. It is also reckoned as the first of its type to employ all feathering blades (turning of the blades edgewise by means of fly weights against a return spring to reduce thrust force and power) for high speed protection on windpumps. This feature however, is very common on wind electric generating rotors having blades of not more than 3 in number. The earlier units were high speed runners with aerofoiled Zigba wooden blades, while the later ones were slow runners with steel sheet blades (Fig. 1.5). Both types of windpumps have their own pros and cons [6].

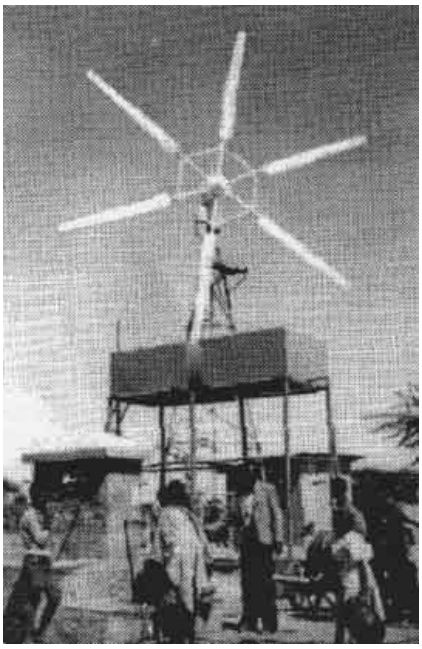

Fig. 1.4: 10 m diameter wind pump

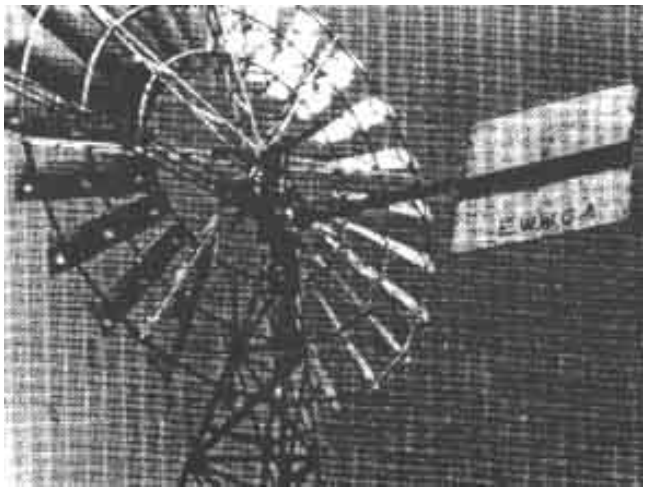

Fig. 1.5: 7 m diameter multi-bladed wind pump

The rotors with high tip-speed ratios (ratio of the blade tip speed to the wind speed) require minimal material for their construction. Nevertheless, their inherent low starting torque feature makes them appropriate only for very high wind speed regimes or require additional torque minimizing devices, a clutch for example, as used by RADS, if they are to be operated in the low wind speed areas. On the other hand, rotors with more blades (high material consumption) run slower but they are able to pump with more forces. These types of windpumps are suited for low wind speed regimes [6].

Equatorial Business Group's (EGB) Initiatives: - The Energy Division of EBG has embarked on the manufacture of a 6 metre diameter, multi-bladed windpump. This windpump is mainly based on Tozzi and Bardi's design, an Italian windpump manufacturer employing both casting and welding technologies. Orientation of the rotor into the wind is realized by a spring loaded tail vane, while the over-speed control is achieved by eccentrically positioning the rotor axis from the tower centre. The manufacturing of these mills is done partly in EBG's own workshop and by sub-contracting other workshops for components that require special purpose machines [6]. Once again, this venture has vividly demonstrated that windpumps can be manufactured in small engineering workshops in Ethiopia. The attempt has also shown that manufacturing of a product need not necessarily be carried out under one shade. By combining the skilled manpower and machinery of different organizations, high quality products can be manufactured locally [6].

CHAPTER 2

HORIZONTAL-AXIS WIND TURBINES

2.1 INTRODUCTION

A wind turbine is a machine which converts the power in the wind into electricity. This is contrast to a windmill, which is a machine that converts the wind's power into mechanical power.

There are two great classes of wind turbines, horizontal- and vertical-axis wind turbines. Conventional wind turbines, horizontal-axis wind turbines (HAWT), spin about a horizontal axis. As the name implies, a vertical-axis wind turbine (VAWT) spins about a vertical axis.

Today the most common design of wind turbine and the only kind discussed in this thesis in the view of aerodynamic behavior is the horizontal-axis wind turbines. In this chapter, detail information about the conventional horizontal-axis wind turbines will be given but before that some unconventional and innovative horizontal-axis wind turbine concepts will be mentioned.

2.2 HORIZONTAL-AXIS WIND TURBINE CONCEPTS

In Figure 2.1, various concepts for horizontal axis wind turbines are illustrated. A few words are in order to summarize briefly some of these concepts to see the evolutionary process that led to modern horizontal axis wind turbine configurations used all over the world.

Enfield-Andreau type of horizontal axis wind turbine is a unique concept in which mechanical coupling between the turbine and the generator is eliminated by driving the generator pneumatically. The turbine rotor has hollow blades with open tips and acts as a centrifugal air pump. As illustrated in Figure 2.2, air is drawn in through side vents in the tower shell, passing upward to drive an enclosed highs peed air turbine coupled directly to the generator. After flowing through the rotor hub into the hollow turbine blades, it is finally expelled from the blade tips. While the Enfield-Andreau turbine operated successfully, it had a low overall efficiency. High drag losses in the internal flow paths were suspected to be the cause. After it had been operated intermittently, it was shut down permanently after suffering bearing failures at the blade roots [1].

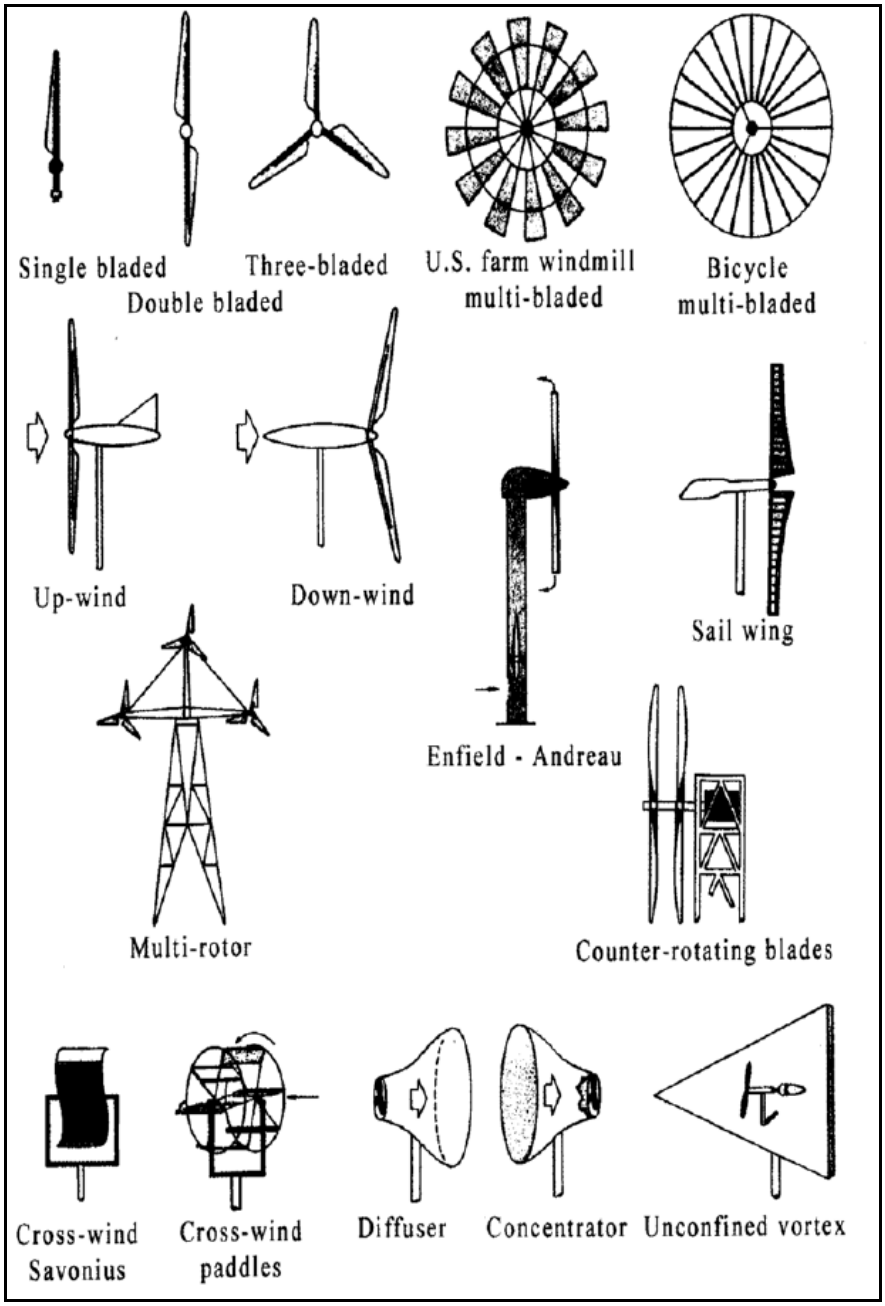

Figure 2.1 various concepts for horizontal-axis wind turbines [2]

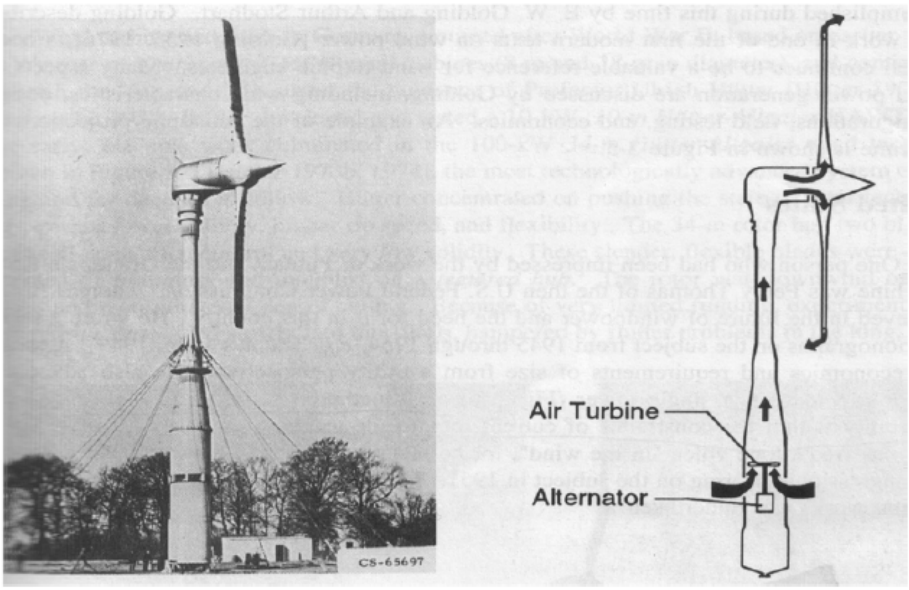

Figure 2.2 Enfield-Andreau turbine (a) General view (b) Diagram of the flow path [1]

The other concept is the multiple rotors in the same plane on a single tower which had been designed as a method of achieving high power levels with rotors of intermediate size. Studies on this concept concluded that it was more cost-effective to use multiple turbines or larger turbines than to pay for the complex structure needed to support. But today no actual design work (much less experimental work) was undertaken [1].

Another unconventional innovative wind turbine concept is a wind turbine composed of counter-rotating blades in other words multiple rotors on the same axis as illustrated in Figure 2.1. This system differs from the multiple rotors on the same plane mentioned just before in that multiple rotors on the same plane increase net swept area while counter-rotating blades on the same axis does share the net swept area. Advocates of such systems usually misunderstand the physics behind wind energy conversion. The effects of induced velocity limit the theoretical maximum power coefficient of two rotors on the same axis to little more than that of a single rotor. Counter-rotation does decrease the rotational energy lost in the wake, but this benefit is trivial compared to the costs of the second rotor and associated gearing. These systems have rarely been successful, much less cost-effective [1].

Another concept that appears periodically is the concentrator. The idea is to channel the wind to increase the productivity of the rotor. The problem was that the cost of building an effective concentrator which can also withstand occasional extreme winds has always been more than the device was worth [2].

2.3 MODERN HORIZONTAL-AXIS WIND TURBINES

All those unconventional horizontal-axis wind turbines described in the previous section led to the conventional modern horizontal-axis wind turbines which are the wind turbine systems with a low-solidity rotor powered by aerodynamic lift driving an electrical generator, with all rotating components mounted on a tower.

Today's modern horizontal-axis wind turbines are generally classified according to the rotor orientation (upwind or downwind of the tower), blade articulation (rigid or teetering), number of blades (generally two or three blades), rotor control (pitch vs. stall) and how they are aligned with the wind (free yaw or active yaw).

Figure 2.3 shows typical upwind and downwind configurations along with definitions for blade coning and yaw orientation. The term upwind rotor and downwind rotor denote the location of the rotor with respect to the tower. The downwind turbines were favored initially in the world, but the trend has been toward greater use of upwind rotors with a current splint between 55% upwind and 45% downwind configurations [7]. Small wind generators are usually of the upwind type for two principle reasons: (1) a simple tail vane is all that is needed to keep the blades pointed into the wind and (2) a furling mechanism that turns the blades out of the wind stream to protect the machine from high winds is easier for design and fabricate for an upwind rotor. The downwind configuration is usually preferred for larger machines, where a tail vane would not be practical. One problem with the downwind configuration is tower shadow. The tower acts as a barrier to the wind stream and each time a rotating blade passes the tower it is subjected to the changes in wind speed, which causes stresses that vary with the exact amount of wind blocked by the rotor [1].

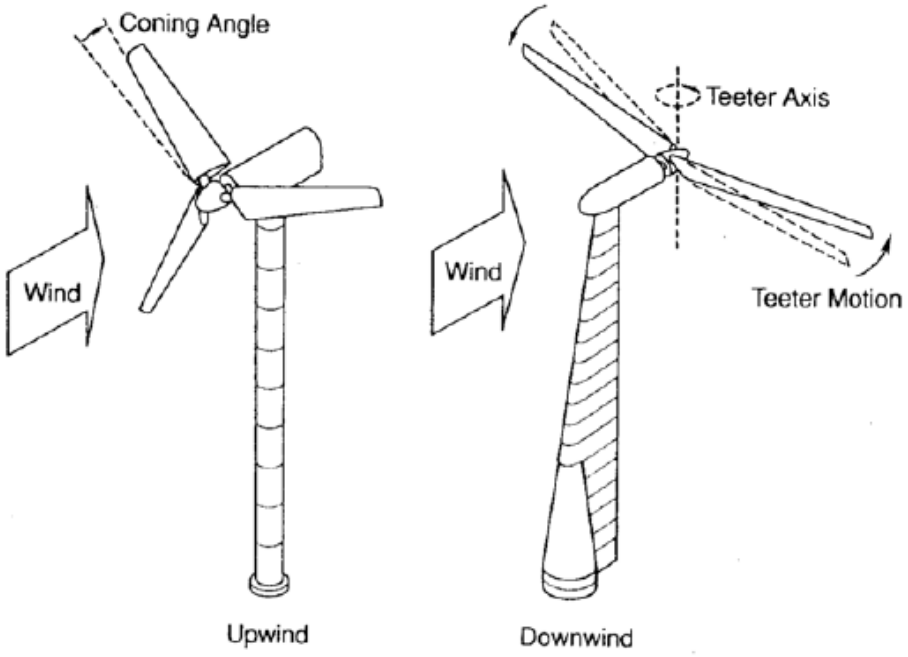

Figure 2.3 Schematic of the two common configurations. Upwind, rigid hub, three-bladed and downwind, teetered, two-bladed turbine [7]

The principal subsystems of a typical horizontal-axis wind turbine as shown in Figure 2.4 include [2]:

- The rotor, consisting of the blades and the supporting hub
- The power train, which includes the rotating parts of the wind turbine (exclusive of the rotor); it usually consists of shafts, gearbox, coupling, a mechanical brake and the generator
- The nacelle structure and main frame; including wind turbine housing, bedplate and the yaw system
- The tower and the foundation
- The machine controls
- The balance of the electrical system, including cables, switchgear, transformers and possibly electronic power converters

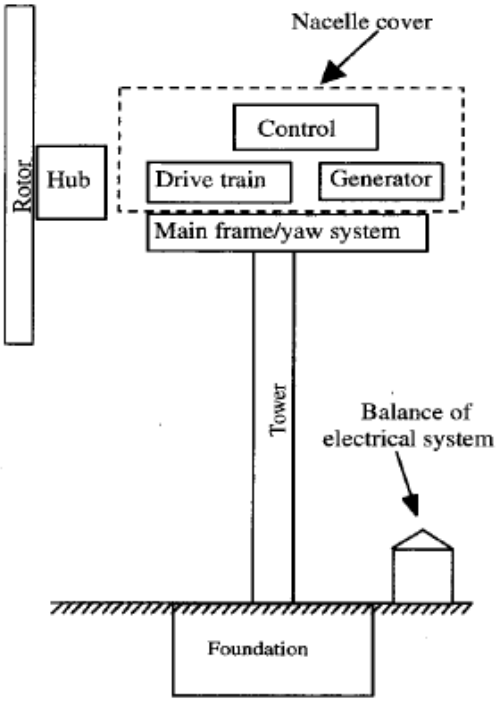

Figure 2.4 Major components of a horizontal-axis wind turbine [2]

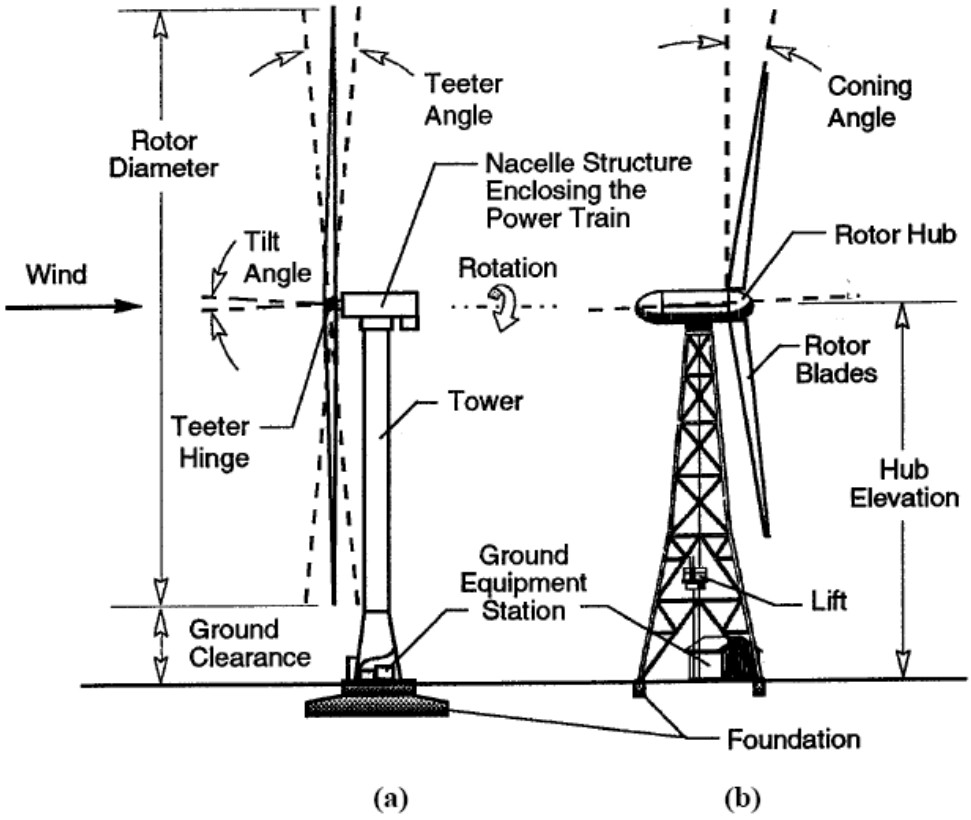

Figure 2.5 Nomenclature and subsystems of HAWT (a) Upwind rotor (b) Downwind rotor

2.3.1 THE ROTOR SUBSYSTEM: The rotor consists of the hub and blades of the wind turbine. These are often considered to be its most important components from both performance and overall cost standpoint. The rotor may be single-, double-, three-, or four-bladed, or multi-bladed. A single-bladed wind rotor requires a counter-weight to eliminate vibration but this design is not practical where icing on the one blade could throw the machine out of balance. The two bladed rotor was the most widely used because it is strong and simple and less expensive than the three-bladed rotor, but in the recent times three-bladed rotor type becomes more widely used one in that the three-bladed rotor distributes stresses more evenly when the machine turns, or yaws, during changes in wind direction. For example a two-bladed rotor with a tail vane would yaw in a series of jerking motions because at the instant the rotor was vertical it offered no centrifugal force resistance to the horizontal movement of the tail vane in following changes in wind direction. At the instant the two-bladed rotor is in the horizontal position its centrifugal force, which is at maximum, resists the horizontal movement of the tail vane. The three-bladed rotor cures this problem, which produces a high level of vibration in the machine, by creating a steady centrifugal force against which the tail vane moves smoothly to shift the direction of the wind turbine [8].

An unconed rotor is one in which the spanwise axes of all of the blades lie in the same plane. Blade axes in a coned rotor are tilted downwind from a plane normal to the rotor axis, at a small coning angle. This helps to balance the downwind bending of the blade caused by aerodynamic loading with upwind bending by radial centrifugal forces. Tower clearance (the minimum distance between a blade tip and the tower) is influenced by blade coning, rotor teetering and elastic deformation of the blades under load. Often an axis-tilt angle is required to obtain sufficient clearance.

Two general types of rotor hubs are rigid and teetered. In a typical rigid hub, each blade is bolted to the hub and the hub is rigidly attached to the turbine shaft. The blades are, in effect, cantilevered from the shaft and therefore transmit all of their dynamic loads directly to it. To reduce this loading on the shaft, a two-bladed HAWT rotor usually has a teetered hub, which is connected to the turbine shaft through a pivot called a teeter hinge, as shown in Figure 2.5(a).

Teeter motion is a passive means for balancing air loads on the two blades, by cyclically increasing the lift force on one while decreasing it on the other. Teetering also reduces the

cyclic loads imposed by a two-bladed rotor on the turbine shaft to levels well below those caused by two blades on a rigid hub.

A three-bladed rotor has usually a rigid hub. In this case, cyclic loads on the turbine shaft are much smaller than those produced by a two-bladed rotor with a rigid hub, because three or more blades form a dynamically symmetrical rotor: one with the same mass moment of inertia about any axis in the plane of the rotor and passing through the hub.

A wide variety of materials have been used successfully for HAWT rotor blades, including glass-fiber composites, laminated wood composites, steel spars with non-structural composite fairings and welded steel foils. Whatever the blade material, HAWT rotor hubs are almost always fabricated from steel forgings, castings or weldments.

2.3.2 THE POWER-TRAIN SUBSYSTEM: The power train of a wind turbine consists of the series of mechanical and electrical components required to convert the mechanical power received from the rotor hub to electrical power. A typical HAWT power train consists of a turbine shaft assembly (also called a primary shaft), a speed increasing gearbox, a generator drive shaft (also called a secondary shaft), rotor brake and an electrical generator, plus auxiliary equipment for control, lubrication and cooling functions.

2.3.3 THE NACELLE STRUCTURE SUBSYSTEM: The HAWT nacelle structure is the primary load path from the turbine shaft to the tower. Nacelle structures are usually a combination of welded and bolted steel sections. Stiffness and static strength are the usual design drivers of nacelle structures.

2.3.4 THE TOWER SUBSYSTEM AND THE FOUNDATION: A HAWT tower raises the rotor and power train to the specified hub elevation, the distance from the ground to the center of the swept area. The stiffness of a tower is a major factor in wind turbine system dynamics because of the possibility of coupled vibrations between the rotor and tower. Located in the ground equipment station are those components which are necessary for properly interfacing the HAWT with the electric utility or other distribution system.

2.3.5 THE CONTROLS: The control system for a wind turbine is important with respect to both machine operation and power production. Wind turbine control involves the following three major aspects and the judicious balancing of their requirements [2]:

- Setting upper bounds on and limiting the torque and power experienced by the drive train

- § Maximizing the fatigue life of the rotor drive train and other structural components in the presence of changes in the wind direction, speed, as well as start-stop cycles of the wind turbine
- § Maximizing the energy production

2.3.6 THE BALANCE OF ELECTRICAL SUBSYSTEM: In addition to the generator, the wind turbine utilizes a number of other electrical components. Some examples are cables, switchgear, transformers and power electronic converters, yaw and pitch motors.

2.4 AERODYNAMIC CONTROLS OF HAWTS

Horizontal-axis wind turbines use different types of aerodynamic control to achieve peak power and optimum performance control. Nearly all turbines use an induction or synchronous generator interconnected with the utility grid. These generators maintain a constant rotor speed during normal operation, so aerodynamic control is needed only to limit and optimize power output. Variable speed control has been considered as a means of improving the aerodynamic efficiency of the rotor and reducing dynamic loads. This type of control results in the rotor speed changing to maintain a constant ratio between blade tip speed and wind speed (tip speed ratio).

Medium and large-scale HAWT rotors usually contain a mechanism for adjusting blade pitch, which is the angle between the blade chord line and the plane of rotation. This pitch-change mechanism, which may control the angle of the entire blade (full-span pitch control) or only that of an outboard section (partial span pitch control), provides a means of controlling starting torque, peak power, and stopping torque. Peak power is controlled by adjusting blade pitch angle to progressively lower angles of attack to control increasing wind loading. Pitch control offers the advantage of more positive power control, decreasing thrust loads as blades pitch toward feather in high winds and low parked rotor loads while the turbine is not operating in extreme winds. One disadvantage of pitch control is the lack of peak power control during turbulent wind conditions.

Some HAWTs have fixed-pitch stall-controlled blades, avoiding the cost and maintenance of pitch-change mechanisms by relying on aerodynamic stall to limit peak power. Passive power regulation is achieved by allowing the airfoils to stall. As wind speed increases stall progresses outboard along the span of the blade causing decreased lift and increased drag. One disadvantage of stall-controlled rotors is that they must withstand steadily increasing

thrust loads with increasing wind speed because drag loads continue to increase as the blade stalls. Another disadvantage is the difficulty of predicting aerodynamic loads in deep stall.

In addition to partial-span and full-span pitch control, several types of aerodynamic brakes have been used for stall-controlled rotors. A simplified form of aerodynamic control mechanism is a tip brake or tip vane, in which a short outboard section of each blade is turned at right angles to the direction of motion, stopping the rotor by aerodynamic drag or at least limiting its speed. Pitchable tips and pivoting tip vane have been used with reasonable success.

A yaw drive mechanism is also required so that the nacelle can turn to keep the rotor shaft properly aligned with the wind. An active yaw drive (one which turns the nacelle to a specified azimuth) contains one or two motors (electric or hydraulic), each of which drives a pinion gear against a bull gear and an automatic yaw control system with its wind direction sensor mounted on the nacelle. A passive yaw drive permits wind forces to orient the nacelle.

2.5 PERFORMANCE PARAMETERS OF HAWTS

The power performance parameters of a HAWT can be expressed in dimensionless form, in which the power coefficients, C_p and the tip-speed ratio, λ are used. These are given in equation 2.5.1 and 2.5.2 respectively;

$$C_p = \frac{P}{0.5\,\rho U_\infty^3 \pi R^2} \quad \text{.....2.5.1}$$

$$\lambda = \frac{\Omega R}{U_\infty} \quad \text{.....2.5.2}$$

Note that in equation 2.5.2, tip-speed ratio is defined for a fixed wind speed. A sample C_p & λ curve is given in Figure 2.6 for a typical HAWT operating at fixed pitch.

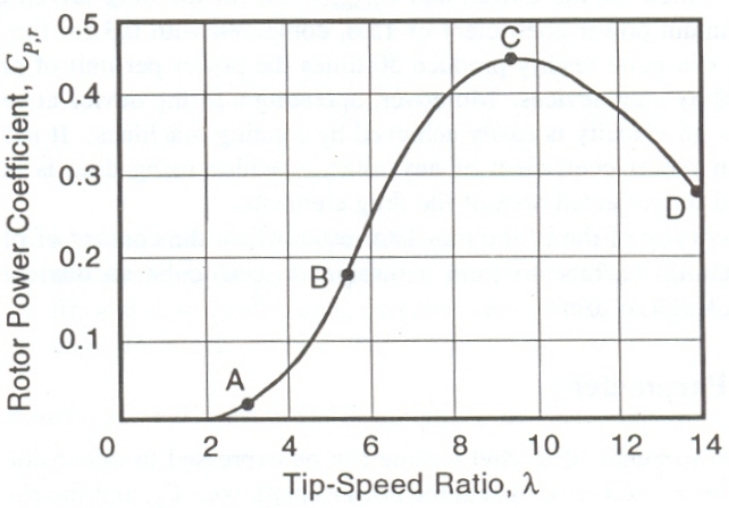

Figure 2.6 Typical plot of rotor power coefficient vs. tip-speed ratio for HAWT with a fixed blade pitch angle

To give a few comments on the operating points A, B, C and D shown in Figure 2.6 will help reading such C_p & I curves of HAWTs. The left-hand side of Figure 2.6 following the path ABC is controlled by blade stall. Local angles of attack (angles between the relative wind angle and the blade chord line) are relatively large as point A is approached. The right-hand side of the same figure following the path CD is controlled by drag, particularly 'skin friction' because the angles of attack are small as point D is approached. At fixed pitch maximum power occurs in the stall region when the lift coefficient is near its peak value over much of the blade.

Apart from the power coefficient, the thrust coefficient, which will be used as well in the subsequent chapters for characterizing the different flow states of a rotor is defined as;

$$C_T = \frac{T}{0.5\,\rho U_\infty^2 \pi R^2} \quad \text{.....2.5.3}$$

2.6 CLASSIFICATION OF HAWTS

Because the interconnection of wind turbines to utilities becomes their principal application, the average size of HAWTs has grown. The question of 'size classification' has been raised, as well. HAWTs are classified as shown in Table 2.1 according to their diameters and/or their rated powers [1].

Table 2.1 Scale classification of wind turbines [1]

Scale	Rotor Diameter	Power Rating
Small	Less than 12m	Less than 40 kW
Medium	12m to 45m	40kW to 999kW
Large	46m and larger	1.0MW and larger

In Figure 2.7 scales of HAWTs are given for the prescribed rated capacity to provide better understanding the relation between the rated capacity of a HAWT with its rotor diameter and tower height.

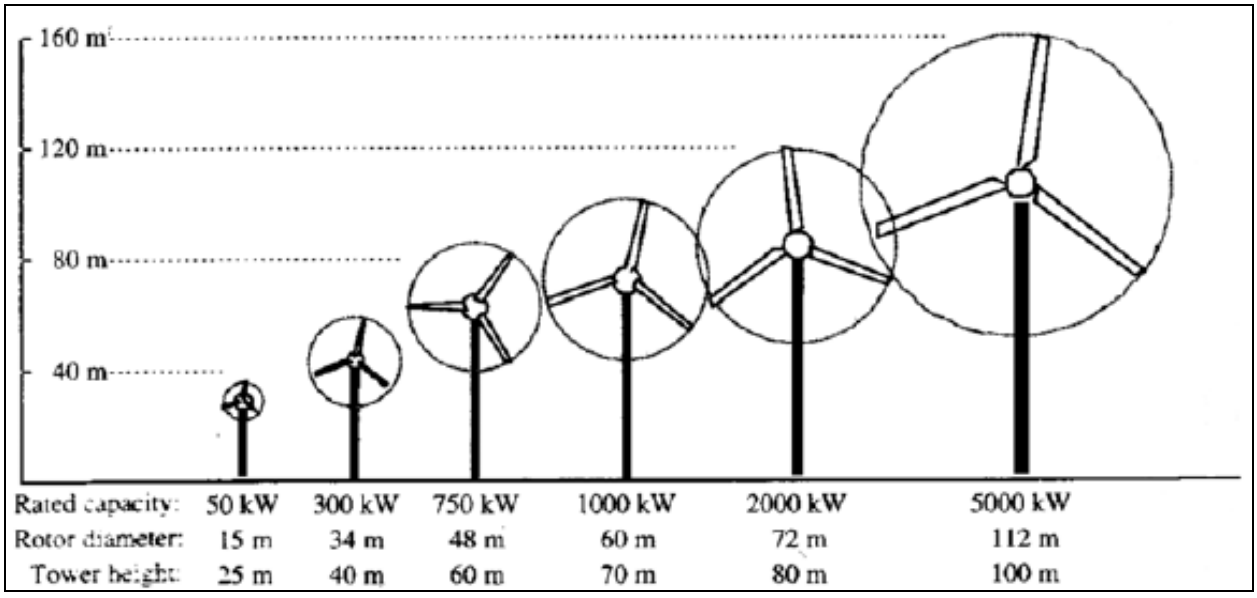

Figure 2.7 Representative size, height and diameter of HAWTs [2]

2.7 CRITERIA IN HAWT DESIGN

Before ending this chapter, a few words to be mentioned in ref [8] about the criteria in HAWT design and construction include:

- Number of turbine blades
- Rotor orientation; downwind or upwind rotor
- Turbine torque regulation
- Turbine speed; fixed or variable rotor speed
- Blade material, construction method and profile (airfoil section)
- Hub design; rigid, teetering or hinged
- Power control via aerodynamic control (stall control) or variable pitch blades (pitch control)
- Orientation by self aligning action (free yaw) or direct control (active yaw)
- Types of mechanical transmission and generator; synchronous or induction generator; gearbox or direct drive transmission
- Type of tower; steel or reinforced –concrete shell or steel truss with tension cables

CHAPTER 3

AERODYNAMICS OF HAWTs

3.1 INTRODUCTION

Wind turbine power production depends on the interaction between the rotor and the wind. The wind may be considered to be a combination of the mean wind and turbulent fluctuations about the mean flow. Experience has shown that the major aspects of wind turbine performance (mean power output and mean loads) are determined by the aerodynamic forces generated by the mean wind. Periodic aerodynamic forces caused by wind shear, off-axis winds, rotor rotation, randomly fluctuating forces induced by turbulence and dynamic effects are the source of fatigue loads and are a factor in the peak loads experience by a wind turbine. These are, of course, important, but can only be understood once the aerodynamics of steady state operation has been understood. Accordingly, this chapter focuses primarily on steady state aerodynamics.

The chapter starts with the analysis of an idealized wind turbine rotor. The discussion introduces important concepts and illustrates the general behavior of wind turbine rotors and the airflow around wind turbine rotors. The analysis is also used to determine theoretical performance limits for wind turbines.

General aerodynamic concepts are then introduced. The details of momentum theory and blade-element theory are developed. The combination of two theories, called strip theory or blade-element momentum theory (BEM) is then studied to outline the governing equations for the aerodynamic design and power prediction of a wind turbine rotor which will be used in the next chapter.

The last section of this chapter discusses the vortex theory. Vortex theory is another approach for aerodynamic design of wind turbine rotors, but here only its concepts related to the former two theories are explained in order to make some definitions in these theories more understandable.

3.2 THE ACTUATOR DISK THEORY AND THE BETZ LIMIT

A simple model, generally attributed to Betz (1926) can be used to determine the power from an ideal turbine rotor, the thrust of the wind on the ideal rotor and the effect of the rotor operation on the local wind field. The simplest aerodynamic model of a HAWT is known as 'actuator disk model' in which the rotor becomes a homogenous disk that removes energy from the wind. Actuator disk theory is based on a linear momentum theory developed over 100 years ago to predict the performance of ship propeller.

The theory of the ideal actuator disk is based on the following assumptions [9]:

- Homogenous, incompressible, steady state fluid flow
- No frictional drag
- The pressure increment or thrust per unit area is constant over the disk
- The rotational component of the velocity in the slipstream is zero. Thus the actuator disk is an ideal mechanism which imparts momentum to the fluid in the axial direction only
- There is continuity of velocity through the disk
- An infinite number of blades

A complete physical representation of this actuator disk may be obtained by considering a close pair of tandem propellers or turbine blades rotating in opposite direction and so designed that the element of torque at any radial distance from the axis has the same value for each blade in order that there shall be no rotational motion in the slipstream; also each turbine actual blade must be replaced with its small number of blades by another of the same diameter having a very large number of very narrow equal frictionless blades, the solidity at any radius being the same as for the actual turbine and finally to have the blade angles suitably chosen to give a uniform distribution of thrust over the whole disk.

The analysis of the actuator disk theory assumes a control volume, in which the control volume boundaries are the surface of a stream tube and two cross-sections of the stream tube as shown in Figure 3.1.

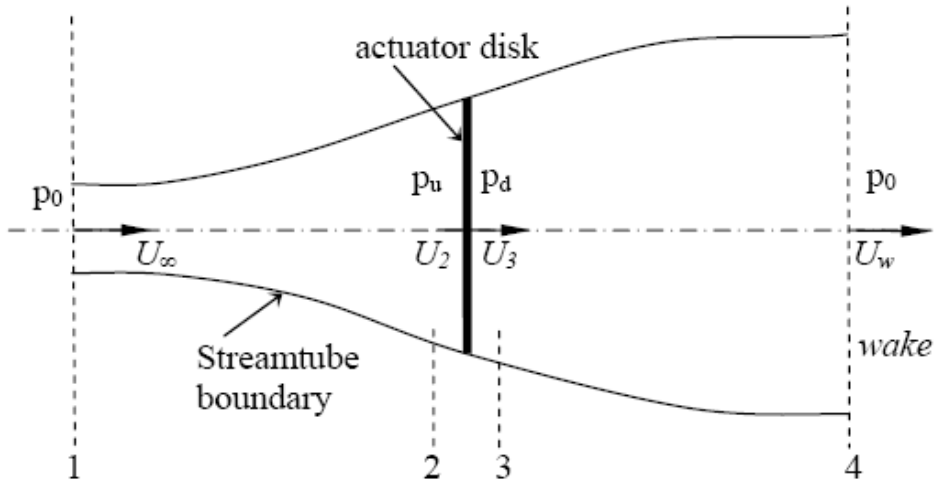

Figure 3.1 Idealized flow through a wind turbine represented by a non-rotating, actuator disk

The only flow is across the ends of the stream tube. The turbine is represented by a uniform "actuator disk" which creates a discontinuity of pressure in the stream tube of air flowing through it. Note also that this analysis is not limited to any particular type of wind turbine.

From the assumption that the continuity of velocity through the disk exists;

$$U_2 = U_3 = U_R$$

For steady state flow, air mass flow rate through the disk can be written as;

$$\dot{m} = \rho * A * U_R \quad \text{.....3.1.1}$$

Applying the conservation of linear momentum to the control volume enclosing the whole system, the net force can be found on the contents of the control volume. That force is equal and opposite to the thrust, T which is the force of the wind on the wind turbine. Hence from the conservation of linear momentum for a one-dimensional, incompressible, time-invariant flow the thrust is equal and opposite to the change in momentum of air stream;

$$T = -\dot{m}(U_\infty - U_W) \quad \text{.....3.1.2}$$

No work is done on either side of the turbine rotor. Thus the Bernoulli function can be used in the two control volumes on either side of the actuator disk. Between the free-stream and upwind side of the rotor (from section 1 to 2 in Figure 3.1) and between the downwind side of the rotor and far wake (from section 3 to 4 in Figure 3.1) respectively;

$$p_o + \frac{1}{2}\rho U_\infty^{\,2} = p_u + \frac{1}{2}\rho U_R^{\,2} \quad \text{.....3.1.3}$$

$$p_d + \frac{1}{2}\rho U_R^2 = p_o + \frac{1}{2}\rho U_W^2 \quad \text{.....3.1.4}$$

The thrust can also be expressed as the net sum forces on each side of the actuator disk;

$$T = A * p' \quad \text{.....3.15}$$

Where,

$$p' = (p_u - p_d) \quad \text{.....3.1.6}$$

By using equations 3.1.3 and 3.1.4, the pressure decrease, p' can be found as;

$$p' = \frac{1}{2}\rho (U_\infty^2 - U_w^2) \quad \text{.....3.1.7}$$

And by substituting equation 3.1.7 in to equation 3.1.5

$$T = \frac{1}{2}\rho A(U_\infty^2 - U_w^2) \quad \text{.....3.1.8}$$

By equating the thrust values from equation 3.1.2 in which substituting equation 3.1.1 in place of $\dot{m}$ and equation 3.1.8, the velocity at the rotor plane can be found as;

$$U_R = \frac{U_\infty + U_w}{2} \quad \text{.....3.1.9}$$

Thus, the wind velocity at the rotor plane, using this simple model, is the average of the upstream and downstream wind speeds.

If an axial induction factor (or the retardation factor), a is defined as the fractional decrease in the wind velocity between the free stream and the rotor plane, then

$$a = \frac{U_\infty - U_R}{U_\infty} \quad \text{.....3.1.10}$$

$$U_R = U_\infty (1 - a) \quad \text{.....3.1.11}$$

$$U_w = U_\infty (1 - 2a) \quad \text{.....3.1.12}$$

The velocity and pressure distribution are illustrated in Figure 3.2. Because of continuity, the diameter of flow field must increase as its velocity decreases and note that there occurs sudden pressure drop at rotor plane which contributes the torque rotating turbine blades.

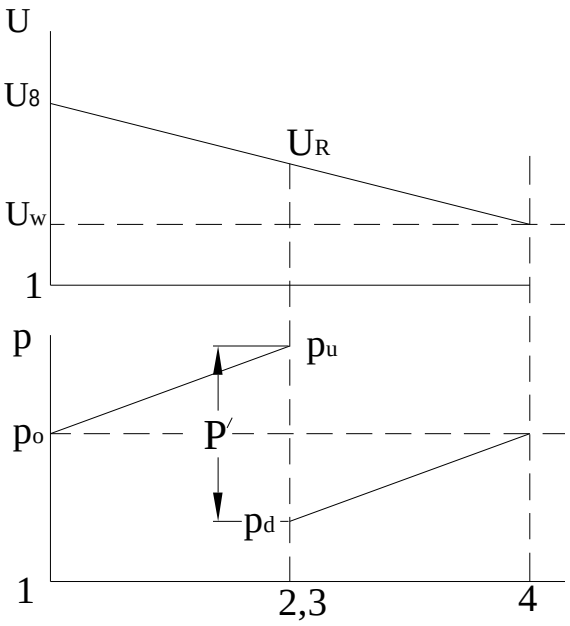

Figure 3.2 Velocity and pressure distribution along stream tube

The power output, P is equal to the thrust times the velocity at the rotor plane;

$$P = T * U_R$$

Using equation 3.1.8,

$$P = \frac{1}{2} \rho A(U_\infty^{\ 2} - U_w^{\ 2})U_R$$

And substituting for U_R and U_w from equations 3.1.11 and 3.1.12,

$$P = 2\rho * A * a(1-a)^2 * U_\infty^{\ 3} \quad \text{.....3.1.12}$$

Using equation 2.5.1, the power coefficient C_p becomes;

$$C_P = 4a(1-a)^2 \quad \text{.....3.1.13}$$

The maximum C_p is determined by taking the derivative of equation 3.1.13 with respect to a and setting it equal to zero yields;

$$(C_P)_{\max} = \frac{16}{27} = 0.5926$$

When, a = 1/3

This result indicates that if an ideal rotor were designed and operated such that the wind speed at the rotor were 2/3 of the free stream wind speed, then it would be operating at the point of maximum power production. This is known as the Betz limit.

From equations 3.1.8, 3.1.11 and 3.1.12 the axial thrust on the disk can be written in the following form;

$$T = 2\,\mathrm{r}Aa(1-a)U_{\infty}^{2} \quad \ldots\ldots\ldots\ldots\ldots\ldots\ldots\ldots\ldots\ldots 3.1.14$$

Similarly to the power coefficient, thrust coefficient can be found as by use of equation 2.5.3;

$$C_T = 4a(1-a)^2 \quad \ldots\ldots\ldots\ldots\ldots\ldots\ldots\ldots\ldots\ldots\ldots 3.1.15$$

Note that C_T has a maximum of 1.0 when a = 0.5 and the downstream velocity is zero. At maximum power output (a =1/3), C_T has a value of 8/9.

In conclusion, the actuator disk theory provides a rational basis for illustrating that the flow velocity at the rotor is different from the free-stream velocity. The Betz limit $C_{p,\max} = 0.593$ shows the maximum theoretically possible rotor power coefficient that can be attained from a wind turbine. In practice three effects lead to a decrease in the maximum achievable power coefficient;

- Rotation of wake behind the rotor
- Finite number of blades and associated tip losses
- Non-zero aerodynamic drag

3.3 THE GENERAL MOMENTUM THEORY

The axial momentum theory of the previous section was developed on the assumption that there was no rotational motion in the slipstream and that the turbine blades could be replaced by an actuator disk which produced a sudden decrease of pressure in the fluid without any change of velocity. More generally, the slipstream will have a rotational motion by the reaction of the torque of the blade and this rotational motion implies a further loss of energy. To extend the theory to include the effects of this rotational motion, it is necessary to modify the qualities of the actuator disk by assuming that it can also impart a rotational component to the fluid velocity while the axial and radial components remain unchanged.

Using a streamtube analysis, equations can be written that express the relation between the wake velocities (both axial and rotational) and the corresponding wind velocities at the rotor disk. In Figure 3.4 an annular streamtube model of this flow illustrating the rotation of the wake is shown for making the visualization clear. And Figure 3.5 illustrates the geometry of this streamtube model of wind flow through a HAWT.

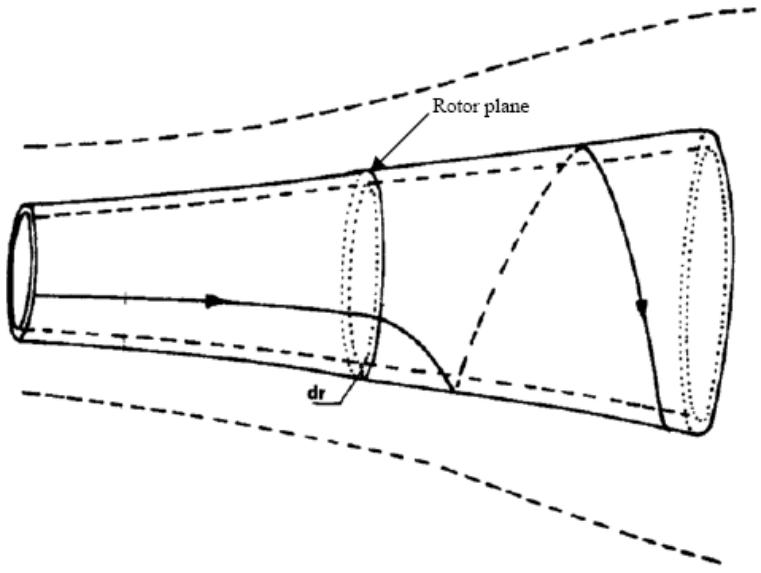

Figure 3.4 Streamtube model of flow behind rotating wind turbine blade

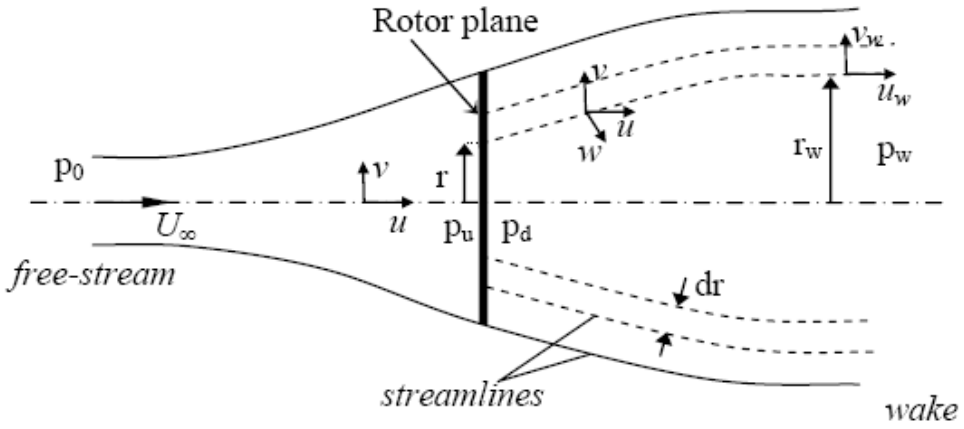

Figure 3.5 Geometry of the streamtube model of flow through a HAWT rotor

Referring to the Figure 3.5, let r be the radial distance of any annular element of the rotor plane, and let u and v be respectively the inflow (the flow immediately in front of the rotor plane) axial and radial components of the fluid velocity. Let P_u be the inflow pressure and let p' be the decrease of outflow (the flow immediately behind the rotor plane) pressure associated with an angular velocity w. In the final wake let P_w be the pressure, u_w be the axial velocity and w_w be the angular velocity at a radial distance r_w from the axis of the slipstream.

By applying the condition of continuity of flow for the annular element is;

$$u_w * r_w * dr_w = u * r * dr \quad \text{.....3.2.1}$$

And the condition for constancy of angular momentum of the fluid as it passes down the slipstream is;

$$w_w * r_w^{\,2} = w * r^2 \quad \text{.....3.2.2}$$

Also since the element of torque of the radial blade element is equal to the angular momentum extracted in unit time to the corresponding annular element of the slipstream;

$$dQ = \rho * u * w * r^2 dA \quad \text{.....3.2.3}$$

Where, $dA = 2\pi * r * dr$

For constructing the energy equation, Bernoulli's equation can be used separately from free-stream to inflow conditions and from outflow to wake conditions;

$$H_o = p_o + \frac{1}{2}\,\mathrm{r}\,U_\infty^{\,2}$$

$$= p_u + \frac{1}{2}\,\mathrm{r}\,(u^2 + v^2)$$

$$H_1 = p_d + \frac{1}{2}\,\mathrm{r}\,(u^2 + v^2 + w^2 * r^2)$$

$$= p_w + \frac{1}{2}\,\mathrm{r}\,(u_w^{\,2} + w_w^{\,2} * r_w^{\,2})$$

Hence,

$$H_o - H_1 = p' - \frac{1}{2}\,\mathrm{r} * w^2 * r^2 \quad \text{……..….3.2.4}$$

Equation 3.2.4 shows that the decrease of total pressure head passing through the blade element is below the thrust per unit area p, by a term representing the kinetic energy of the rotational motion imparted to the fluid by the torque of the blade.

The expressions for the total pressure head also give;

$$p_o - p_w = \frac{1}{2}\,\mathrm{r}\,(u_w^{\,2} - U\infty^2) + \frac{1}{2}\,\mathrm{r} * w_w^{\,2} * r_w^{\,2} + (H_o - H_1)$$

$$= \frac{1}{2}\,\mathrm{r}\,(u_w^{\,2} - U\infty^2) + \frac{1}{2}\,\mathrm{r}\,(w_w^{\,2} * r_w^{\,2} - w^2 * r^2) + P' \quad \text{……3.2.5}$$

To find the pressure drop, p, Bernoulli's equation can be applied between inflow and outflow relative to the blades which are rotating with an angular velocity • . Note that the flow behind the rotor rotates in the opposite direction to the rotor, in reaction to the torque exerted by the flow on the rotor. Hence the angular velocity of the air relative to the blade increases from • to (• + w), while the axial component of the velocity remains constant. The result is;

$$p' = \frac{1}{2}\,\mathrm{r}\,[(\Omega + w)^2 - \Omega^2]$$

$$= \mathrm{r}\,(\Omega + \frac{w}{2}) * w * r^2 \quad \text{……3.2.6}$$

Finally, combining this result (equation 3.2.6) with the previous equations 3.2.2 and 3.2.5, the drop of pressure in the wake becomes;

$$p_o - p_w = \frac{1}{2}\,\mathrm{r}\,(u_w^{\,2} - U\infty^2) + \mathrm{r}\,(\Omega + \frac{w}{2}) * w_w * r_w^{\,2} \quad \text{…..…3.2.7}$$

The pressure gradient in the wake balances the centrifugal force on the fluid and is governed by the following equation;

$$\frac{dp_w}{dr_w} = \rho * w_w^{\,2} * r_w \quad \text{.....3.2.8}$$

And then differentiating equation 3.2.7 relative to r_w and equating to equation 3.2.8, a differential equation is obtained connecting the axial and rotational velocities in the wake,

$$\frac{1}{2}\frac{d}{dr_w}[U_\infty^{\,2} - u_w^{\,2}] = (w_w + \Omega)\frac{d}{dr_w}(w_w * r_w^{\,2}) \quad \text{.....3.2.9}$$

The equation of axial momentum for the blade element, which can be established rigorously by a simple extension of the analysis of the previous section,

$$T = \int \rho * u_w(U_\infty - u_w)dA + \int (p_o - p_w)dA_w$$

and in the differential form;

$$dT = \rho u_w(U_\infty - u_w)dA + (p_o - p_w)dA_w \quad \text{.....3.2.10}$$

also from the pressure decrease at the rotor plane, dT can alternatively be written as;

$$dT = p'dA \quad \text{.....3.2.11}$$

By inserting equation 3.2.6 into its place in equation 3.2.11,

$$dT = \rho(\Omega + \frac{w}{2})wr^2 dA \quad \text{.....3.2.12}$$

Finally, combining equation 3.2.1, 3.2.5, 3.2.10 and 3.2.12,

$$\frac{1}{2}[U_\infty^{\,2} - u_w]^2 = \left[\frac{\Omega + w_w/2}{u_w} - \frac{\Omega + w/2}{U\infty}\right]u_w w_w r_w^{\,2} \quad \text{.....3.2.13}$$

It should be emphasized that the equation of axial momentum is based on the assumption that the axial force due to the pressure on the lateral boundary of the streamline is equal to the pressure force, $(p_o A_o - p_w A_w)$ over its ends. This assumption implies that the mutual interference between various annular elements has been neglected but the actual deviations from the conditions represented by equation 3.2.12 are believed to be extremely small in general. The other assumptions made for deriving the general momentum equations so far are that the rotor was treated as having very large number of very narrow blades (infinite number of blades) resulting in negligible radial component of the velocity of the fluid and the air is incompressible and inviscid, i.e., fluid drag is zero [10].

Equations 3.2.1, 3.2.2, 3.2.9 and 3.2.13, though rather complex in form, suffice to determine the relationship between the thrust and torque of the blade and the flow in the slipstream. If, for example, the angular velocity w_w is known as a function of the radius r in the wake, equation 3.2.9 determines the axial velocity, u_w and then equation 3.2.13, taken in conjunction with equation 3.2.1 and equation 3.2, determines the axial and rotational velocities at the rotor plane. The thrust and torque of the rotor are then obtained from equation 3.2.12 and equation 3.2.3 respectively. Owing to the complexity of these equations, however, it is customary to adopt certain approximations based on the fact that the rotational velocity in the slipstream is generally very small.

An exact solution of the general momentum equations can be obtained when the flow in the slipstream is irrotational except along the axis. This condition implies that the rotational momentum wr^2 has the same value for all radial elements. Then by virtue of equation 3.2.11, the axial velocity, u_w is constant along a radius because this equation's right-hand side is zero.

Defining the axial velocities u and u_w as

$$u = U_\infty(1-a)$$

$$u_w = U_\infty(1-b)$$

After some algebraic manipulations, it can be obtained from equation 3.2.13,

$$a = \frac{b}{2}\left[1 - \frac{(1-a)b^2}{4\mathrm{l}^2(b-a)}\right] \quad \text{.....3.2.14}$$

Examination of equation 3.2.14 shows that the axial velocity reduction of the rotor disk is always approximately one-half the reduction in the far-wake for the tip-speed ratio above 2, which is the same result, reached in the previous section when the wake rotation was neglected.

For the approximate solution, the following assumption is made. The angular velocity w imparted to the slipstream is very small compared with the angular velocity • of the blades and it is therefore possible to simplify the general equations by neglecting certain terms involving w^2 [10]. On this basis of approximation the pressure p_w in the wake is equal to the initial pressure p_o of the air and the decrease of pressure p' across the rotor disk is equal to the decrease of total pressure head $(H - H_o)$. The relationships connecting the

thrust and axial velocity are then the same as in the simple momentum theory, the axial velocity u at the rotor disk is the arithmetic mean of the axial velocity $U\infty$ and the slipstream velocity u_w , and the element of thrust is

$$dT = 2\rho u(u - U\infty)dA$$

$$= 4\pi\rho U_\infty^{\ 2} a(1-a)rdr \quad \text{.....3.2.15}$$

Alternatively, from equation 3.2.6,

$$dT = p'dA$$

$$= 2\pi\rho(\Omega + w/2)wr^3 dr$$

And defining angular induction factor, $a' = w/2\Omega$

$$dT = 4\pi\rho\Omega^2 a'(1+a')r^3 dr \quad \text{.....3.2.16}$$

Equating the two expressions for the thrust given in equation 3.2.15 and equation 3.2.16, a relationship is obtained between axial induction factor, a and angular induction factor a',

$$\frac{a(1-a)}{a'(1+a')} = \frac{\Omega^2 r^2}{U_\infty^{\ 2}} = \lambda_r^{\ 2} \quad \text{.....3.2.17}$$

The element of torque is obtained from equation 3.2.3 as following;

$$dQ = \rho uwr^2 dA$$

$$= 4\pi\rho U\infty\Omega a'(1-a)r^3 dr \quad \text{.....3.2.18}$$

The power generated at each radial element, dP is given by the following equation;

$$dP = \Omega dQ \quad \text{.....3.2.19}$$

By substituting dQ from equation 3.2.18 into equation 3.2.19 and using the definition of local tip speed ratio, λ_r the expression for the power generated at each radial element becomes;

$$dP = \frac{1}{2}\rho AU_\infty^{\ 3}\left[\frac{8}{\lambda^2}a'(1-a)\lambda_r^{\ 3} d\lambda_r\right] \quad \text{.....3.2.20}$$

The incremental contribution to the power coefficient from each annular ring is given by;

$$dC_p = \frac{dP}{\frac{1}{2}\rho U_\infty A} \quad \text{.....3.2.21}$$

By inserting equation 3.2.20 into equation 3.2.21 and integrating elemental power Coefficient from local tip speed ratio at the hub, λ_h to the tip speed ratio, C_p is obtained as;

$$C_p = \frac{8}{\lambda^2}\int_{\lambda_h}^{\lambda} a'(1-a)\lambda_r^{\,3}\,d\lambda_r \quad \text{.....3.2.22}$$

In order to integrate equation 3.2.22, it is needed to relate the variables a, a' and λ_r. By solving equation 3.2.17, a' in terms of a,

$$a' = -\frac{1}{2} + \frac{1}{2}\sqrt{1+\frac{4}{\lambda_r^{\,2}}a(1-a)} \quad \text{.....3.2.23}$$

The aerodynamic conditions for the maximum possible power production occur when the term $a'(1-a)$ in equation 3.2.22 is at its greatest value. Substituting the value for a' from equation 3.2.23 into the term $a'(1-a)$ and setting the derivative with respect to a and equating to zero yields;

$$\lambda_r^{\,2} = \frac{(1-a)(1-4a)^2}{(1-3a)} \quad \text{.....3.2.24}$$

And substituting equation 3.2.24 into equation 3.2.17, it is found that for maximum power in each annular ring,

$$a' = (1-3a)/(4a-1) \quad \text{.....3.2.25}$$

If equation 3.2.24 is differentiated with respect to a, a relationship between $d\lambda_r$ and da at those conditions is obtained;

$$2\lambda_r d\lambda_r = \left[6(4a-1)(1-2a)^2/(1-3a)^2\right]da \quad \text{.....3.2.26}$$

Now, substituting the equations 3.2.24, 3.2.25 and 3.2.26 into the equation 3.2.22 gives;

$$C_{p,\max} = \frac{24}{\lambda^2}\int_{a_1}^{a_2}\left[\frac{(1-a)(1-2a)(1-4a)}{(1-3a)}\right]^2 da \quad \text{.....3.2.27}$$

Where a_1 : Corresponding axial induction factor for $\lambda_r = \lambda_h$

a_2 : Corresponding axial induction factor for $\lambda_r = \lambda$

Also from equation 3.2.24;

$$\lambda^2 = (1-a_2)(1-4a_2)/(1-3a_2) \quad \text{.....3.2.28}$$

Equation 3.2.28 can be solved for the values of a that correspond to operation at tip speed ratios of interest. Note also from equation 3.2.28, $a_2 = 1/3$ is the upper limit of the axial induction factor giving an infinitely large tip speed ratio.

Table 3.1 presents a summary of numerical values for $C_{p,\max}$ as a function of λ_r with corresponding values for the axial induction factor at the tip, a_2

Table 3.1 Power coefficient, $C_{p,\max}$ as a function of tip-speed ratio, λ and a_2

λ	a_2	$C_{P,\max}$
0.5	0.2983	0.289
1.0	0.3170	0.416
1.5	0.3245	0.477
2	0.3279	0.511
2.5	0.3297	0.533
5	0.3324	0.570
7.5	0.3329	0.581
10	0.3330	0.585

The result of general momentum theory shows that the higher the tip-speed ratio, the greater the maximum power coefficient.

3.4 BLADE-ELEMENT THEORY

The momentum theories, which are developed in the previous sections, are based on a consideration of the mean axial and rotational velocity in the slipstream and determine the thrust and torque of a blade from the rate of decrease of momentum of the fluid. The theories determine an upper limit to the power coefficient of any blade, depending on the free-stream wind velocity and on the power extracted, but they restrict the understanding of the effect of rotor geometry (i.e. blade airfoil section, chord and twist). The blade-element theory is an alternative method of analyzing the behavior of blades due to their motion through air.

As shown in Figure 3.7, for this analysis, it is assumed that the blade is divided into N sections (or elements) and the aerodynamic force acting on each blade element can be estimated as the force on suitable airfoil characteristics of the same cross-section adopted for the blade elements. Finally assuming that the behavior of each element is not affected by the adjacent elements of the same blade, the force on the whole blade can be derived by adding the contributions of all the elements along the blade.

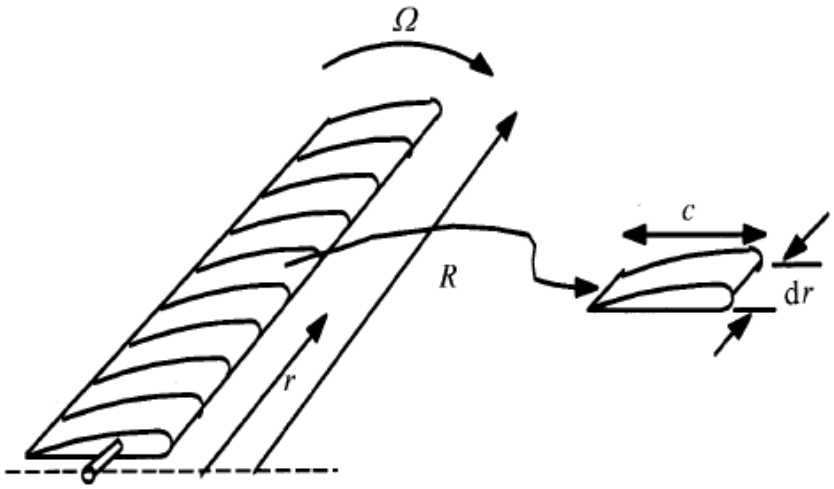

Figure 3.7 Schematic of blade elements

A diagram showing the developed blade element at radius r and the velocities and forces acting on this element is given in Figure 3.8.

The relative wind velocity U_{rel} is the vector sum of the wind velocity at the rotor $U_\infty(1-a)$ (the vector sum of the free-stream wind velocity, U_∞ and the induced axial velocity $-aU_\infty$) and the wind velocity due to rotation of the blade. And this rotational component is the

vector sum of the blade section velocity, Ωr and the induced angular velocity $a'\Omega r$. Hence the relative wind velocity will be as shown on the velocity diagram in Figure 3.8. The minus sign in the term $U_\infty(1-a)$ is due to the retardation of flow while the air approaching the rotor and the plus sign in the term $\Omega r(1+a')$ as shown in Figure 3.8 is due to the flow of air in the reverse direction of blade rotation after air particles hit the blades and so give torque.

In the mean time let the existence of the axial and angular induction factors assumed, their evaluation will be given in the subsequent section.

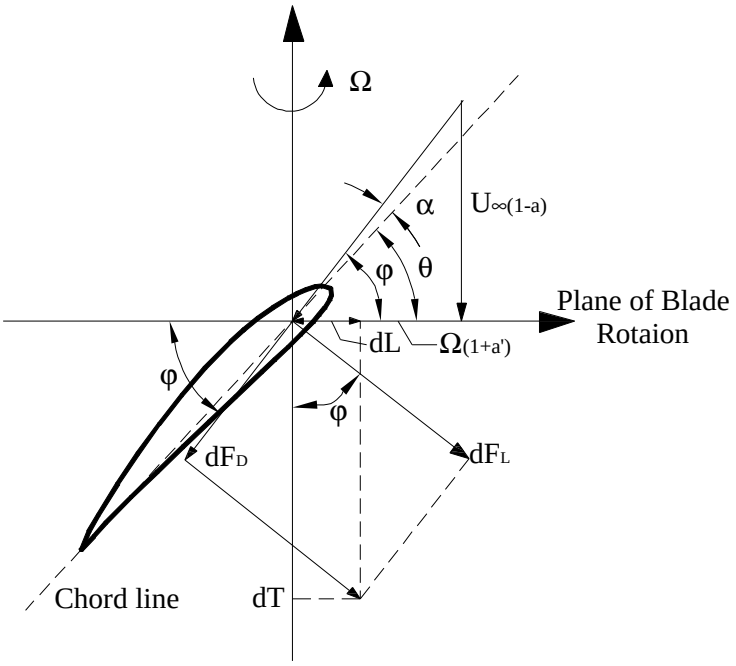

Figure 3.8 Blade Geometry for analysis of a HAWT

From Figure 3.8 the following relationships can be determined;

$$U_{rel} = \frac{U_\infty(1-a)}{\sin(\phi)} \quad \text{.....3.3.1}$$

$$\tan(\phi) = \frac{U_\infty(1-a)}{\Omega r(1+a')} = \frac{(1-a)}{(1+a')\lambda_r} \quad \text{.....3.3.2}$$

$$dF_D = C_D \frac{1}{2} \rho U_{rel}^2 c\,dr \quad \text{.....3.3.3}$$

$$dF_L = C_L \frac{1}{2} \rho U_{rel}^2 c\,dr \quad \text{.....3.3.4}$$

$$dT = dF_L \cos(\phi) + dF_D \sin(\phi) \quad \text{.....3.3.5}$$

$$dL = dF_L \sin(\phi) - dF_D \cos(\phi) \quad \text{……..…..3.3.6}$$

If the rotor has B number of blades, the total normal and tangential force on the element at a distance r by rearranging equation 3.3.5 and 3.3.6 with the use of equation 3.3.1, 3.3.3 and 3.3.4;

$$dT = B\frac{1}{2}\rho U_{rel}(C_L \cos(\phi) + C_D \sin(\phi))cdr \quad \text{……...…....3.3.7}$$

$$dL = B\frac{1}{2}\rho U_{rel}(C_L \sin(\phi) - C_D \cos(\phi))cdr \quad \text{……...3.3.8}$$

The elemental torque due to the tangential forces, dL operating at a distance r from the center is given by;

$$dQ = rdL \quad \text{…….3.3.9}$$

Hence the elemental torque by inserting equation 3.3.8 into equation 3.3.9;

$$dQ = B\frac{1}{2}\rho U_{rel}(C_L \sin(\phi) - C_D \cos(\phi))crdr \quad \text{……..….3.3.10}$$

From the velocity diagram in Figure 3.8, relative wind velocity can be written as below;

$$U_{rel} = \frac{U\infty(1-a)}{\sin(\phi)} \quad \text{……..3.3.11}$$

And by defining solidity ratio, σ as following;

$$\sigma = \frac{Bc}{2\pi r} \quad \text{……..……3.3.12}$$

and inserting equations 3.3.11 and 3.3.12 into equations 3.3.7 and 3.3.10, the general form of elemental thrust and torque equations become;

$$dT = \sigma\pi\rho\frac{U_\infty{}^2(1-a)^2}{\sin^2(\phi)}(C_L \cos(\phi) - C_D \sin(\phi))rdr \quad \text{……3.3.13}$$

$$dQ = \sigma\pi\rho\frac{U_\infty{}^2(1-a)^2}{\sin^2(\phi)}(C_L \sin(\phi) - C_D \cos(\phi))r^2 dr \quad \text{……3.3.14}$$

Thus, from blade element theory, two equations (3.3.13 and 3.3.14) have been obtained. They define the normal force (thrust) and the tangential force (torque) on an annular rotor section as a function of the flow angles at the blades and airfoil characteristics.

Here it is convenient to consider in turn the following assumptions which are the bases of developing blade element theory [11]:

- The assumption that the behavior of an element is not affected by the adjacent elements of the same blade
- The airfoil characteristics to be adopted for the element

The independence of blade elements, assumed in the blade element theory and also in all later developments of theory, is analogous to the assumption adopted in the general momentum theory that the thrust on an elementary annulus of a rotor may be expressed as $dT = 2\rho u(u - U_\infty)dA$ (equation 3.2.15). In the discussion of general momentum theory it was pointed out that this equation could not be established rigorously. Similarly, in the blade element theory, it is not possible to give a rigorous proof of the independence of the blade elements and the validity of the assumption must be justified by an appeal to suitable experimental results. If the assumption valid, the thrust on the blade element at radial distance r with the blade angle θ should be independent of the variation of the blade angle along the remainder of the blade. A check of the assumption can therefore be obtained by taking two propellers of different pitch with blades of the same plan form and section and by rotating the blades of one rotor so that the blade angles of the two rotors have the same value at a chosen radial distance r. The thrust distribution along the blades should then show the same element of thrust on the blade elements under examination. By means of a series of experiments [12] has been established the independence of the blade elements over the principal part of the blades.

The second assumption states that two-dimensional airfoil characteristics can be used for the blade elements. Airfoil two-dimensional characteristics are usually determined from tests of a rectangular airfoil of different aspect ratio. Hence the lift and drag characteristics are dependent on aspect ratio. But in the fully-attached regime, airfoil section characteristics are not generally affected by aspect ratio, and since HAWT rotors operate in the fully-attached regime of the flow while extracting maximum energy from the wind, two-dimensional (i.e. infinite aspect ratio) can be used in predicting performance. However, when two-dimensional data are used, a tip-loss factor must be added as will be described in the next chapter.

3.5 BLADE ELEMENT-MOMENTUM (BEM) THEORY

In the general momentum theory attention was directed to the motion of the fluid and the forces acting on the blades were determined. The defect of the general momentum theory was that it gave no indication of the shape of blade required to produce the reactions considered.

The principle of the blade element theory was to consider the forces experienced by the blades of the rotor in their motion through the air and this theory was therefore intimately concerned with the geometrical shape of the blade.

In order to bridge the gap between these two theories, the blade element momentum theory (BEM) which is also known as strip theory has been developed. BEM theory relates rotor performance to rotor geometry and particularly important prediction of this theory is the effect of finite blade number.

The assumptions for BEM theory are obviously the combination of those which were made for general momentum and blade element theory. The foremost assumption in BEM theory is that individual streamtubes (the intersection of a streamtube and the surface swept by the blades) can be analyzed independently of the rest of the flow as assumed before for the blade element theory.

A second assumption associated with the development of BEM theory is that spanwise flow is negligible, and therefore airfoil data taken from two-dimensional section tests are acceptable as assumed before in again blade element theory. A third assumption is that flow conditions do not vary in the circumferential direction, i.e. axisymmetric flow. With this assumption the streamtube to be analyzed is a uniform annular ring centered on the axis of revolution as assumed before in general momentum theory.

BEM theory refers to the determination of a wind turbine blade performance by combining the equations of general momentum theory and blade element theory. In this case by equating the elemental thrust force equations from general momentum theory and blade element theory (equations 3.2.15 and 3.3.13 respectively) the following relationship is obtained;

$$\frac{a}{(1-a)} = (\sigma C_L)\frac{\cos(\phi)}{4\sin^2(\phi)}\left[1+(C_D/C_L)\tan(\phi)\right] \quad \text{.....3.4.1}$$

and equating the elemental torque derived in both general momentum theory and blade element theory (equations 3.2.18 and 3.3.14 respectively);

$$\frac{a'}{(1-a)} = \frac{(\mathrm{s}C_L)}{4\mathrm{l}_r \sin(\mathrm{j})}\left[1-(C_D/C_L)\cot(\mathrm{j})\right] \ldots\ldots\ldots\ldots\ldots\ldots\ldots 3.4.2$$

Equation 3.4.2 can be rearranged by using equation 3.3.2, which relates a, a', j and l_r based on the geometric considerations;

$$\frac{a'}{(1+a')} = \frac{(\mathrm{s}C_L)}{4\cos(\mathrm{j})}\left[1-(C_D/C_L)\cot(\mathrm{j})\right] \ldots\ldots\ldots\ldots\ldots\ldots 3.4.3$$

In the calculation of induction factors a and a', accepted practice is to set C_D zero for the purpose of determining induction factors independently from airfoil characteristics. For airfoils with low drag coefficient, this simplification introduces negligible errors [13]. So equation 3.4.1, 3.4.2 and 3.4.3 can be rewritten considering $C_D \approx 0$

$$\frac{a}{(1-a)} = (\mathrm{s}C_L)\frac{\cos(\mathrm{j})}{4\sin^2(\mathrm{j})} \ldots\ldots\ldots\ldots\ldots\ldots\ldots\ldots\ldots\ldots\ldots 3.4.4$$

$$\frac{a'}{(1-a)} = \frac{(\mathrm{s}C_L)}{4\mathrm{l}_r \sin(\mathrm{j})} \ldots\ldots\ldots\ldots\ldots\ldots\ldots\ldots\ldots\ldots\ldots 3.4.5$$

$$\frac{a'}{(1+a')} = \frac{(\mathrm{s}C_L)}{4\cos(\mathrm{j})} \ldots\ldots\ldots\ldots\ldots\ldots\ldots\ldots\ldots\ldots\ldots 3.4.6$$

By using these three equations the following useful relationships result after some algebraic manipulation;

$$C_L = \frac{4\sin(\mathrm{j})}{\mathrm{s}}\frac{(\cos(\mathrm{j})-\sin(\mathrm{j}))}{(\sin(\mathrm{j})+\mathrm{l}_r\cos(\mathrm{j}))} \ldots\ldots\ldots\ldots\ldots\ldots\ldots\ldots 3.4.7$$

$$a = \frac{1}{\left[1+\left[4\sin^2(\mathrm{j})/(\mathrm{s}C_L)\cos(\mathrm{j})\right]\right]} \ldots\ldots\ldots\ldots\ldots\ldots\ldots\ldots 3.4.8$$

$$a' = \frac{1}{\left[\left[4\cos(\mathrm{j})/(\mathrm{s}C_L)\right]-1\right]} \ldots\ldots\ldots\ldots\ldots\ldots\ldots\ldots\ldots 3.4.9$$

$$a/a' = \mathrm{l}_r/\tan(\mathrm{j}) \ldots\ldots\ldots\ldots\ldots\ldots\ldots\ldots\ldots\ldots\ldots 3.4.10$$

To determine the power coefficient of a wind turbine, the power contribution from each annulus is found firstly, then integrated along the blade length and finally using the equation 2.5.1, power coefficient C_p can be obtained.

The elemental power from each blade element was defined in equation 3.2.19 as;

$$dP = \Omega dQ \ldots\ldots\ldots\ldots\ldots\ldots\ldots\ldots\ldots\ldots\ldots 3.2.19$$

And the total power from the rotor is;

$$P = \int_{r_h}^{R} dP = \int_{r_h}^{R} \Omega dQ \quad \text{……..3.2.20}$$

Hence the power coefficient C_p becomes by rewriting equation 2.5.1 here,

$$C_p = \frac{P}{1/2\,\rho U_\infty^3 A} = \frac{\int_{r_h}^{R} \Omega dQ}{1/2\,\rho U_\infty^3 \pi R^2} \quad \text{……..3.4.11}$$

Using the expression for the elemental torque from equation 3.3.14, the power coefficient can be expressed as below,

$$C_p = \frac{2}{\lambda^2}\int \sigma C_L \frac{(1-a)}{\sin(\phi)}\left[1-(C_L/C_D)\cot(\phi)\right]\lambda_r^{\,2} d\lambda_r \quad \text{…….3.4.12}$$

Finally by using equations 3.4.4 and 3.4.10 in equation 3.4.12, the general form of power coefficient expression can be obtained as;

$$C_p = \frac{8}{\lambda^2}\int_{\lambda_h}^{\lambda} \lambda_r^{\,3} a'(1-a)\left[1-(C_D/C_L)\cot(\phi)\right] d\lambda_r \quad \text{……..3.4.13}$$

Note that when, $C_D \approx 0$, the equation above for C_p is the same as the one derived from the general momentum theory (equation 3.2.22). An alternative expression for the power coefficient can be derived after performing the tedious algebra and by inserting equations 3.4.7 and 3.4.8 into equation 3.4.12;

$$C_p = \frac{8}{\lambda^2}\int_{\lambda_h}^{\lambda} \sin^2(\phi)(\cos(\phi)-\lambda_r\sin(\phi))(\sin(\phi)+\lambda_r\cos^*(\phi))\left[1-(C_D/C_L)\cot(\phi)\right]\lambda_r^{\,2} d\lambda_r$$

……3.4.14

Note that even though the axial and angular induction factors were determined assuming the $C_D \approx 0$, the drag is included in the power coefficient calculation. By the same token, the thrust coefficient C_T can be found beginning from the definition of thrust coefficient in the equation 2.5.3 as following;

$$C_T = \frac{4}{\lambda^2}\int_{\lambda_h}^{\lambda} \sin^2(\phi)(\cos(\phi)-\lambda_r\sin(\phi))(\sin(\phi)+\lambda_r\cos^*(\phi))\left[1+(C_D/C_L)\cot(\phi)\right]\lambda_r^{\,2} d\lambda_r \ldots$$

……3.4.15

3.6 VORTEX THEORY

In addition to BEM theory which will be used for rotor performance analysis and blade design of HAWT in this thesis; vortex theory is an alternative theory which provides a method of analyzing the rotor performance. Even though vortex theory is not the scope of this thesis there is a necessity of discussing of this theory briefly without going into its detail. Because the vortex theory explains the origin of axial and angular induction factors which have been already introduced in both general momentum theory and blade element theory without giving any physical meaning about their existence.

The vortex theory depends fundamentally on the conception that the lift of an airfoil section is associated with a circulation of the flow around its contour. According to modern airfoil theory the lift L per unit length of an airfoil section in two-dimensional motion is related to the circulation • around its contour by the following equation;

$$L = \rho U \Gamma \quad \text{.....3.5.1}$$

Applying this concept of airfoil theory to the problem of the rotor blades, it is evident that there must be circulation of the flow around the blades of the rotor in order to produce the aerodynamic force experienced by the blades. In general the circulation Γ around the blade element will vary along the blade, but to explain the mode of action of the blades it is simpler to assume as a first step that the circulation is constant along the whole blade. The existence of this circulation can be expressed also by the statement that there is a vortex line of strength Γ, bound to the blade and running along it from root to tip. But a vortex line can not begin or end abruptly; unless it forms a closed curve in the body, it must be continued as a free vortex line in the fluid and in this latter form it follows the general motion of the fluid as a trailing vortex behind the body. Thus the bound vortex must be continued by two free vortices in the fluid, one springing from the root of the blade and the other from its tip. As shown in Figure 3.9 the free vortex springing from the roots of propeller blades will be straight line along the axis of the propeller and its strength will be $B\Gamma$ for a propeller with B blades. The tip vortices, each of strength Γ, will be of helical shape and will be tracing out the paths described by the tips of the propeller blades.

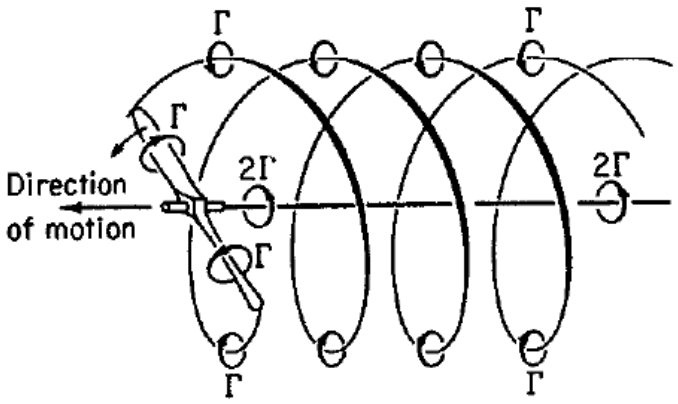

Figure 3.9 Tip and root vortices

Up to this point the vortex system of a rotor or propeller has been based for simplicity on the assumption that the circulation along the blade is constant. More generally, however, the strength of the circulation will vary along the blade and indeed the condition of constant circulation along the whole blade is physically impossible. Because the pressure difference between the top and bottom surface of the blade causes flow and pressure equalization near the blade tips. For an illustration the actual variation of the circulation along the blade is given in Figure 3.10. Due to the variation of the circulation along the blade, trailing vortices will arise, not only at the root and tip of the blade, but from every point of its trailing edge, forming a continual screw like vortex sheet.

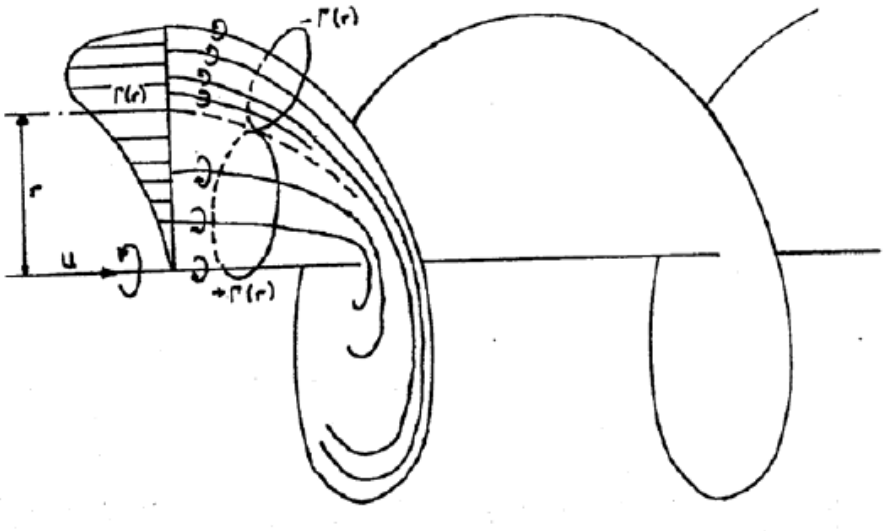

Figure 3.10 Variation of bound circulation along blade length

If $d\Gamma$ is the increase of circulation between the points r and $(r + dr)$ of the blade, then the strength of the helical vortex springing from this element will be $\bullet\, d\Gamma$. The vortex line springing from one blade form a vortex sheet in the form of a screw surface and there will be one such surface for each blade. The slipstream of the rotor consists of these vortex sheets and of the fluid contained between them.

The disturbance of the flow caused by a rotor can be represented as the induced velocity of the completed vortex system, comprising the bound vortices of the propeller blades and the free vortex sheets of the slipstream and the motion of the fluid relative to the propeller is the resultant of the axial velocity and its induced velocity.

Owing to the difficulty of calculating the induced velocity of the system of helical vortex sheets which constitute the slipstream of a rotor, the induced velocity is usually calculated on the assumption that the propeller has a very large number of blades. This assumption implies that the vorticity of the slipstream is distributed throughout the whole of the fluid instead of being concentrated on a few vortex sheets and the vorticity can then be assumed to be grouped in the following manner. Considering first the condition of constant circulation along the blades, the boundary of the slipstream is a cylindrical vortex sheet as shown in Figure 3.11.

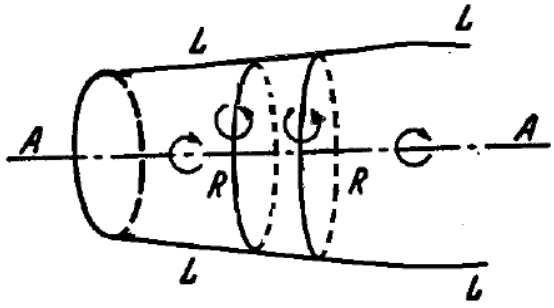

Figure 3.11 Helical vortices replaced by axial and circumferential vortex lines

In place of the helical vortex lines covering the surface, the vorticity of the sheet may be considered a close succession of vortex rings RR whose vorticity represents the decreased axial velocity of the slipstream and a surface of vortex lines LL whose vorticity represents the rotation of the slipstream. The vortex system is completed by the axial vortex AA. More generally, with circulation varying along the blades of the propeller, the whole slipstream must be considered as full of vortex systems of this simpler type.

The induced velocity of the vortex system in the ultimate wake far behind the rotor plane will be an axial velocity $(U_\infty - u_w)$ and an angular velocity w_w, which will be function of the radial coordinate r_w. In this wake the induced velocity of the bound vortices of the blades is negligibly small. At the disc also the bound vortices can not give any component to the axial velocity owing to the symmetrical distribution of this vorticity relative to any arbitrary point of the disc and hence the axial induced velocity $(U_\infty - u)$ will be due wholly to the trailing vortex system.

Also if the expansion of the slipstream can be ignored in calculating these induced velocities, it can easily be seen that the axial induced velocity at the rotor disk is half that in the ultimate wake; for the vortex system is then simply a long cylinder extending indefinitely in one direction from the rotor disk and the induced axial velocity at a point of the wake, where the cylinder extends indefinitely in both directions, must clearly be double that at the corresponding point of the rotor disk. Thus

$$(U_\infty - u) = \frac{1}{2}(U_\infty - u_w)$$

Or

$$u = \frac{1}{2}(U_\infty + u_w) \quad \text{.....3.1.8}$$

Which is the well known equation of the momentum theory described in section 3.1 from which the axial induction factor has been defined, The induced angular velocity w immediately behind the rotor disk can be related to the corresponding angular velocity w_w in the wake by considering the constancy of circulation of the fluid. The ring of fluid of radius r immediately behind the rotor disk has the circulation $2\pi w r^2$ and by the laws of hydrodynamics this circulation must remain constant as the ring of fluid passes down stream. In the wake the radius of the ring has expanded to r_w and there must therefore be a decrease of the angular velocity governed by the equation as described in section 3.2;

$$w r^2 = w_w r_w^2 \quad \text{.....3.2.2}$$

Immediately in front of the rotor disk there can be no such circulation, since the fluid approaching the rotor is in irrotational motion. Also the bound vorticity of the rotor blades must cause equal and opposite induced angular velocities $\pm w'$ immediately before and behind the rotor disk and hence the induced angular velocity of the trailing vortex system

must have the value w' at the rotor disk in order to cancel the effect of the bound vortices in front of the disk. It follows that the total induced angular velocity immediately behind the rotor disk is $2w'$ and this is the angular velocity previously denoted by w. Hence the induced angular velocity of the trailing vortices at the propeller disk is $1/2\,w$ and the angular induction factor in section 3.2 has been defined by taking this value as a basis.

Vortex theory shows also the independence of blade elements which has been assumed in blade element theory in section 3.3 and tried to explained physically. Here it will be explained with the help of vortex theory as well by taking the consideration of the system of trailing vortices which leads to the conclusion that induced flow experienced by the blade elements at radial distance r from the axis depends solely on the forces experienced by these elements and is not influenced by the blade elements at greater or less radial distance. Consider the action of the blade elements dr at radial distance r when the remainder of each rotor blade is inoperative. The trailing vortices which spring from the ends of the element lie on the surfaces of two circular cylinders of radius r and $r + dr$ respectively and the vorticity may be resolved into two components as described before; one having its axis parallel to the rotor axis and the other being circumferential and similar to a succession of vortex rings. The first component of the vorticity acts as the roller bearings between the rotating shell of air bounded by the cylindrical surfaces and the general mass of air. Now the general mass of air can not acquire any circulation about the axis and hence the rotation due to the torque of the blade elements is confined to the region between the two cylindrical surfaces. Hence also the rotational interference due to the vortex system is experienced by those blade elements which gave rise to the vorticity.

A similar argument can be applied to the second component of the vorticity and thus the independence of the blade elements at different radial distances from the axis of the rotor is established [14].

It may be summarized the results of the vortex theory as follows:

- The induced flow at any radius r depends only on the thrust and torque grading at this radius. In other words, the blade elements at differing radii are hydro dynamically independent. This proves the validity of the assumption about this result mentioned in blade element theory in section 3.3

- The induced axial velocity at a blade element is just half the axial velocity in the distant part of the slipstream which comes from the element at that radius. This is in agreement with the findings of the actuator disk theory of section 3.1
- The induced circumferential or rotational velocity of inflow at a blade element is just the half the rotational velocity in the distant part of the slipstream which comes from the elements at that radius which is what was done while defining angular induction factor in the general momentum theory in section 3.2.

Before closing this section a few words about the advantages and disadvantages of the vortex theory over the BEM theory are the following; the BEM theory offers the method of ease of understanding and use as well as minimal computation requirements. However there are a number of situations where it is not reasonable to expect BEM methods over the vortex methods since vortex methods offer the greatest accuracy. Though methods are available for incorporating some complex effects such as yawed flow and unsteady aerodynamics into a BEM analysis, it is much more desirable to seek analytical methods of vortex theory which are fundamentally better suited to complex flows. The greatest obstacle to widespread use of vortex methods is the computation burden. No programs are currently available that calculate the details of an unsteady, three-dimensional, free wake in a reasonable time, regardless of computer platform [7].

CHAPTER 4

HAWT BLADE DESIGN

4.1 INTRODUCTION

In this chapter, the application of BEM theory on the HAWT blade design and analyzing the aerodynamic performance of a rotor will be explained.

BEM theory, as previously developed, does not account the effect of blade numbers of a rotor. In other words, the equations of BEM theory were derived assuming infinite number of blades of a rotor. This chapter begins with introducing the concept of tip-loss factor and the generally recommended expression for including tip losses in HAWT blade design is given. The governing equations developed in BEM theory will then be modified in order to take the tip losses in to account.

In the next section flow states in which HAWTs are operating will be examined. At which values of axial induction factor the application of BEM theory becomes invalid will be explained and the Glauert empirical relationship will then be given in order to proceed the blade design for those values of axial induction factor.

Since the HAWT blades are made from airfoils to transform the kinetic energy in the wind into useful energy, subsequent section is left to the introduction of airfoil selection criteria in HAWT blade design. Most used airfoil families are described as well.

After giving all these necessary knowledge for a blade design, the blade design procedure for an optimum rotor and power performance prediction procedure for the designed blade shape are given. The output of the BLADE DESIGN PROGRAM performed for the airfoil NACA 4412 are also put in this section as an example.

The chapter is ended with the results and explanatory figures showing the effect of some parameters relating to the blade design.

It should be noted here that various methods [15,16,17,18,19] for HAWT blade design and predicting performance of a rotor have been studied and the important concepts [20,21] for design procedure have been used while developing the user-interface computer program, BLADE DESIGN PROGRAM.

4.2 THE TIP-LOSS FACTOR

There was an assumption; the rotor has an infinite number of blades which was used in all theories discussed in the previous chapter. With the aid of this assumption radial velocity of the flow across the rotor plane and in the wake has been always neglected and by so the derivations of governing equations have been established. But near the boundary of the slipstream the air tends to flow around the edges of the blade tips and acquires an important radial velocity. Because the pressure on the suction side of a blade is lower than on the pressure side which causes the air to flow around the tip from the lower to upper surface, reducing lift and hence power production near the tip.

A number of methods have been suggested for including the effect of tip losses. An approximate method of estimating the effect of this radial flow and hence including the effect of tip losses has been given by L.Prandtl. Prandtl tip loss model is generally recommended for the following reasons;

- Prandtl model prediction are in qualitative agreement with the behavior of HAWT rotors,
- Calculations of rotor power and thrust made with Prandtl model are in good agreement with test data,
- BEM theory calculations made with Prandtl model show good agreement with calculations made with vortex theory,
- The Prandtl model is easier to program and use

The expression obtained by Prandtl for tip-loss factor is given by the following equation [22];

$$F = (2/\mathrm{p})\cos^{-1}\left[\exp\left[\frac{-(B/2)[1-(r/2)]}{(r/R)\sin \mathrm{j}}\right]\right] \quad \text{.....4.2.1}$$

The application of this equation for the losses at the blade tips is to provide an approximate correction to the system of equations summarized in section 3.4.2 for predicting rotor performance and blade design.

The physical fact represented by the tip correction is virtually that the maximum decrease of axial velocity $(U_\infty - u_w)$ or $2aU_\infty$ in the slipstream occurs only on the vortex sheets and that the average decrease of axial velocity in the slipstream is only a fraction F of this velocity.

Thus, to order of approximation of the analysis the correct form of the axial momentum equation (equation 3.2.15) will be taken to be [2];

$$dT = 4F\rho U_{\infty}^{2} a(1-a)rdr \quad \text{.....4.2.2}$$

Similarly, also the angular momentum equation (equation 3.2.18) will be assumed to be [2];

$$dQ = 4F\rho U_{\infty}^{2} a'(1-a)r^{3}dr \quad \text{.....4.2.3}$$

Thus the effect of the tip-loss is to reduce slightly the thrust and torque contributed by the elements near the tips of the blades.

Equations derived in section 3.3 are all based on the definition of the forces used in blade element theory and remain unchanged. When the forces from the general momentum theory are set equal using the method of BEM theory as performed before, the derivation of the flow condition is changed.

Carrying the tip-loss factor through the calculations, the changes (through equations 3.4.4 to 3.4.9 and 3.4.14) will be as following;

$$\frac{a}{(1-a)} = (\sigma C_L)\frac{\cos\phi}{4F\sin^2\phi} \quad \text{.....4.2.4}$$

$$\frac{a'}{(1-a)} = \frac{(\sigma C_L)}{4\lambda_r F\sin\phi} \quad \text{.....4.2.5}$$

$$\frac{a'}{(1+a')} = \frac{(\sigma C_L)}{4F\cos\phi} \quad \text{.....4.2.6}$$

$$C_L = \frac{4F\sin\phi(\cos\phi - \lambda_r\sin\phi)}{\sigma(\sin\phi + \lambda_r\cos\phi)} \quad \text{.....4.2.7}$$

$$a = \frac{1}{\left[1+\left[4F\sigma\sin^2\phi/(\sigma C_L)\cos\phi\right]\right]} \quad \text{.....4.2.8}$$

$$a' = \frac{1}{\left[\left[4F\cos\phi/(\sigma C_L)\cos\phi\right]-1\right]} \quad \text{.....4.2.9}$$

$$C_p = \frac{8}{\lambda^2}\int_{\lambda_h}^{\lambda} F\sin^2(\phi)(\cos(\phi)-\lambda_r\sin(\phi))(\sin(\phi)+\lambda_r\cos^*(\phi))\left[1-(C_D/C_L)\cot(\phi)\right]\lambda_r^{2}d\lambda_r$$

.....4.2.10

Even though the tip-loss factor has been accounted for the development of the computer program of the blade design and power performance prediction in this thesis, for the purpose of simplifying the calculations without including the tip-loss factor, an effective-radius

of the rotor may be defined for the diminished thrust and torque output of the tip regions. This effective radius is generally taken as about 3% smaller than the tip radius. Note that from equation 4.2.1 it can be seen that F is always between 0 and 1 and in this empirical approach the following definition can be set;

F=1 if $0 < r < r_e$

F=0 if $r_e \le r \le R$

$r_e \approx 0.97R$

4.3 HAWT FLOW STATES

Measured wind turbine performance closely approximates the results of BEM theory at low values of the axial induction factors but general momentum theory is no longer valid at axial induction factors greater that 0.5, because according to the equation 3.1.10, the wind velocity in the far wake would be negative. In practice, as the axial induction factor increases above 0.5, the flow patterns through the wind turbine become much more complex than those predicted by the general momentum theory.

The thrust coefficient represented by the equation 3.1.14 can be used to characterize the different flow states of a rotor. Figure 4.1 shows flow states and thrust force vectors T associated with a wide range of axial induction factors.

According to this figure, for r negative induction factors $(a < 0)$ it is simple to continue the analysis to show that the device will act as a propeller producing an upwind force (i.e. $C_T < 0$) that adds energy to the wake. This is typical of the propeller state. The operating states relevant to HAWTs are designated by the windmill state and the turbulent wake state. The windmill state is the normal operating state. The windmill state is characterized by the flow conditions described by general momentum theory for axial induction factors less than about 0.5. As illustrated by the data in Figure 4.1 obtained on wind turbines, above a =0.5, rotor thrust increases up to 2 with increasing induction factor in the turbulent wake state, instead of decreasing as predicted by the equation 3.1.14. While general momentum theory no longer describes the turbine behavior, Glauert's empirical formula for axial induction factor from 0.4 to 1.0 are often used in HAWT rotor design for predicting wind turbine flow states.

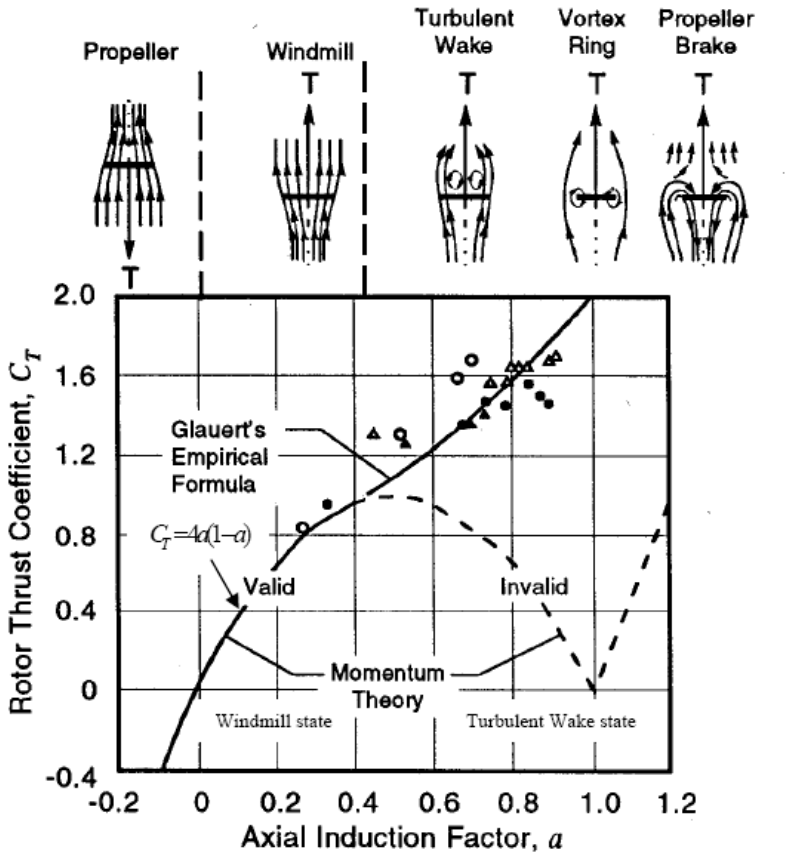

Figure 4.1 Relationship between the axial induction factor, flow state and thrust of a rotor [1]

When the induction somewhat over unity, the flow regime is called the vortex ring state and when a >2.0 the rotor reverses the direction of flow which is termed propeller brake state with power being added to flow to create downwind thrust on the rotor.

In the turbulent wake state, as stated before, a solution can be found by using the Glauert empirical relationship between the axial induction factor, a and the thrust coefficient, C_T in conjunction with the blade element theory. The empirical relationship developed by Glauert, including tip losses is [2];

$$a = (1/F)\left[0.143 + \sqrt{0.0203 - 0.6427(0.88 - C_T)}\right] \quad \text{……..……4.3.1}$$

This equation is valid for a > 0.4 or equivalently for $C_T > 0.96$

The Glauert empirical relationship was determined for the overall thrust coefficient for a rotor. It is customary, however, to assume that it applies equally to equivalently local thrust coefficients for each blade section. The local thrust coefficient C_{Tr} can be defined for each annular rotor section as;

$$C_{T_r} = \frac{dT}{1/2\,\rho U_\infty^{\,2} 2\pi dr} \quad \text{……..4.3.2}$$

From the equation 3.3.13 for the elemental thrust force from blade element theory, the local thrust coefficient becomes;

$$C_{T_r} = \sigma (1-a)^2 (C_L \cos\phi + C_D \sin\phi)/\sin^2\phi \quad \text{……..4.3.3}$$

In order to include the blade design and power performance prediction of highly loaded HAWTs which are operating at high tip-speed ratios, the Glauert empirical formula is used in the developing of the computer program. It firstly calculates the local thrust coefficient for each blade section according to the equation 4.3.3 and if $C_{Tr} < 0.96$ then uses the previously derived equations for the blade design. If $C_{Tr} > 0.96$ then it estimates axial induction factor using equation 4.3.1 and this new value of axial induction factor is used in the equations for the design.

4.4 AIRFOIL SELECTION IN HAWT BLADE DESIGN

HAWT blades use airfoils to develop mechanical power. The cross-sections of HAWT blades have the shape of airfoils. The width and length of the blade are functions of the desired aerodynamic performance, the maximum desired rotor power, the assumed airfoil parameters and strength calculations. Hence designing

HAWT blade depends on knowledge of the properties of airfoils. The most significant flow factor influencing the behavior of airfoils is that of viscosity which is characterized by the Reynolds number of the airfoil/fluid combination. The Reynolds number Re is defined by:

$$\mathrm{Re} = \frac{U_{rel} c}{\nu} \quad \text{……..4.4.1}$$

Airfoils in use on modern wind turbines range in representative chord size from about 0.3 m on a small-scale turbine over 2 m on a megawatt-scale rotor. Tip speeds typically range from approximately 45 to 90 m/s. Then for HAWT airfoils Reynolds number range from about 0.5 million to 10 million. This implies that turbine airfoils generally operate beyond sensitive.

It should be noted that there are significant differences in airfoil behavior at different Reynolds numbers. For that reason it must be made sure that appropriate Reynolds number data are available for the blade design.

The lift and drag characteristics of airfoils show also significant aspect-ratio dependence at angles of attack larger than 30 deg. But in the fully-attached region in which HAWT is

operating under windmill state are not greatly affected by aspect-ratio, so that two-dimensional (i.e. infinite aspect-ratio) data can be used in blade design at low angles of attack. However, when two-dimensional data are used, tip-loss factor must be added as described in equation 4.2.1.

In this thesis what has been considered in constructing the airfoil database from the computer program XFOIL which will be mentioned in the next chapter includes these considerations; two-dimensional data with Reynolds number in the order of 1 million.

There are evidently many engineering requirements into the selection of a wind turbine airfoil. These include primary requirements related to aerodynamic performance, structural, strength and stiffness, manufacturability and maintainability.

The usual assumption is that high lift and low drag are desirable for an airfoil and that the drag-to-lift ratio g which is known as glide ratio as given below is a critical consideration [23];

$$g = \frac{C_D}{C_L} \qquad \text{.....4.4.2}$$

Airfoils for HAWTs are often designed to be used at low angles of attack, where lift coefficients are fairly high and drag coefficients are fairly low(i.e. fairly low glide ratio). Many different standard airfoils developed for aircraft have been used on HAWTs. The NACA 230XX series and NACA44XX series airfoils have been used on many modern HAWT units. The NACA 63-2XX series airfoils have demonstrated the best overall performance characteristics of the NACA airfoil families.

The experienced gained from these traditional airfoils has highlighted the shortcomings of such airfoils for HAWT application. Consequently, a new airfoil family has been developed. The name SERI designates the classification of these airfoils of this family which is now being used on commercial HAWTs.

In this thesis, NACA4412 airfoil characteristics has been obtained and included in the airfoil database of the BLADE DESIGN program as an example.

4.5 BLADE DESIGN PROCEDURE

Designing a blade shape from a known airfoil type for an optimum rotor means determining the blade shape parameters; chord length distribution and twist distribution along the blade length for a certain tip-speed ratio at which the power coefficient of the rotor is maximum. Therefore first of all the change of the power coefficient of the rotor with respect to tip-speed ratio should be figured out in order to determine the design tip-speed ratio, λ_d corresponding to which the rotor has a maximum power coefficient. The blade design parameters will then be according to this design tip-speed ratio.

As it can be seen from the equation 4.2.10, the overall power coefficient, C_P depends on the relative wind angle (ϕ), local tip-speed ratio λ_r, the glide ratio ($\frac{C_D}{C_L}$) and the tip loss factor (F). To get maximum C_P value from this equation is only possible to make the elemental power coefficient maximum for each blade element. In other words, the term in the integral of the mentioned equation should be maximum for each blade element in order to get maximum overall power coefficient from the summation of each.

Since the airfoil type is selected before, the glide ratio included in this term can be chosen so as to it gets maximum value. This can be found from the two dimensional polar diagram of that airfoil. So the other variables left in the term are the relative wind angle and local tip-speed ratio because the variable, tip-loss factor depends also on these two variables for an assumed blade number as it can be seen from the equation 4.2.1. Hence a relationship can be established between the relative wind angle and local tip-speed ratio to determine the optimum relative wind angle, ϕ_{opt} for a certain local tip-speed ratio. The condition is given below;

$$\phi_{opt} \rightarrow MAX\left\{F \sin^2\phi\,(\cos\phi - \lambda_r \sin\phi)(\sin\phi + \lambda_r \cos\phi)[1-(C_D/C_L)\cot\phi\,]\right\}$$

When the optimum relative wind angle values are plotted with respect to the corresponding local tip-speed ratio values at which the elemental power coefficient is maximum for a wide range of glide ratios, the relationship has be found to be nearly independent of glide ratio and tip-loss factor. Hence the condition given before can be rearranged as following;

$$\phi_{opt} \approx MAX\left\{\sin^2\phi\,(\cos\phi - \lambda_r \sin\phi)(\sin\phi + \lambda_r \cos\phi)\right\}$$

Therefore a general relationship can be found between optimum relative wind angle and local tip-speed ratio which will be applicable for any airfoil type by taking the partial derivative of the term above, i.e.;

$$\frac{\partial}{\partial \varphi}\left\{\sin^2\varphi\,(\cos\varphi - \lambda_r \sin\varphi)(\sin\varphi + \lambda_r \cos\varphi)\right\} \ldots\ldots\ldots\ldots\ldots\ldots 4.5.1$$

Equation 4.5.1 reveals after some algebra [2];

$$\varphi_{opt} = (2/3)\tan^{-1}(1/\lambda_r) \ldots\ldots\ldots\ldots\ldots\ldots\ldots\ldots\ldots\ldots\ldots\ldots 4.5.2$$

Having found the solution of determining the optimum relative wind angle for a certain local tip-speed ratio, the rest is nothing but to apply the equations from equation 4.2.7 to 4.2.10, which were derived from the blade-element momentum theory and modified including the tip loss factor, to define the blade shape and to find out the maximum power coefficient for a selected airfoil type.

The procedure of blade design begins with dividing the blade length into N elements. The local tip-speed ratio for each blade element can then be calculated with the use of equation 2.5.2 and 3.2.17 as given below;

$$\lambda_{r,i} = \lambda\,(r_i / R) \ldots\ldots\ldots\ldots\ldots\ldots\ldots\ldots\ldots\ldots\ldots\ldots 4.5.3$$

Then according to equation 4.5.2 the optimum relative wind angle for each blade element is determined;

$$\varphi_{opt,i} = (2/3)\tan^{-1}(1/\lambda_{r,i}) \ldots\ldots\ldots\ldots\ldots\ldots\ldots\ldots\ldots\ldots\ldots\ldots 4.5.4$$

From the equation 4.2.1 the tip loss factor for each blade element is found;

$$F_i = (2/\pi)\cos^{-1}\left[\exp\left[\frac{-(B/2)[1-(r_i/2)]}{(r_i/R)\sin\varphi_{opt,i}}\right]\right] \ldots\ldots\ldots\ldots\ldots\ldots\ldots 4.5.5$$

The chord-length distribution can then be calculated for each blade element by using equation 4.2.7;

$$c_i = \frac{8\pi r_i F_i \sin\varphi_{opt,i}}{BC_{L,design}} \frac{(\cos\varphi_{opt,i} - \lambda_{r,i}\sin\varphi_{opt,i})}{(\sin\varphi_{opt,i} + \lambda_{r,i}\cos\varphi_{opt,i})} \ldots\ldots\ldots\ldots\ldots\ldots\ldots 4.5.6$$

Where, $C_{L,design}$, is chosen such that the glide ratio is minimum at each blade element. The twist distribution can be determined from the following equation which can be easily derived from the velocity diagram shown in Figure 3.8;

$$q_i = j_{opt,i} - a_{design} \quad \text{.....4.5.7}$$

Where, a_{design}, is again the design angle of attack at which $C_{L,design}$ is obtained

Finally, the power coefficient is determined using a sum approximating the integral in equation 4.2.10;

$$C_p = \sum_{i=1}^{N} \left[\left(\frac{8\Delta l_r}{l^2} \right) F_i \sin^2 j_{opt,i} (\cos j_{opt,i} - l_{r,i} \sin j_{opt,i}) ... \right.$$
$$\left. (\sin j_{opt,i} + l_{r,i} \cos j_{opt,i}) \left[1 - (C_D / C_L) \cot j_{opt,i} \right] l_{r,i}^2 \right] \quad \text{.....4.5.8}$$

As a result, for a selected airfoil type and for a specified tip-speed ratio and blade length (i.e. rotor radius), the blade shape can be designed for optimum rotor and from the calculation of power coefficient the maximum power that can be extracted from the wind can then be found for any average wind velocity.

4.6 RESULTS

In this chapter, design of a HAWT blade has been explained and the solution method shown via the equations derived from BEM theory. Tip-loss factor and drag effect have also been considered in these equations. The method of determining blade shape for optimum performance of a turbine has been developed, and finally power performance calculation methods have been established. And the airfoil NACA 4412 was used while performing these methods and illustrated with figures as an example.

In addition to these studies, the effect of some parameters relating to the blade design have also been investigated for the purpose of keeping in mind what should be considered while designing a blade shape for the best performance and the results are given with figures following this section.

As an example, the blade chord-length and twist distribution for an optimum three-bladed rotor at the design tip-speed ratio $\lambda_d = 9.8$ is tabulated in Table 4.1 for the airfoil NACA 4412 whose lift coefficient and drag coefficient values are taken at Re =1x10^6. In Figure 4.2 chord-length distribution with respect to radial location of each blade element both of which are normalized with blade radius is shown.

Figure 4.4 shows the maximum achievable power coefficients for a HAWT with 3 blades. It can be seen that the fewer the blades the lower the possible C_P at the same tip-speed ratio. For that reason most wind turbines use two or three blades and in general most two-bladed wind turbines use a higher tips peed ratio than most three-bladed wind turbines. Thus, there is little practical difference in the maximum achievable C_P value between typical two- and three bladed designs, assuming no drag. Moreover, the effect of the number of blades is negligible at high design tip-speed ratios.

Looking at the effect of glide ratio on maximum achievable power coefficients for a three-bladed rotor, there is clearly a significant reduction in maximum achievable power as the airfoil drag increases. It can be seen that it clearly benefits the blade designer to use or design airfoils with low glide ratio.

The variations in twist angle and chord-length along the blade for different tip speed ratios are shown in Figure 4.3 and Figure 4.2.

Radial thrust coefficient which is a measure of loading of rotor in the wind direction has also been calculated for the designed blade. Again normal (thrust) force and tangential force is also calculated for the designed blade and shown in Table 4.2

In Figure 4.4 and Figure 4.5, the views of blade elements of NACA 4412 airfoil for the designed blade are shown. As it can be seen from these figures, twist distribution of designed blade is not smooth. Figure 4.6 and Figure 4.7 show the blade elements of NACA 4412 in isometric view for the designed and modified blade.

Lastly, three-dimensional views of the designed and modified blade made from the airfoil NACA 4412 are illustrated in Figure 4.8, Figure 4.9 and Figure 4.10 for visualization.

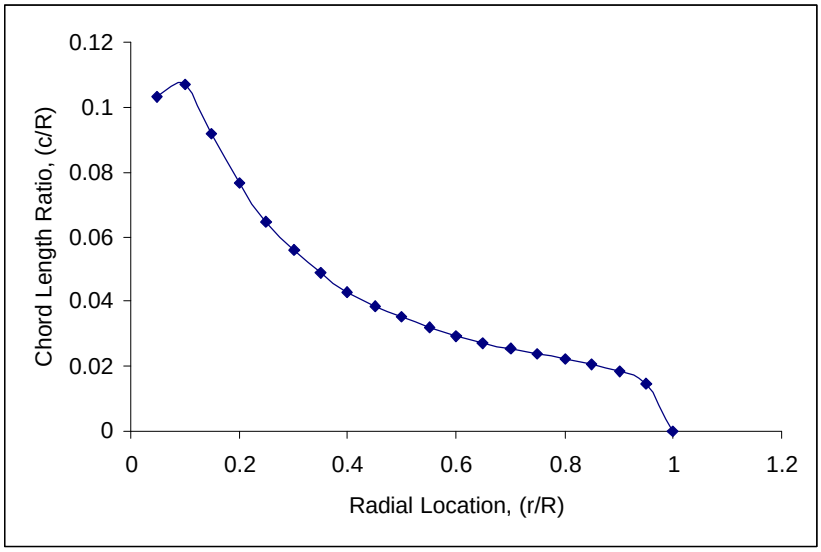

Figure 4.2 Chord-length distributions for the designed blade

Similarly twist distribution with respect to radial location is illustrated in Figure 4.3. Finally the power coefficient variation with respect to tip-speed ratio is given graphically in Figure 4.4. From this figure it can be seen that the design tip-speed ratio should be taken to as 9.8 where the power coefficient is at maximum value for the designed blade design.

Table 4.1 Blade Chord and Twist Distribution for a Three-Bladed HAWT
(Airfoil NACA 4412, $C_{L,design} = 1.074$ $a_{design} = 5.5^0$ $g = 0.0075$)

Radial location (r/R)	Chord-length ratio (c/R)	Twist angle • (deg)
0.05	0.1029119	37.09676399
0.1	0.10714652	24.88581704
0.15	0.09156339	17.31757454
0.2	0.0765285	12.52057351
0.25	0.06471749	9.302319021
0.3	0.05567643	7.023347008
0.35	0.0486787	5.33586003
0.4	0.04315736	4.040694175
0.45	0.03871421	3.017456938
0.5	0.03507337	2.189747102
0.55	0.03204155	1.507005574
0.6	0.02948045	0.934555645
0.65	0.02728802	0.447874681
0.7	0.02538446	0.029158231
0.75	0.02369765	-0.33481864
0.8	0.02213842	-0.65407672
0.85	0.02054043	-0.93634291
0.9	0.01849297	-1.18766828
0.95	0.0148069	-1.41285729
1	0	-1.61577198

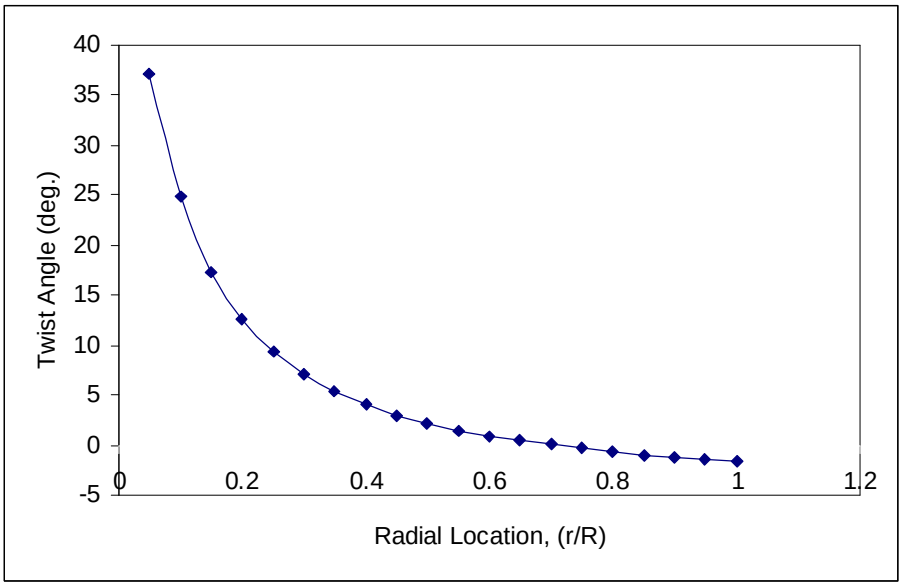

Figure 4.3 Twist distributions for the designed blade

Table 4.2. The variations normal (thrust) force and tangential force along the blade

Radial location (m)	Normal (thrust) force (N)	Tangential force(N)
0.039495	0.341713	0.309489
0.078989	0.744628	0.429151
0.118484	1.155334	0.475908
0.157979	1.564343	0.495964
0.197474	1.971117	0.505093
0.236968	2.376221	0.509142
0.276463	2.78016	0.510563
0.315958	3.18328	0.510505
0.355453	3.585808	0.509554
0.394947	3.987888	0.508033
0.434442	4.389583	0.506129
0.473937	4.790825	0.503946
0.513432	5.191204	0.501517
0.552926	5.589235	0.498772
0.592421	5.980015	0.495374
0.631916	6.347668	0.490233
0.671411	6.641209	0.480003
0.710905	6.69701	0.454516
0.7504	5.969695	0.381589
0.789895	0	0

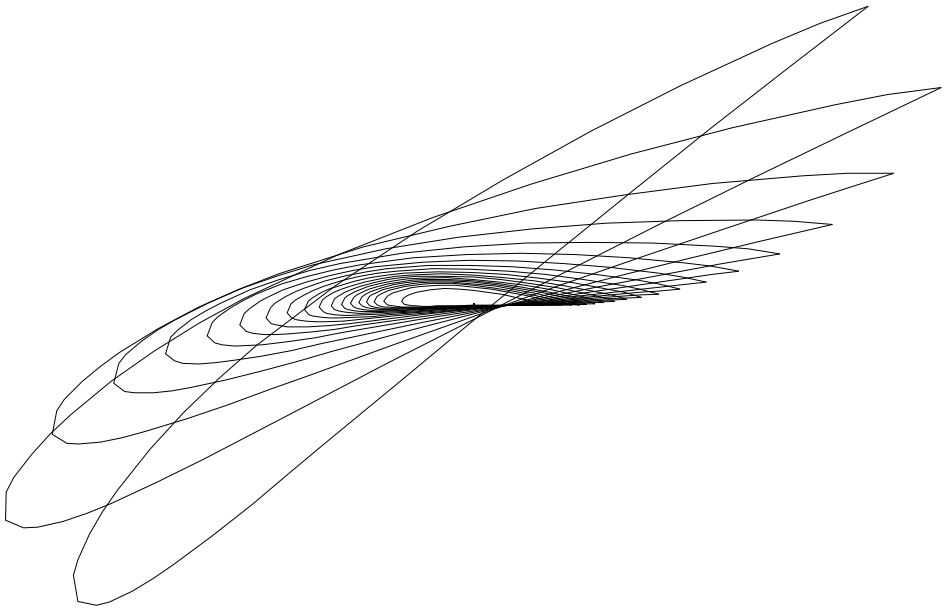

Figure 4.4 Views of blade elements from root towards tip

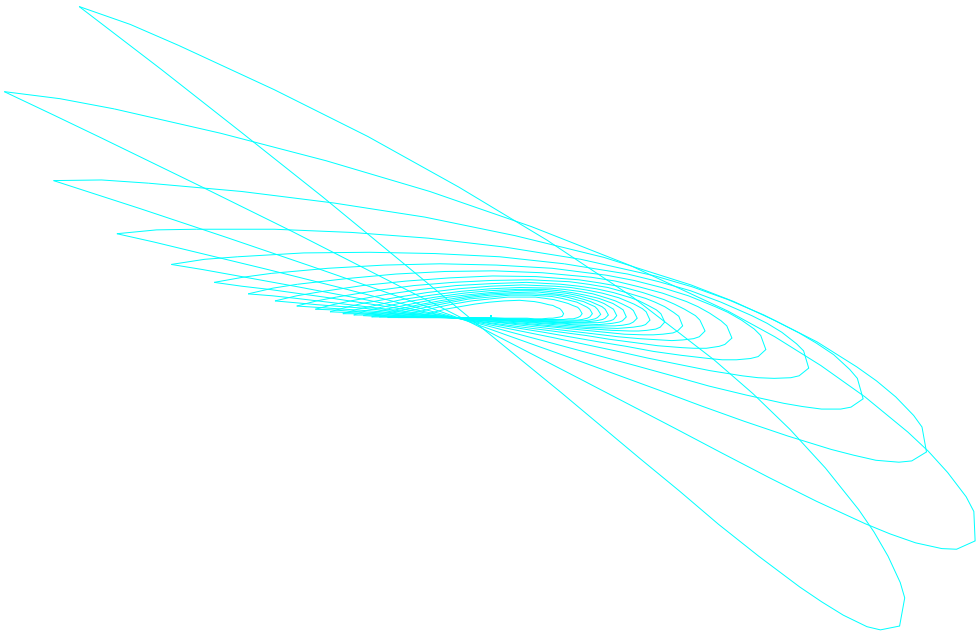

Figure 4.5 Views of blade elements from tip towards root

Figure 4.6 Isometric views of the blade elements

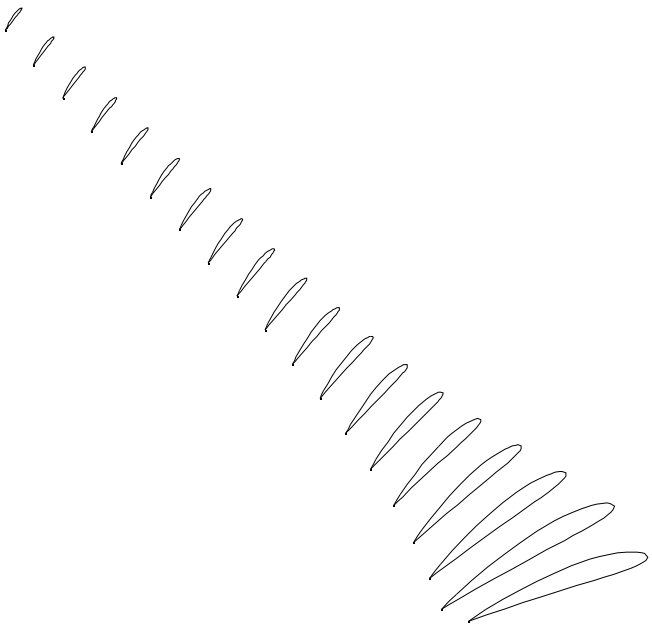

Figure 4.7 SE Isometric views of the blade elements

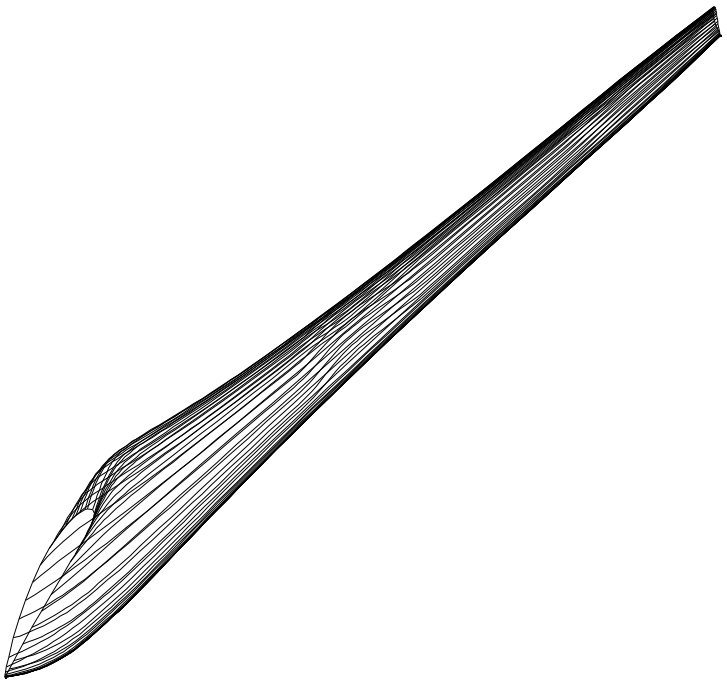

Figure 4.8 Three-dimensional wire frame model of the designed blade

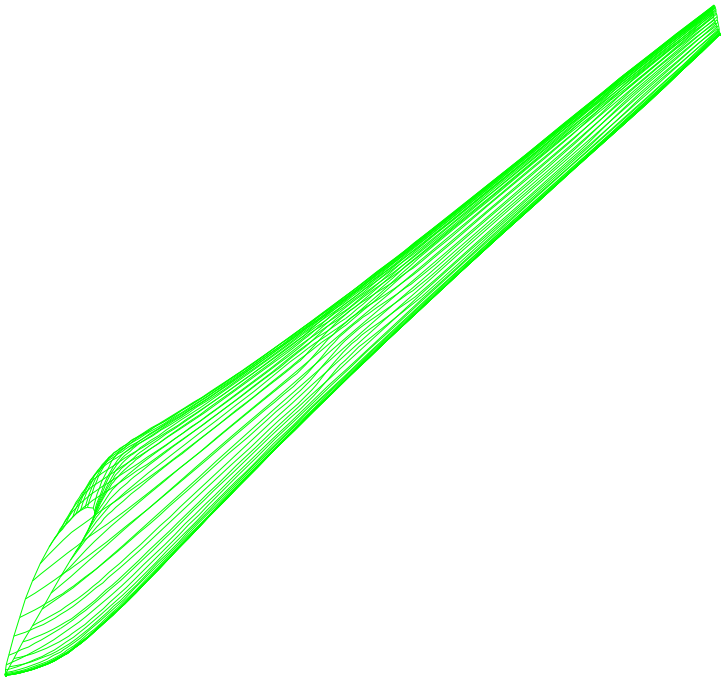

Figure 4.9 Three-dimensional solid model of the designed blade

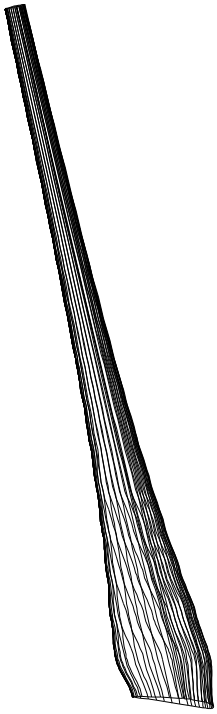

Figure 4.10 Three-dimensional solid model of the designed blade

CHAPTER 5

COMPUTER PROGRAM FOR BLADE DESIGN PROGRAM

5.1 INTRODUCTION

The computer programs XFOILP4 and VISUALBASIC are utilized during the study of this thesis. This chapter focuses on these programs, results from the programs and their applications in computer-aided design of horizontal-axis wind turbine blades.

XFOIL is firstly introduced by giving its capabilities on the analysis of an existing airfoil, design and redesign of new airfoil geometric parameters. Since the aerodynamic characteristics of an airfoil should be known numerically before designing a blade and all the information and experimental results performed on airfoils were given graphically in literature, XFOIL is very well fitted for obtaining lift coefficient and drag coefficient data with respect to angle of attack. In this thesis only the function of this program related to the viscous analysis of existing airfoils has been used. The required data are obtained from the program by performing on various existing airfoil types and used for the subsequent studies of blade design. The procedure to obtain the data is described and the results of the program are also compared with the results given in literature to show that the program XFOIL gives fairly close values.

User-interface computer program, BLADE DESIGN PROGRAM written by using visual basic is then described. General view and working flow chart of the program are presented with the explanation of important properties and capabilities of the program. All the commands and their functions in the program are also introduced for the users of this program.

Lastly sample blade design studies are given by specifying a set of input values. According to these input values, the program is executed and the corresponding outputs are illustrated in tabulated form and also compared with C_P & •, c/R & r/R and • & r/R figures for both designed and modified blades.

5.2 XFOILP4

XFOIL is an interactive program for the design and analysis of subsonic isolated airfoils. It consists of a collection of menu-driven routines which perform various useful functions such as:

- Viscous (or incviscid) analysis of an existing airfoil, allowing
    - Forced or free transition
    - Transitional separation bubbles
    - Limited trailing edge separation
    - Lift and drag predictions just beyond maximum lift coefficient
    - Karman-Tsien compressibility correction
- Airfoil design and redesign by interactive specification of a surface speed distribution via screen cursor or mouse. Two such facilities are implemented:
    - Full-Inverse, based on a complex-mapping formulation
    - Mixed-Inverse, allowing relatively
- Airfoil redesign by interactive specification of new geometric parameters such as:
    - New max. thickness and/or camber
    - New LE (leading edge) radius
    - New TE (trailing edge) thickness
    - New camberline via geometry specification
    - New camberline via loading change specification
    - Explicit contour geometry (via screen cursor)
- Drag polar calculation with fixed or varying Reynolds and/or Mach number
- Writing and reading of airfoil geometry and polar save files
- Plotting of geometry, pressure distribution and polars

XFOIL was written by Mark Drela in 1986 with the name XFOIL 1.0 and after undergoing numerous revisions, upgrades and enhancements it becomes now strongly geared to practical airfoil development with its final revision name XFOILP4. Further explanation about the use of XFOIL program can be found in reference [26], here only the part of XFOIL program which was extensively used for the development of blade design program will be described.

If it is remembered from the airfoil selection criteria in section 4.4, the design angle of attack should be selected such that the glide ratio is minimum at that value of angle of attack. Therefore the variation of lift coefficients and drag coefficients of an airfoil with respect to angle of attack in the fully-attached regime are required. XFOIL gives these data in a considerably excellent agreement with published polars as shown in Figure 5.1 and Figure 5.2 for the airfoil NACA 4412 as an example. The results of XFOIL has been compared with the reference polar data performed by Abbott and Von Doenhoff [25] and also from the reference Riegels [26] to see the validity of XFOIL results.

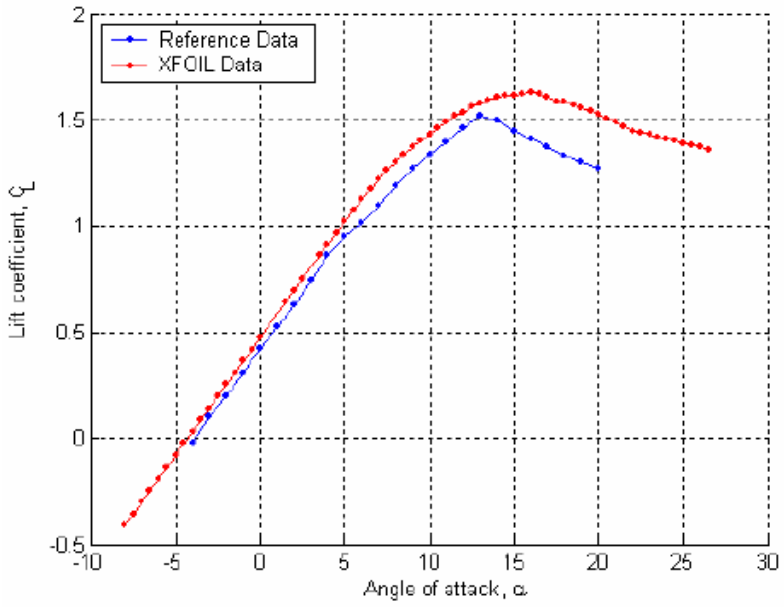

Figure 5.1 Comparison of XFOIL lift coefficient data with data in reference [26]

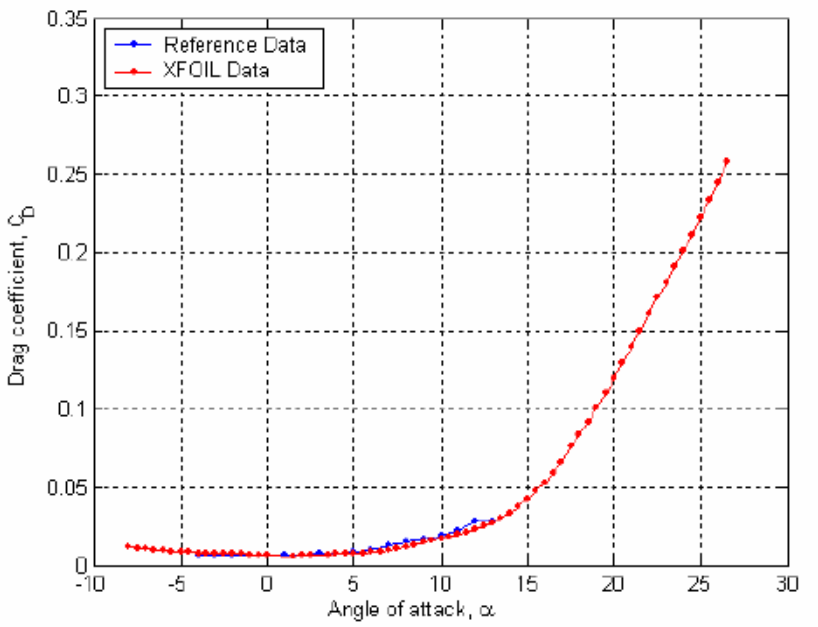

Figure 5.2 Comparison of XFOIL drag coefficient data with data in reference [26]

The results are obtained from the program by giving the coordinates of an airfoil. XFOIL first takes these coordinates and creates the contour geometry of the airfoil and finally by dividing the surface of the airfoil into a certain number of panels, which can be changed by the user, gives the variations of lift coefficient and drag coefficient with respect to angle of attack.

In developing the airfoil database for the blade design program, the characteristics of airfoil have been obtained with the viscous mode analysis of XFOIL and for the Reynolds number in the order of 1 million and also Mach number has been setted to zero considering that the angular velocity of a HAWT blades does not become so great that the rotational velocity of the blade tips approaches to the velocity of sound.

5.3 BLADE DESIGN PROGRAM

As it was stated before, the main objective of this thesis is to develop a user interface computer program on HAWT blade design. The main purpose of constructing such a program is to collect and represent all the studies of this thesis in a visual and more understandable way and also to provide a design program for the users who are dealing with HAWT blade design. For all of these reasons a user interface computer program on HAWT blade design was written.

The general view of the program and its working flow schematic are illustrated in Figure 5.3 and Figure 5.4 respectively. The main features of the program can be summarized as below:

- The program was written on VISUALBASIC.
- The program gives various error dialog boxes in case of incorrect input data or requesting an output of a command before this command some other commands should be executed firstly and necessary outputs for the requesting command should be firstly obtained. By so the program serves as a guide for the user to perform the design procedure step by step.
- The density of air, ρ is taken as 1.2 kg/m^3 in some algorithms of the program for the calculation of rotor diameter.
- The program includes one input part and four output parts.
- Input part requires the following information; turbine power required in Watt, design wind velocity in m/s, the number of blades supposed to be used on the rotor and airfoil type to be used for the blade profile. Here the design wind velocity is the average wind velocity of an area where the turbine or wind farm of similar turbines is to be set. NACA 4412 airfoils are currently available in the database.
- The output parts are composed of design condition output, blade geometry output, 3-D visualization output and figures output.

Design condition output part gives the information for designed blade. These information are design power coefficient (C_P), corresponding design tip-speed ratio (λ_d) and rotor diameter in meter to be constructed for the specified turbine power input.

Blade geometry output part shows the chord-length in meter and setting angle in degree for each blade element (for each station). The number of stations in the program has been kept constant with 20 because it has been seen that the increase of number of stations does not

change the blade geometry values considerably much. The purpose of putting this output part is that these output information can be used for the prototype production of the design blade in further studies.

3-D visualization output part gives three dimensional views of the designed blade on after exporting to AutoCAD or CATIA windows.

The last output part, figures output part illustrates the results with figures for both designed and modified blade. The first figure shows the variation of power coefficient with tip-speed ratio, the second one shows the output of chord-length distribution, which is normalized with R, with respect to again normalized blade length (r/R) graphically.

- § If it is desired to change the input values for another design, simply 'change inputs' in the input part and press the 'design' button.

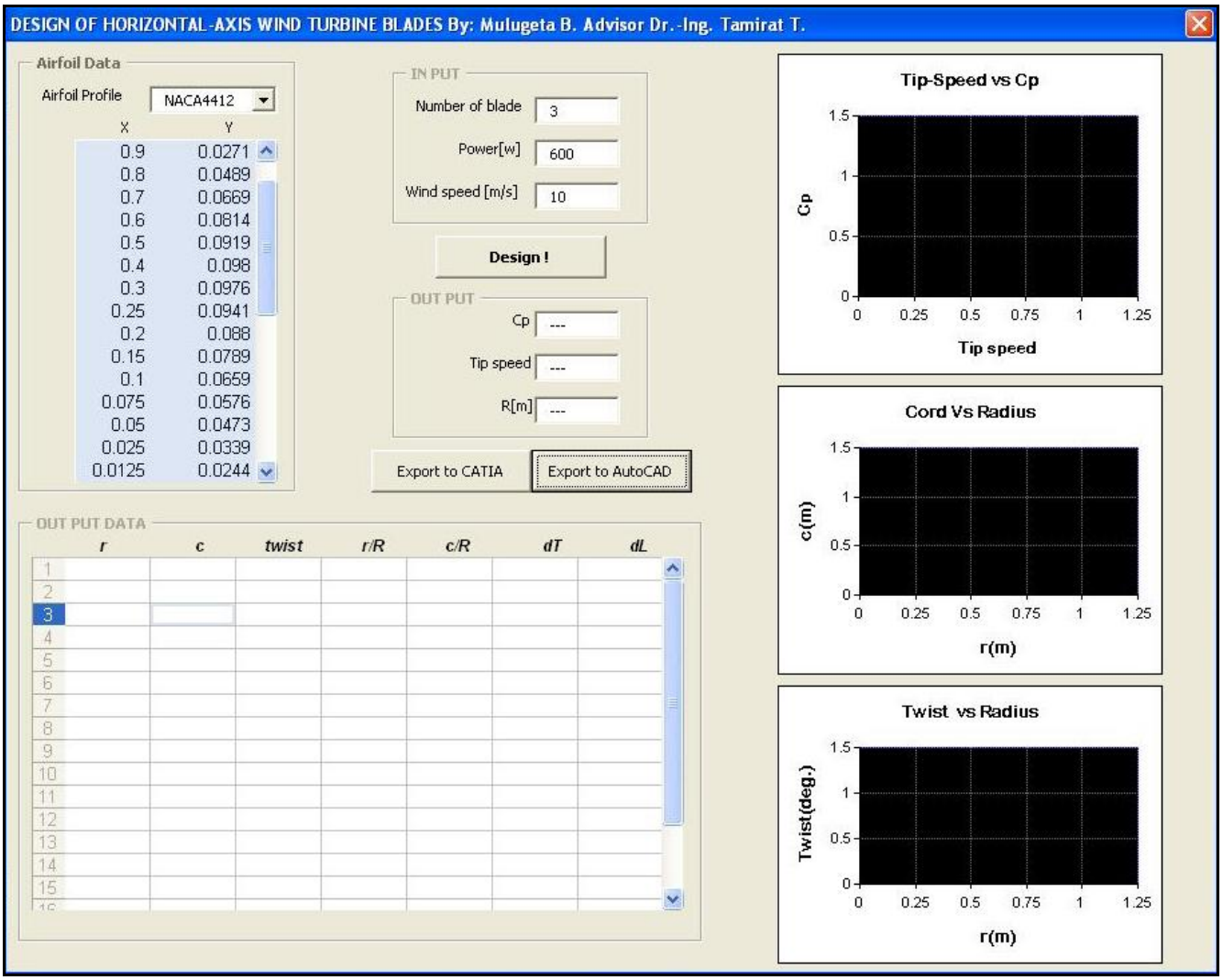

Figure 5.3 General view of BLADE DESIGN PROGRAM

5.4 SAMPLE BLADE DESIGN ON BLADE DESIGN PROGRAM

In this section a sample blade design will be demonstrated on blade design program according to the following inputs:

Turbine power required, P = 600W

Design wind velocity, U_∞ = 10 m/s

Number of blades, B = 3

Airfoil type = NACA 4412

First task is to find the design power coefficient which is dependent on the selected airfoil type. Then the design tip-speed ratio at which the maximum power coefficient (i.e. design power coefficient) can be obtained for the three-bladed rotor. This design tip-speed ratio can be used to determine the rotational velocity of the rotor at design condition. Finally rotor diameter is found out with the known values of design power coefficient and design wind velocity and required power. (Equation 2.5.1)

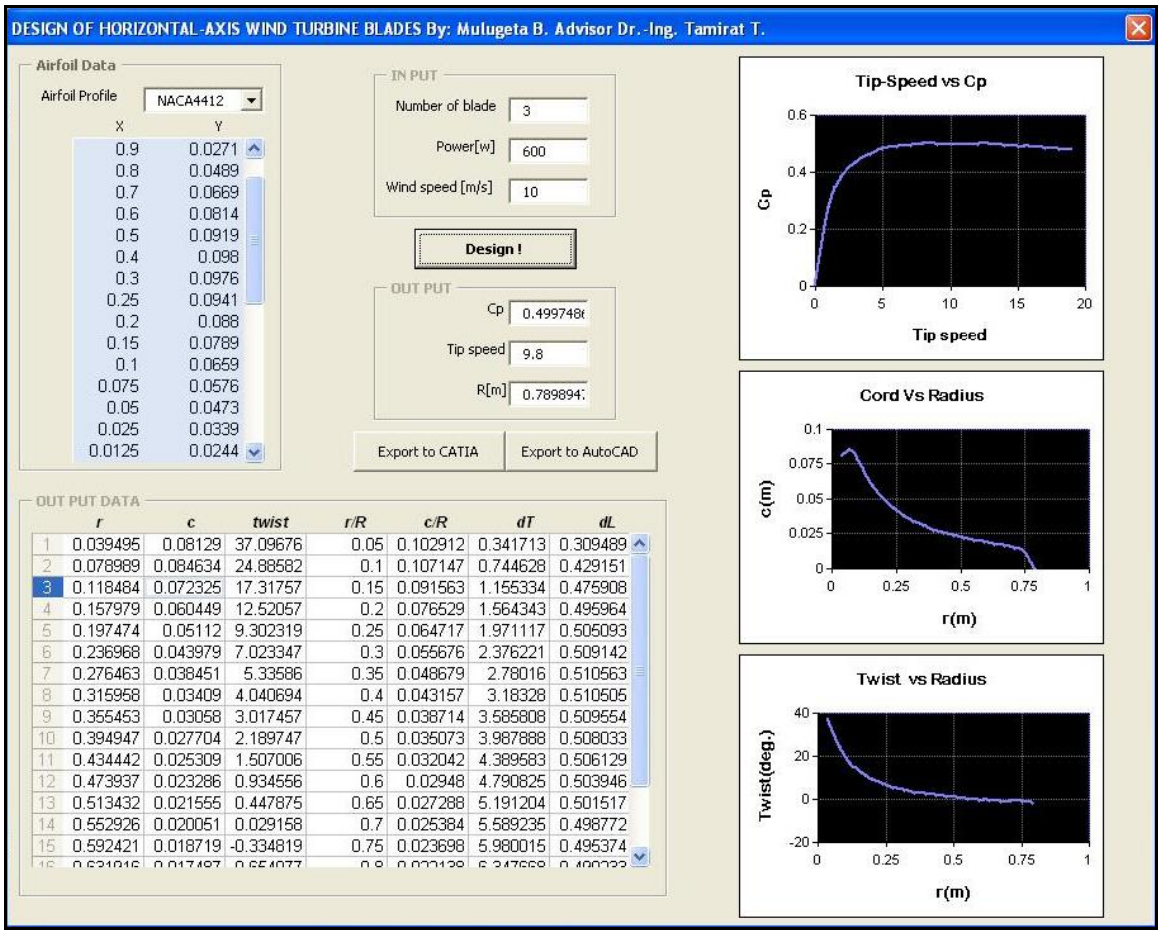

Figure 5.5 Output from the program performed for the sample blade design case (P= 600W, U_∞ = 10 m/s, B=3, NACA4412 airfoil)

CHAPTER 6

STRUCTURAL DESIGN OF HAWT BLADE

6.1 INTRODUCTION

Structural design of HAWT blades is as important as their aerodynamic design. The dynamic structural loads which a rotor will experience play the major role in determining the lifetime of the rotor. Obviously, aerodynamic loads are a major source of loading and must be well understood before the structural response can be accurately determined and also the blade geometry parameters are required for dynamic load analysis of wind turbine rotors. Such a study on the dynamic load analysis of HAWT blades might also use the outputs of BLADE DESIGN PROGRAM.

6.2 BASIS FOR DESIGN LOADS

6.2.1 Sources of loading

The sources of loading to be taken into account may be catagorized as follows:

- Aerodynamic loads,
- Gravitational loads,
- Inertia loads (including centrifugal and gyroscopic effects), and
- Operational loads arising from actions of the control system (e.g., braking, yawing, blade-pitch control, generator disconnection) [27].

6.2.2 Ultimate loads

The load cases selected for ultimate load design must cover realistic combinations of a wide range of external wind conditions and machine states. It is common practice to distinguish between normal and extreme wind conditions on the one hand, and between normal machine states and fault states on the other. The load cases for design are then chosen from:

- Normal wind conditions in combination with normal machine states,
- Normal wind conditions in combination with machine fault states, or
- Extreme wind conditions in combination with normal machine states.

Extreme and normal wind conditions are generally defined in terms of the worst condition occurring with a 50 year and 1 year return period respectively. It is assumed that machine fault states arise only rarely and are uncorrelated with extreme wind conditions, so that the occurrence of a machine fault in combination with an extreme wind condition is an event with such a high return period that it need not be considered as a load case. However, IEC

61400-1(Germanischer Lloyd's Regulation for the Certification of Wind Energy Conversion Systems) wisely stipulates that if there is some correlation between an extreme external condition and a fault state, then the combination should be considered as a design case [27].

6.2.3 Fatigue loads

A typical wind turbine is subjected to a severe fatigue loading regime. The rotor of a 600 kW machine will rotate some $2x10^8$ times during a 20 year life, with each revolution causing a complete gravity stress reversal in the low speed shaft and in each blade, together with a cycle of blade out-of-plane loading due to the combined effects of wind shear, yaw error, shaft tilt, tower shadow and turbulence.

The design fatigue load spectrum should be representative of the loading cycles experienced during power production over the full operational wind speed range, with the numbers of cycles weighted in accordance with the proportion of time spent generating at each wind speed. For completeness, load cycles occurring at start-up and shut-down and, if necessary, during shut-down, should also be included. It is generally assumed that the extreme load cases occur so rarely that they will not have a significant effect on fatigue life [27].

6.2.4 Partial safety factors for loads

Limit-state design requires the design load for a component to be calculated as the sum of the products of each characteristic load and the appropriate partial load factor. The partial safety factors for ultimate loads stipulated by IEC 61400-1. The IEC 61400-1 classifies load cases involving a machine fault as normal. IEC 61400-1 observes that in many cases, especially where varying loads result in dynamic load effects, the loads from various sources cannot be evaluated separately. In these situations, the standard requires the use of a single partial load factor equal to the highest of the factors for the relevant design situation. The partial safety factor for fatigue loads is taken as unity. For Unfavorable loads the aerodynamic and Inertia source of loading the partial factor of safety is 1.3 and 1.2 respectively and for Favorable loads it is 0.9 for both [27].

6.3 BLADE LOADS DURING OPERATION

6.3.1 Deterministic and stochastic load components

It is normal to separate out the loads due to the steady wind on the rotating blade from those due to wind speed fluctuations and analyse them in different ways. The periodic loading on the blade due to the steady spatial variation of wind speed over the rotor swept area is termed the deterministic load component, because it is uniquely determined by a

limited number of parameters – i.e., the hub-height wind speed, the rotational speed, the wind shear, etc. On the other hand, the random loading on the blade due to wind speed fluctuations (i.e., turbulence) has to be described probabilistically, and is therefore termed the stochastic load component. In addition to wind loading, the rotating blade is also acted on by gravity and inertial loadings. The gravity loading depends simply on blade azimuth and mass distribution, and is thus deterministic, but the inertial loadings may be affected by turbulence – as, for example, in the case of a teetering rotor – and so will sometimes contain stochastic as well as deterministic components [27].

6.3.2 Deterministic Aerodynamic Loads

Steady, uniform flow perpendicular to plane of rotor

The application of momentum theory to a blade element, which is described in Section 3.5.3, enables the aerodynamic forces on the blade to be calculated at different radii. Equations (3.4.1) and (3.4.2) are solved iteratively for the flow induction factors, a and a', at each radius, enabling the flow angle, the angle of attack, and hence the lift and drag coefficients to be determined. The solution of the equations is normally simplified by omitting the C_D term in Equation (3.4.1) – an approximation which is justified, because C_D/C_L is negligibly small away from the root area [27]. For loadings on the outboard portion of the blade, allowance for tip loss must be made, so Equations (3.4.1) and (3.4.2) are replaced by Equations (3.4.4) and (3.4.5) in Section 3.5, (with the omission of the C_D term in Equation (3.4.1) again being permissible). These equations can be arranged to give the following expressions for the forces per unit length on an element perpendicular to the plane of rotation and in the direction of blade motion, known as the out-of-plane (normal or trust) and in-plane (tangential) forces respectively:

Out-of-plane (normal or trust) force per unit length:

$$dT = dF_L \cos \mathrm{j} + dF_D \sin \mathrm{j} \quad \text{……..…6.1(a)}$$

In-plane (tangential) force per unit length:

$$dL = dF_L \sin \mathrm{j} - dF_D \cos \mathrm{j} \quad \text{……6.2 (a)}$$

Alternatively, out-of-plane force per unit length can be described as:

$$dT = (\cos \mathrm{j} * 0.5 * C_L * \mathrm{r} * U_{rel}{}^2)cdr + (\sin \mathrm{j} * 0.5 C_D * \mathrm{r} * U_{rel}{}^2)cdr \quad \text{……6.1(b)}$$

Similarly, In-plane force per unit length can be described as:

$$dL = (\sin \text{j} * 0.5 * C_L * \text{r} * U_{rel}^{\ 2})cdr - (\cos \text{j} * 0.5 C_D * \text{r} * U_{rel}^{\ 2})cdr \quad \ldots\ldots\ldots 6.2 \text{ (b)}$$

The variation of the in-plane and out-of-plane forces with radius is shown in Figure 6.1 for a typical machine operating in a steady 10 m/s wind speed.

It is evident that the out-of-plane load per unit length increases approximately linearly with radius, in spite of the reducing blade chord until the effects of tip loss are felt beyond about 75 percent of tip radius. Integration of these forces along the blade then yields in-plane and out-of-plane aerodynamic blade bending moments.

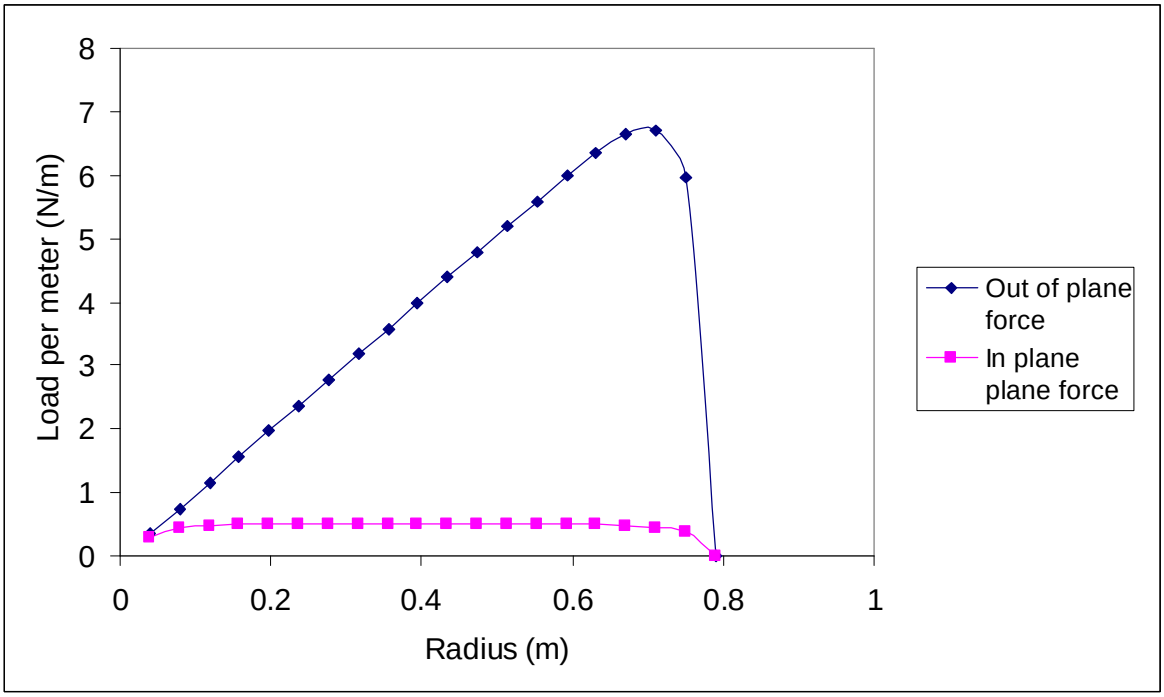

Figure 6.1 Distribution of Blade In-plane and Out-of-plane Aerodynamic Loads during Operation of Typical 1.6 m Diameter in a Steady, Uniform 10 m/s Wind

6.3.3 Gravity loads

Gravity loading on the blade results in a sinusoidally varying edgewise bending moment which reaches a maximum when the blade is horizontal, and which changes sign from one horizontal position to the other. It is thus a major source of fatigue loading. The maximum gravity moment is:

$$W = \int_0^R m(r) r dr \quad \ldots\ldots\ldots 6.3$$

6.3.4 Deterministic inertia loads

Centrifugal loads

For a rigid blade rotating with its axis perpendicular to the axis of rotation, the centrifugal forces generate a simple tensile load in the blade which at radius r^* is given by the expression $\Omega^2 \int_{r^*}^{R} m(r) r dr$. As a result, the fluctuating stresses in the blade arising from all loading sources always have a tensile bias during operation. Thrust loading causes flexible blades to deflect downwind, with the result that the centrifugal forces generate blade out-of-plane moments in opposition to those due to the thrust. This reduction of the moment due to thrust loading is known as centrifugal relief. The phenomenon is non-linear, so iterative techniques are required to arrive at a solution. Greater centrifugal relief can be obtained by coning the rotor so that the blades are inclined downwind in the first place. A balance can be struck so that the maximum forward out-of-plane moment due to centrifugal loads in very low wind is approximately equal to the maximum rearward out-of plane moment due to the thrust loading in combination with centrifugal loads during operation in rated wind [27].

Gyroscopic loads

When an operating machine yaws, the blades experience gyroscopic loads perpendicular to the plane of rotation.

Braking loads

Rotor deceleration due to mechanical braking introduces edgewise blade bending moments which are additive to the gravity moments on a descending blade.

Teeter loads

Blade out-of-plane root bending moments can be eliminated entirely by mounting each blade on a hinge so that it is free to rotate in the fore–aft direction. Although centrifugal forces are effective in controlling the cone angle of each blade at normal operating speeds, the need for alternative restraints during start-up and shut-down means that such hinges are rarely used. However, in the case of two bladed machines, it is convenient to mount the whole rotor on a single shaft hinge allowing fore–aft rotation or 'teetering', and this arrangement is frequently adopted in order to reduce out-of-plane bending moment fluctuations at the blade root, and to prevent the transmission of blade out-of-plane moments to the low speed shaft.

6.3.5 Stochastic aerodynamic loads – analysis in the frequency domain

The random loadings on the blade due to short-term wind speed fluctuations are known as stochastic aerodynamic loads. The wind speed fluctuations about the mean at a fixed point in space are characterized by a probability distribution – which, for most purposes, can be assumed to be normal –and by a power spectrum which describes how the energy of the fluctuations is distributed between different frequencies.

6.4. BLADE MATERIAL

The blades are designed and constructed to carry loads resulting from normal operation, gust, or turbulence, which induce major alternating stresses, and therefore the material used must be capable of resisting fatigue. Modern wind turbine blades are commonly constructed from some form of composite material. A composite material is formed from two or more discrete component materials, which in combined has different, ideally improved properties than exhibited individually. The most commonly used types of composite material in the wind turbine industry are glass fiber-reinforced plastics (GRP). GRP dominates the market because it provides the necessary properties at a low cost. The important characteristics of GRP are good mechanical properties, good corrosion resistance, high temperature tolerance, ease of manufacture, and favorable cost. More importantly, composite materials enable structures to be designed to provide significant advantages such as weight reduction, over traditional engineering materials, whilst maintaining the required levels of performance and reliability [28].

The ideal material for blade construction will combine the necessary structural properties namely high strength to weight ratio, fatigue life and stiffness – with low cost and the ability to be formed into the desired aerofoil shape [27]. For comparative purposes, values are also presented of:

- § compressive strength-to-weight ratio,
- § fatigue strength as a percentage of compressive strength,
- § stiffness-to-weight ratio,

It is evident that glass- and carbon-fiber composites (GFRP and CFRP) have a substantially higher compressive strength-to-weight ratio compared with the other materials. However, this apparent advantage is not as decisive as it appears, for example the relatively low Young's modulus of these composites means that resistance to buckling of the thin skins governs the design rather than simple compression yielding.

With similar reason as well stated before the material Glass/epoxy with 50% fiber volume fraction and unidirectional fibers (all fibers running longitudinally) lay-up material is selected, and its structural properties are:

Ultimate tensile strength (UTS) =860-900MPa,

Ultimate compressive strength (UCS) =720Mpa

Specific Gravity=1.85, Young's Modulus, E=38GPa [27].

6.5 LOAD CONDITIONS

The blade is modeled as a cantilever as shown below. The loads on the blade in this case are the drag and gravity. Look at the fig.6.2 below to see these loads

To simplify the design of wind mill structures, it is well to understand the loads which try to break apart these machines. These loads are centrifugal force and blade bending. There are others, but lesser important.

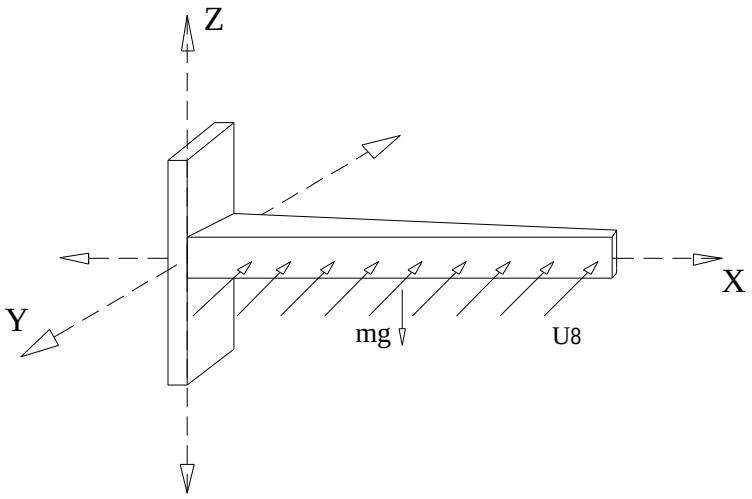

Fig.6.2 (a) Blade with fixed at one end and uniformly distributed wind load

A structural analysis was then carried out using a cantilever beam analysis, with the help of CATIA V5 R16 Finite Element Software.

From BLADE DESINE PROGRAM the aerodynamic forces are calculated as follows:

The total trust Force on the single blade is:

$$dT = (\cos \mathrm{j} * 0.5 * C_L * \mathrm{r} * U_{rel}^{\ 2})cdr + (\sin \mathrm{j} * 0.5 C_D * \mathrm{r} * U_{rel}^{\ 2})cdr$$ Summing up the elemental trust forces along the blade from BLADE DESINE PROGRAM gives the total trust on the blade

$$T = 73.28649N$$

The total tangential on the single blade is:

$dL = (\sin \mathrm{j} * 0.5 * C_L * \mathrm{r} * U_{rel}{}^2)cdr - (\cos \mathrm{j} * 0.5 C_D * \mathrm{r} * U_{rel}{}^2)cdr$ Summing up the elemental tangential forces along the blade from BLADE DESINE PROGRAM give the total trust on the blade

$$L = 9.075481N$$

6.6 FEM ANALYSIS

A solid FEA model of a twisted blade experiencing a combined load is created. Since there is no planes of symmetry exist and therefore model simplifications cannot be made. This model is handled with solid elements. There are two main types of solid elements available in CATIA V5, linear and parabolic. Both are referred to as tetrahedron elements and shown below.

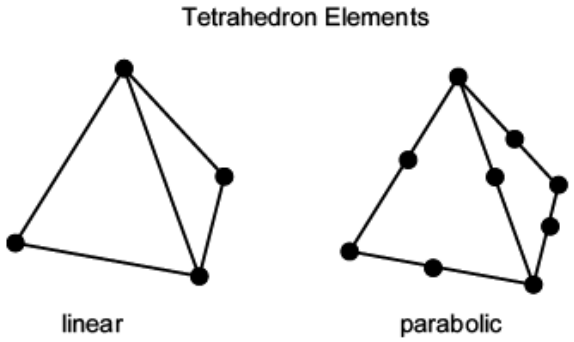

Fig.6.2 (b) Mesh elements

The linear tetrahedron elements are faster computationally but less accurate. On the other hand, the parabolic elements require more computational resources but lead to more accurate results. Another important feature of parabolic elements is that they can fit curved surfaces better. In general, the analysis of bulky objects requires the use of solid elements. In our case the analysis is done with linear tetrahedron element in catia and solid 185 element in ansys. It is used for the 3-D modeling of solid structures. It is defined by eight nodes having three degrees of freedom at each node: translations in the nodal x, y, and z directions. It also has mixed formulation capability for simulating deformations of nearly incompressible elastoplastic materials, and fully incompressible hyper elastic materials.

Creation of the solid Part is achieved after exported form the BLADE DESIGN PROGRAM to CATIA or AutoCAD and lofted to make the blade elements solid. Selecting the proper material in CATIA material library and applying a trust load of 75N or 2,344 Pa in the positive y-axis direction, CATIA and ansys will perform the detail FEM analysis.

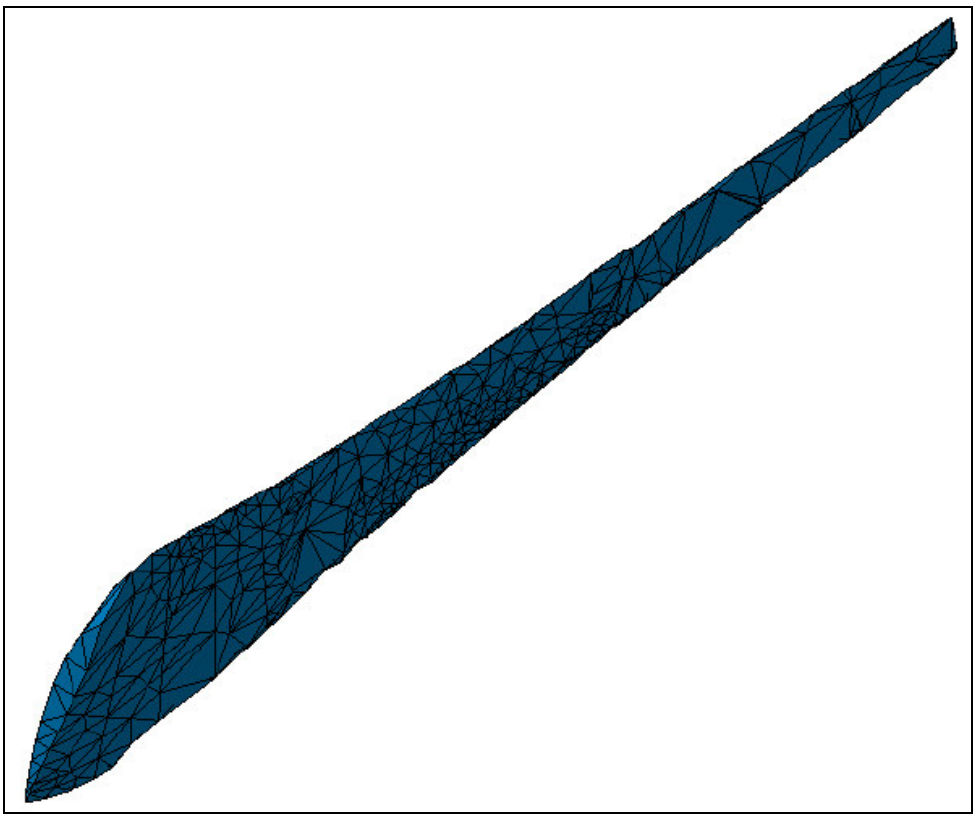

Fig. 6.3 (a) The generated mesh in CATIA with the correct material property

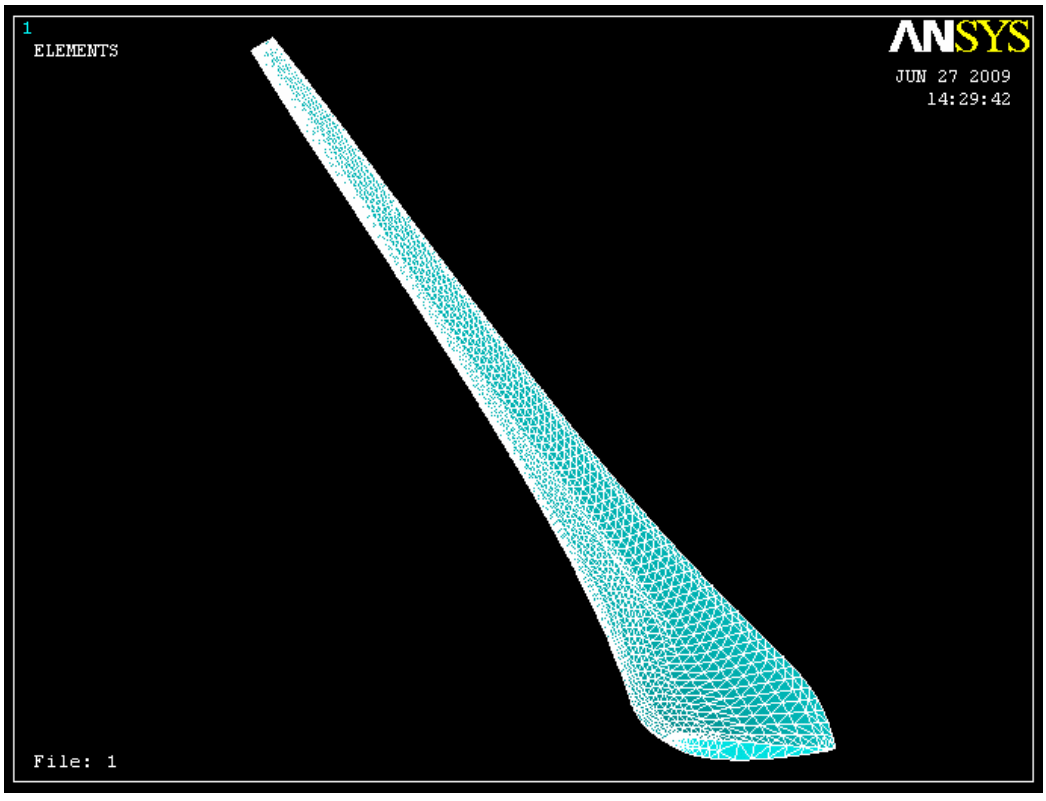

Fig. 6.3 (b) The generated mesh in ANSYS with the correct material property

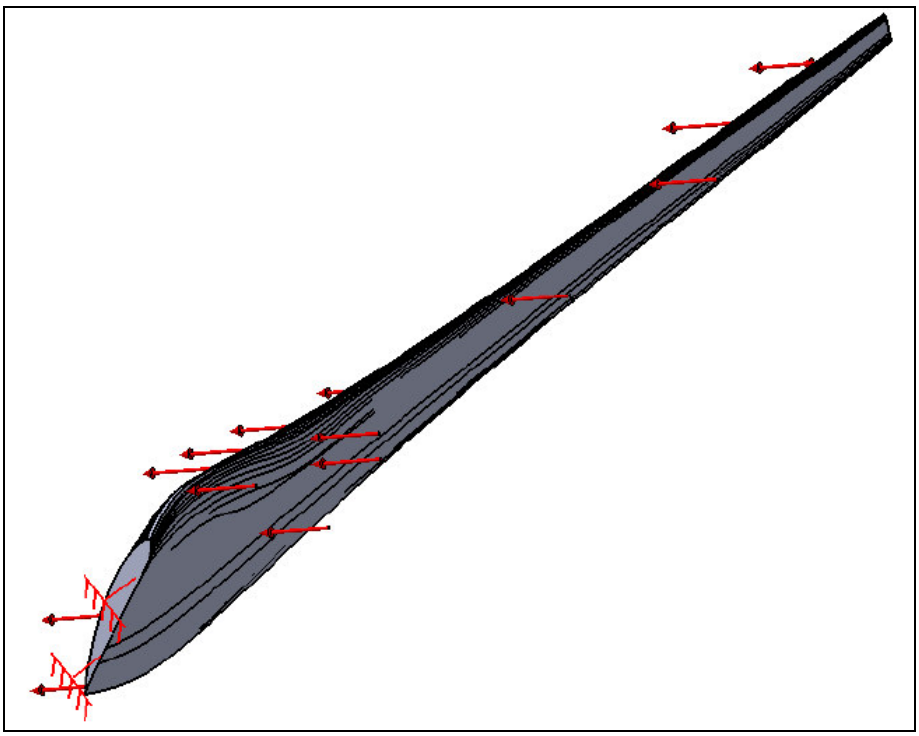

Fig. 6.4 Blade with load and displacement boundary condition in CATIA

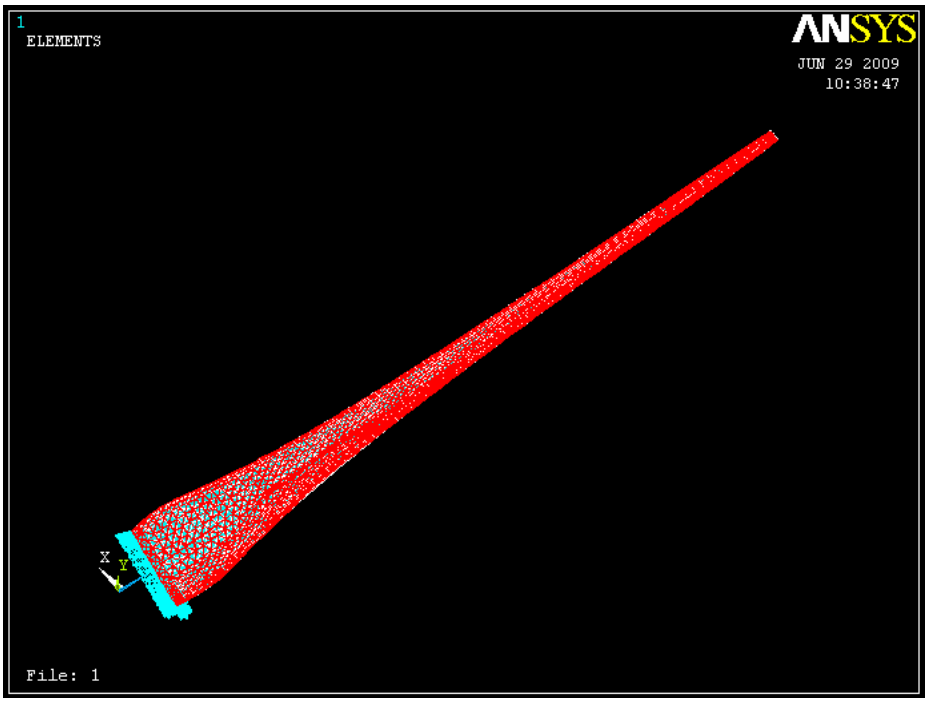

Fig. 6.5 Blade with load and displacement boundary condition in ANSYS

In the above figure, you can see that the blade is clamped. The Clamp condition means that the displacements in all three directions are zero. The Distributed trust force of 75N or a pressure of 2,344Pa is applied in the positive y-direction. It is possible to apply forces in the local direction specified by the user. Upon selection of the appropriate face, the force symbols will appear as shown above. After applying all the displacement and load boundary conditions and computing, the analysis can be run.

The resulting deformed shape is displayed below. The deformation image can be very deceiving because one could have the impression that the blade actually displaces to that extent. Keep in mind that the displacements are scaled considerably so that one can observe the deformed shape. Although the scale factor is set automatically, one can easily change this value.

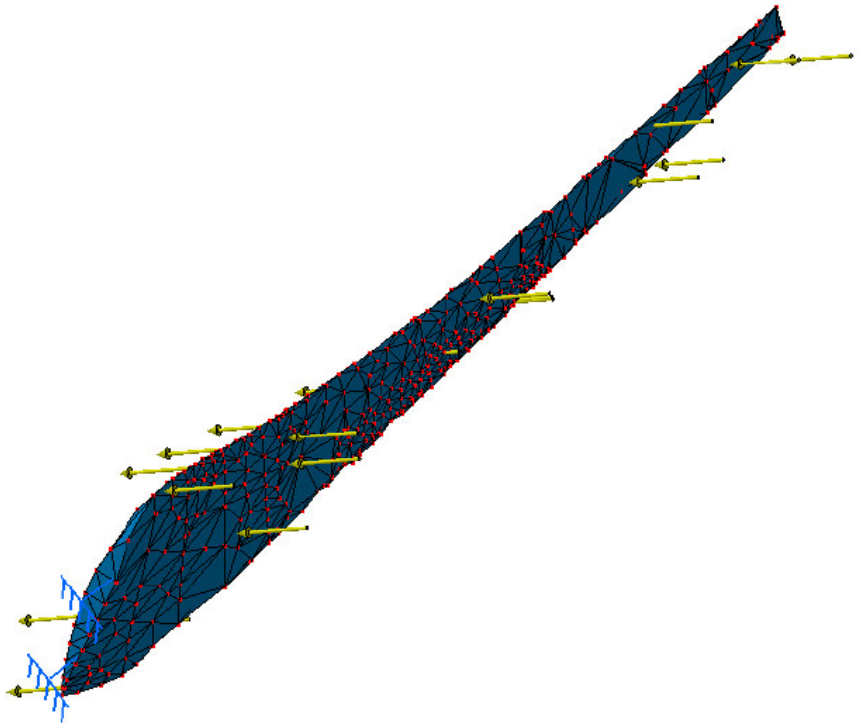

Fig. 6.6 Deformed Blade in CATIA

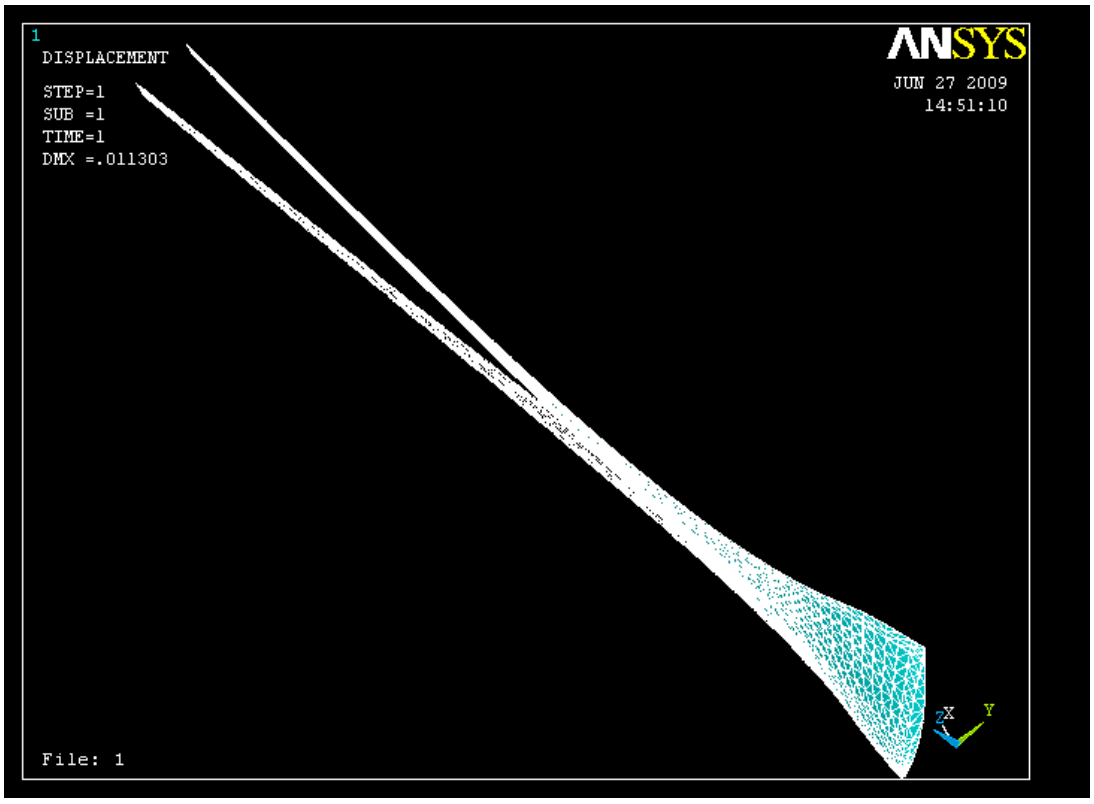

Fig. 6.7 Displaced and undisplaced Blade in ANSYS

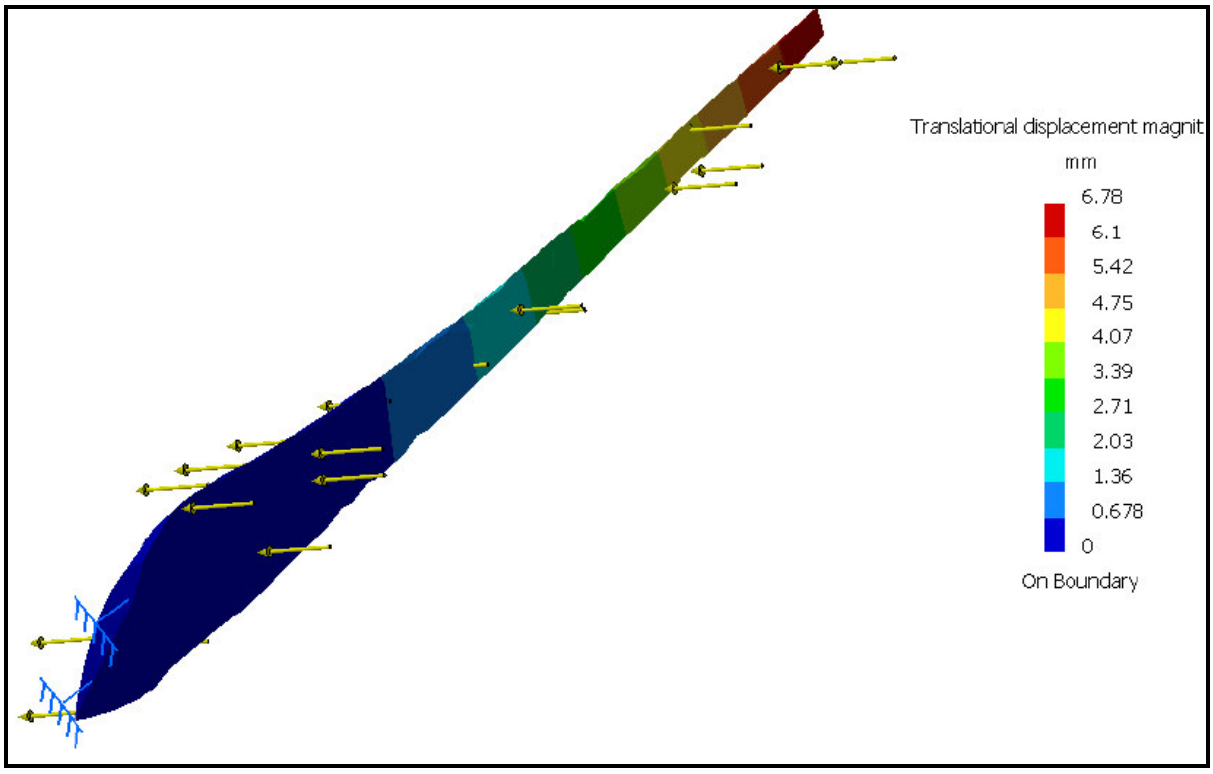

Fig. 6.8 (a) The contour plot of the displacement field in CATIA

The contour legend indicates a maximum displacement of 6.78mm in catia and 11mm in ansys.

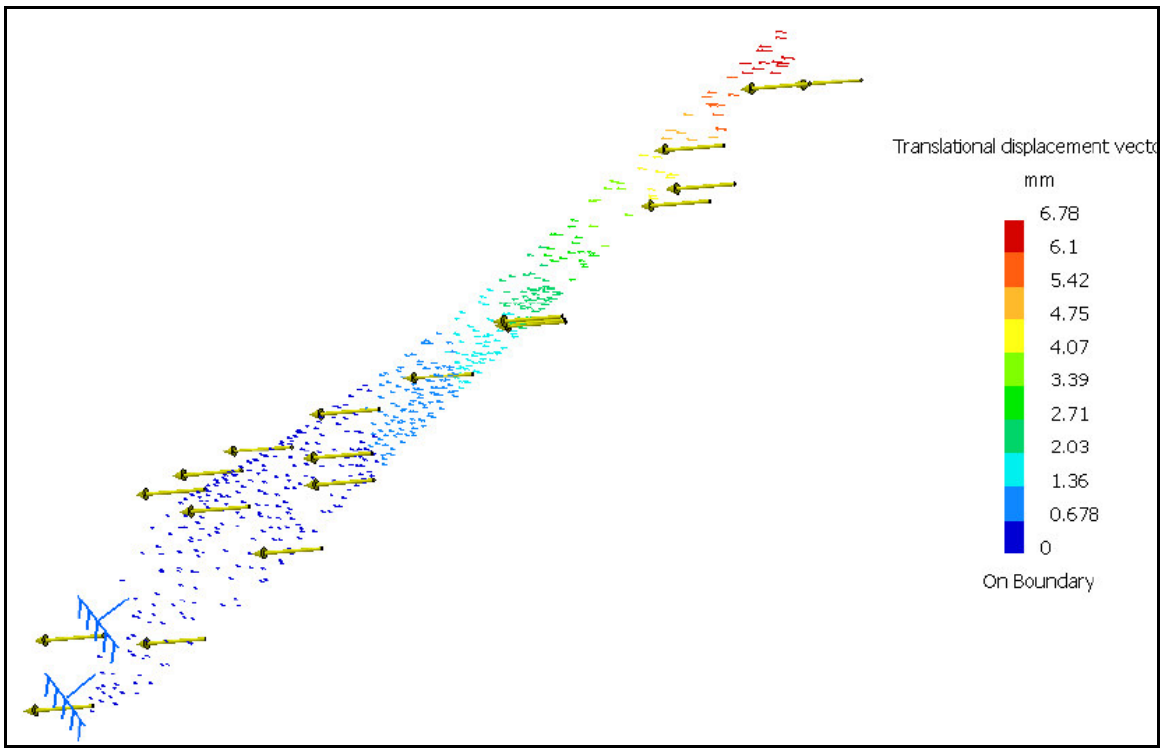

Fig. 6.8 (b) The vector plot of the displacement field in CATIA

The color and the length of arrows represent the size of the displacement. Clearly, the maximum displacement is at the tip of the blade, in the positive y-direction as expected.

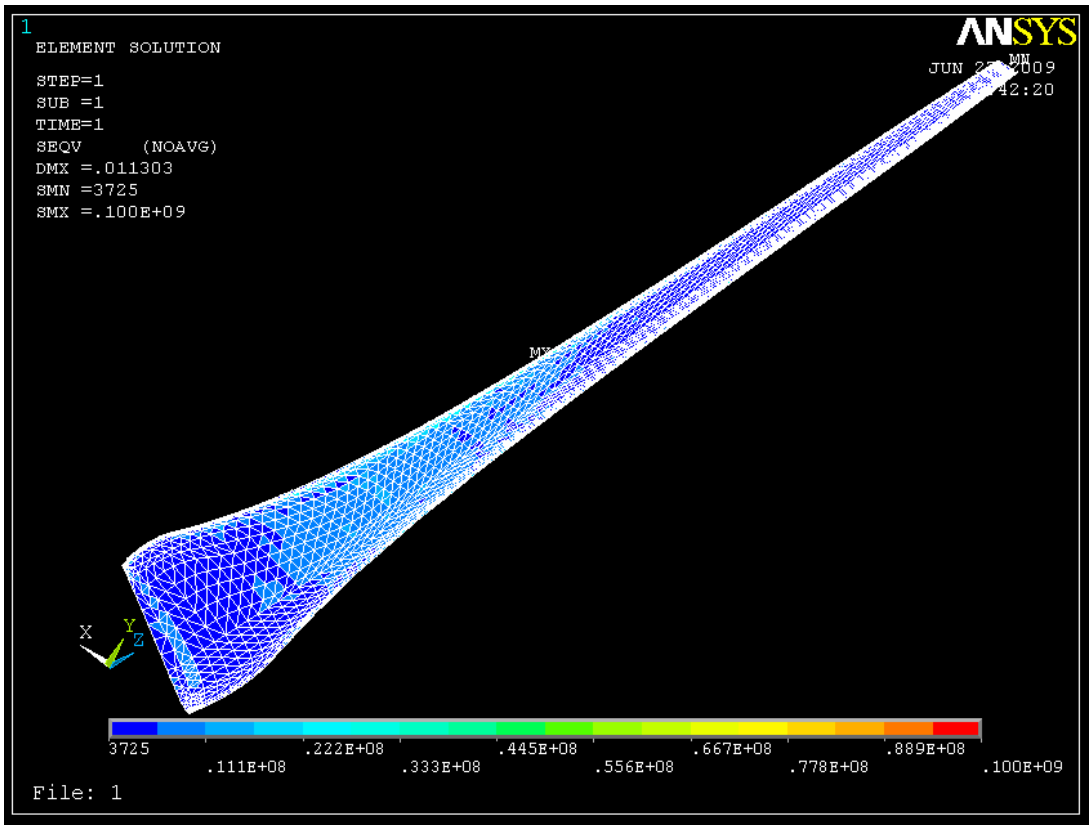

Fig. 6.9 The contour plot of the elemental Von Mises stress in ANSYS

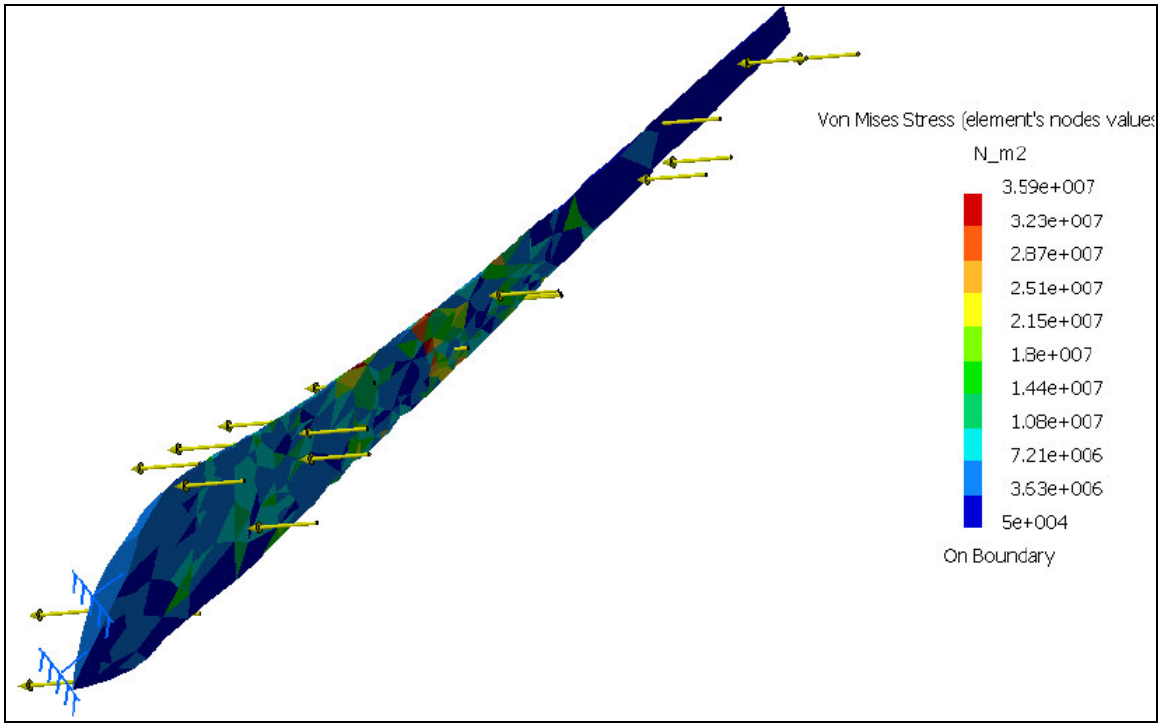

Fig. 6.10 The contour plot of the elemental Von Mises stress in CATIA

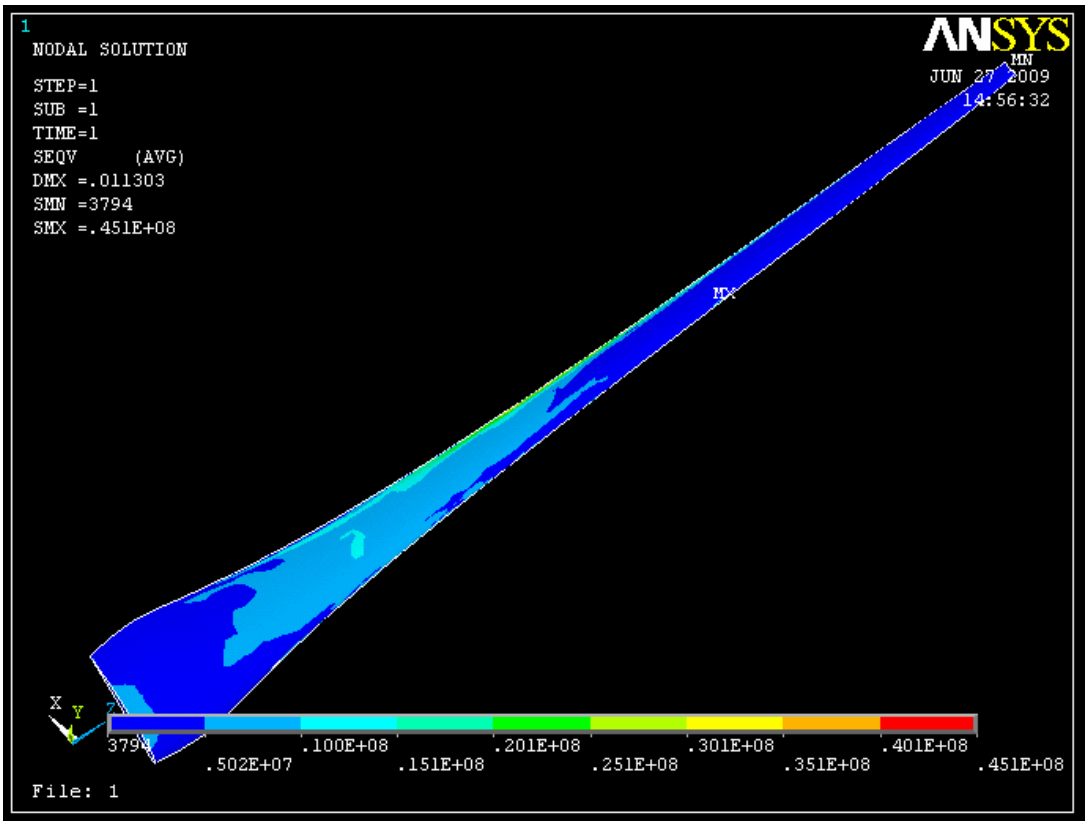

Fig. 6.11 The contour plot of the nodal Von Mises stress in ANSYS

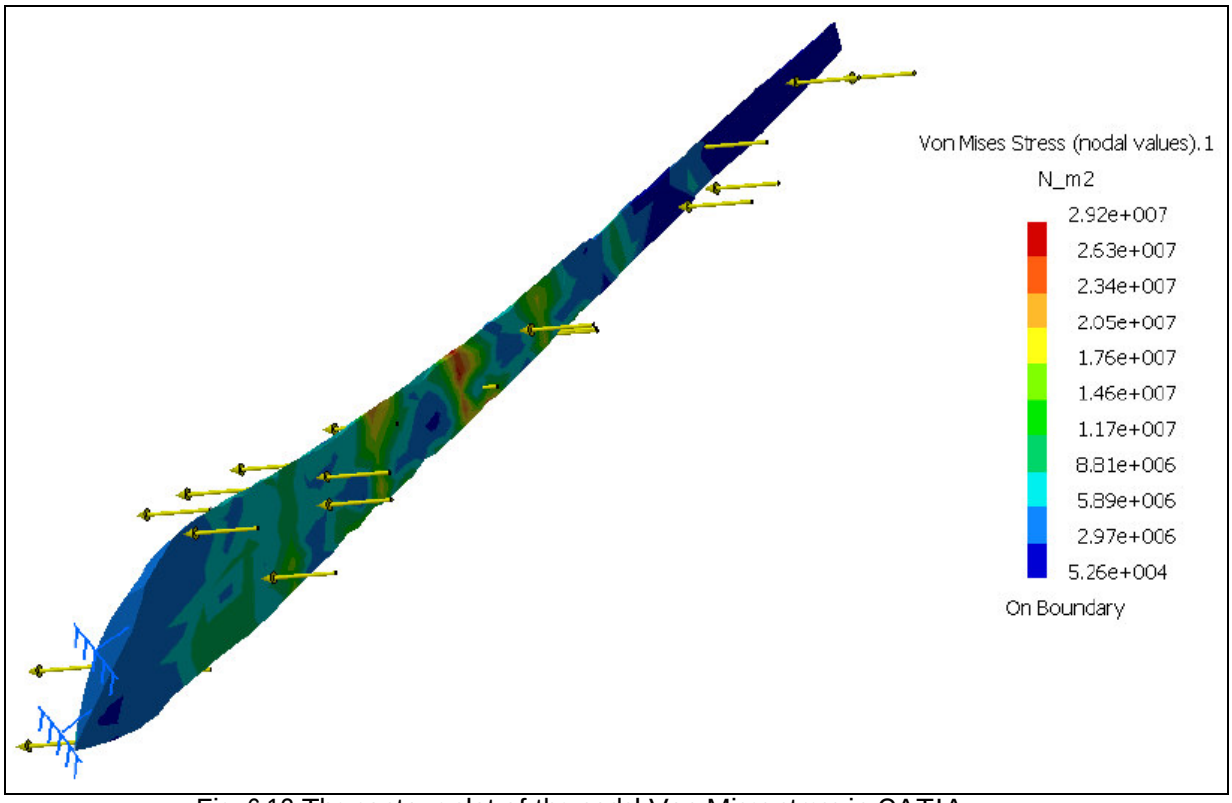

Fig. 6.12 The contour plot of the nodal Von Mises stress in CATIA

The maximum elemental Von Mises stress value in ansys is 100MPa where as in catia 36Mpa in both cases which is below the yield strength of the selected material. The maximum nodal stress value in ansys is 45.1Mpa where as in catia is 29.2Mpa. The global maximum and minimum are found and their location is pin-pointed in a contour plot as displayed below.

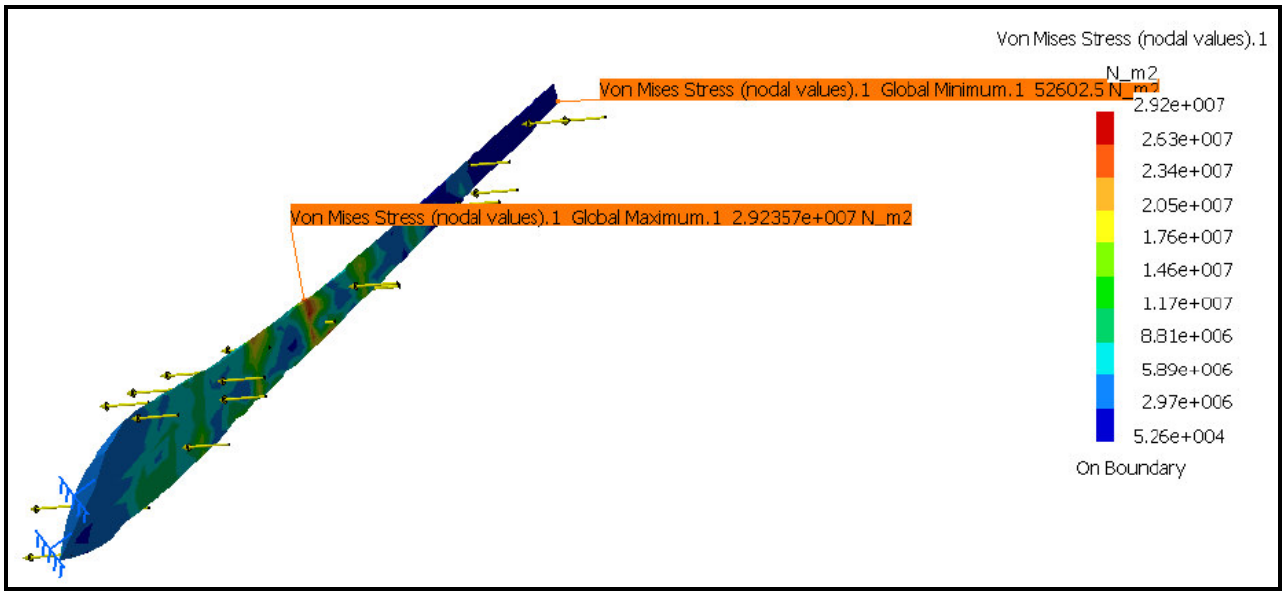

Fig. 6.13 The Extrema of the nodal Von Mises stress in CATIA

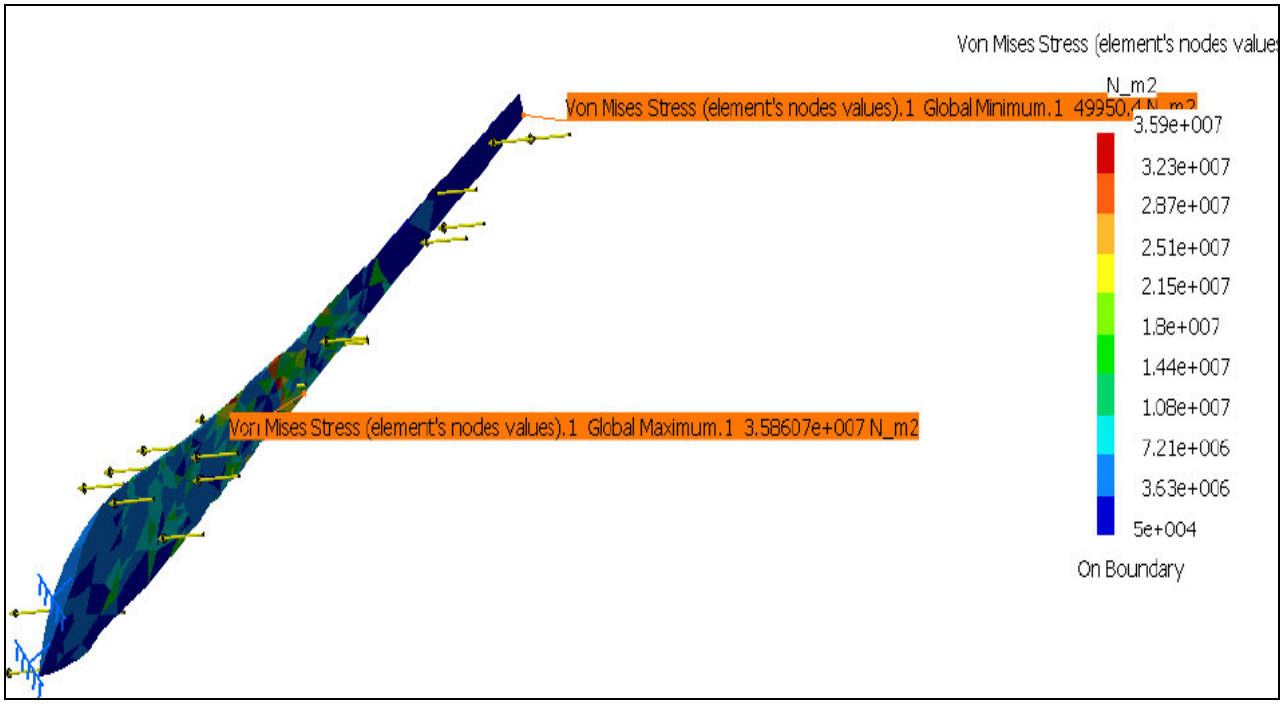

Fig. 6.14 The Extrema of the elemental Von Mises stress in CATIA

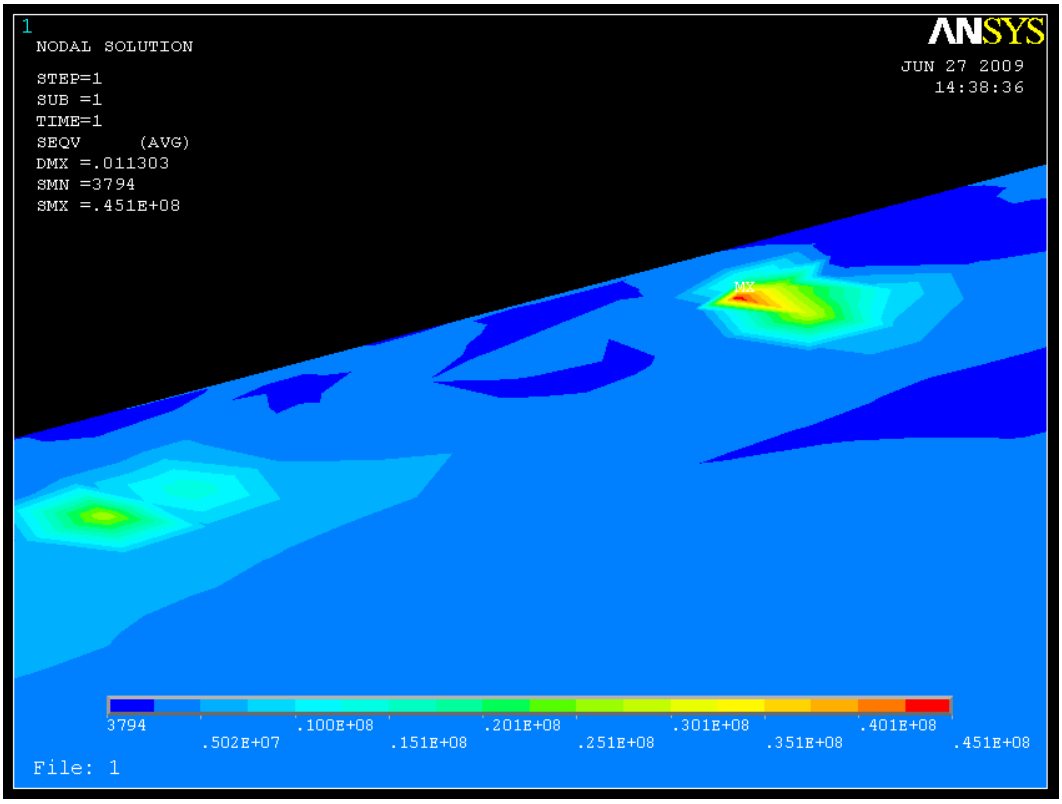

Fig. 6.15 The Extrema of the nodal Von Mises stress in ANSYS

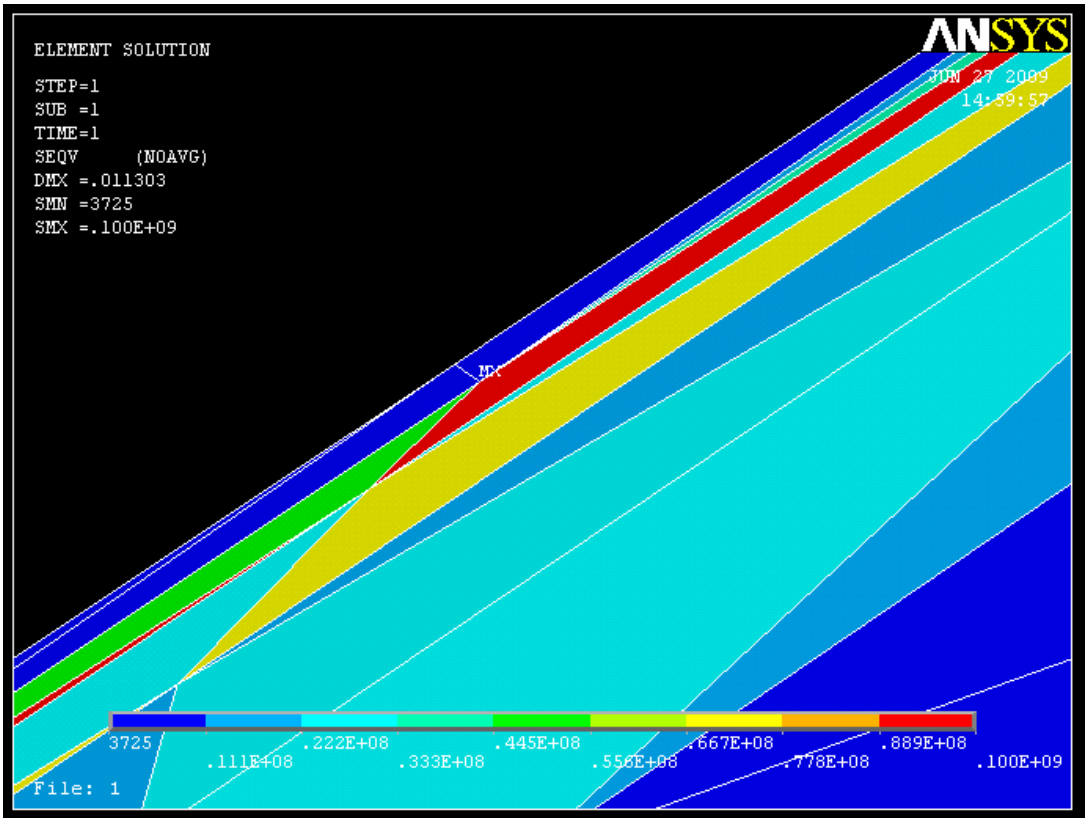

Fig. 6.16 The Extrema of the elemental Von Mises stress in ANSYS

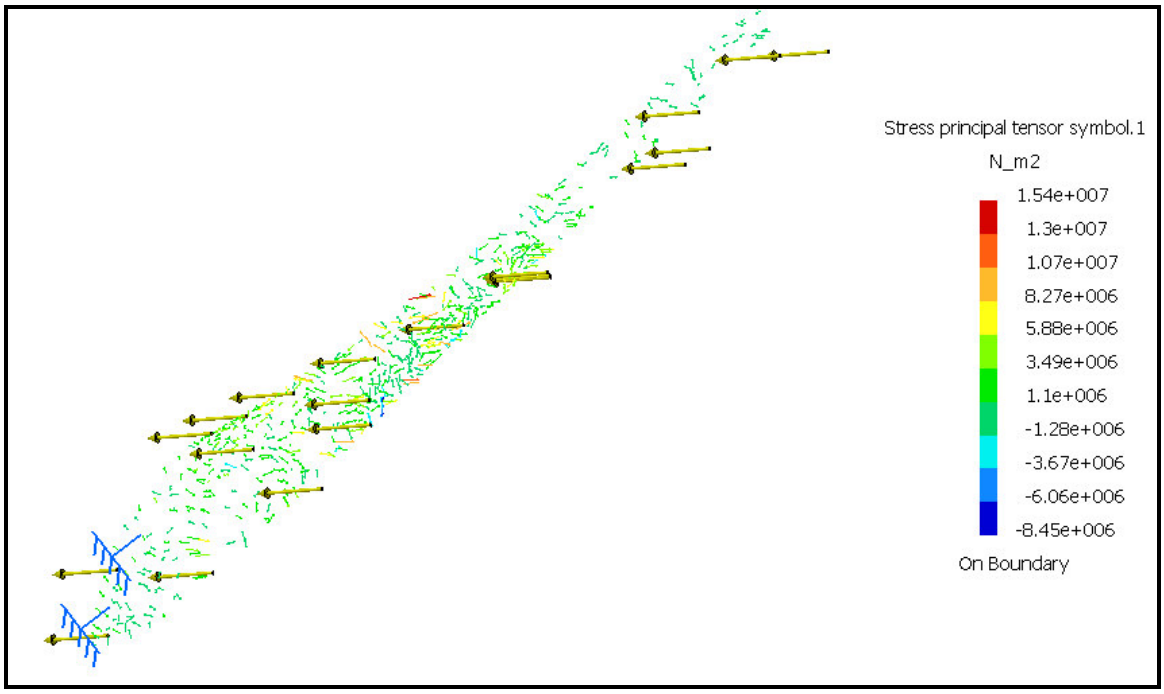

Fig. 6.17 The first principal stresses in CATIA

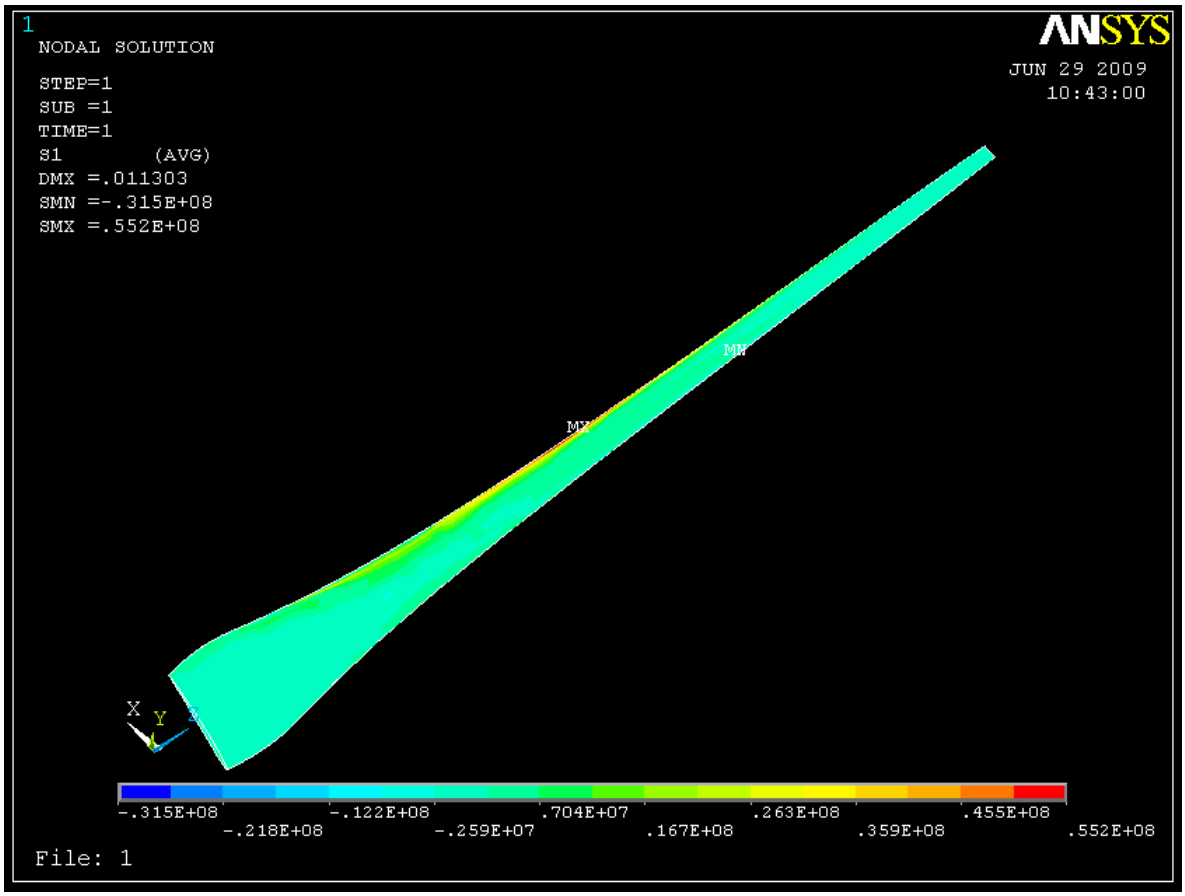

Fig. 6.18 The first principal stresses in ANSYS

CHAPTER 7

CONCLUSION AND FUTURE WORK

In this study, aerodynamic design of horizontal-axis wind turbine blades was investigated and a user-interface computer program called as BLADE DESIGN PROGRAM was written on HAWT blade design software for the use of its outputs in further studies.

Wind turbine blades are the pivot of the other parts of a wind turbine in electricity production since they extract the energy from the wind and carry this energy to generators which produce electricity. The interaction between the wind and the blades is related to the aerodynamic forces acting on the blades. While the wind is passing through the area swept by a rotor it leaves its some part of energy on the blades resulting from this aerodynamic interaction. Then structural analysis of the model is done using ANSYS and CATIA V5 R16.

Aerodynamic theories related to HAWT blade design were investigated extensively. Firstly the simplest aerodynamic model of a HAWT, the actuator disk theory was discussed. The main outcome of this theory is that it is impossible to extract more than 59% of the usable amount of wind energy under the ideal conditions which were stated as the assumptions of this theory.

Since the actuator disk theory is an idealized model which will never be realized for real operation of wind turbines, the general momentum theory is then needed to be discussed. The main outcome of this theory is a measure of the effects of rotation on the relative values of the induced velocities at the rotor and in the wake.

Although the general momentum theory predicts the rotor performance, it fails to give any information about the rotor geometry. This deficiency requires the next discussion which is blade element theory. In the blade element theory, the equations required to find the torque and thrust force on the rotor were found in terms of blade geometry parameters. The results of this theory provide to make relations between the rotor performance and rotor geometry.

The ultimate goal was to relate the results of general momentum theory and blade element theory in order to get the enough equations for HAWT blade design. This was achieved in the discussion of blade element-momentum theory (BEM). After the equations resulted from this theory were obtained, a tip correction method was applied to the theory. In this study, Linearized tip correction method was used to take the effect of number of blades into

account. This method uses Prandtl's tip correction factor which is related to the reduction of the circulation around a rotor blade.

It was also briefly explained about vortex theory for the purpose of giving the physical explanation of induced velocity definitions made in the previous theories. The origin of axial and angular induction factors was explained and the assumptions of the previous theories were clarified with the explanation of this theory.

Blade design was performed beginning with the optimization of blade geometry aerodynamically. Aerodynamic optimization for a wind turbine means to design a blade geometry which gives the maximum power output. For the optimization, it was graphically shown that the effect of airfoil characteristics (glide ratio) and the tip-loss effect were negligible on rotor performance. So the unique relationship was found between the relative wind angle and local tip-speed ratio for the determination of optimum condition for each blade element. For a chosen blade profile and a tip-speed ratio, the setting angle and chord-length variation along the blade length were then calculated together with the power coefficients.

Designed blade has a non-linear twist and taper and more importantly even though it had high power coefficient. Therefore, in future study, the blade geometry may be simplified and performance of modified blade can be examined for the ease of manufacturing.

All the studies on HAWT blade design were presented on a user interface computer program written on VISUALBASIC. User of the blade design program gives the required power output, number of blades, blade profile and design wind velocity as input and the program gives design power coefficient, design tip-speed ratio and rotor diameter as output. In addition to that, blade geometries were listed. Three dimensional views of the blade were what the program does lastly after exported to AUTOCAD or CATIA.

Finally the structural analysis of the blade is checked using CATIA for static case by modeling the blade as a cantilever. The displacement vectors, Von Mises stress and the principal stress results are plotted. The factor of safety is checked.

The studies of this thesis can be surely used for further works. These further works might be either directly parallel to the topic of this thesis to add valuable usefulness on horizontal-axis wind turbine blade design or related to the studies of this thesis to extend the studies on horizontal-axis wind turbines as they are described in the following paragraphs.

If it is recalled that the modification of the designed blade to linearize the blade twist and chord-length distribution using least square method or other alternative methods for modification may also be tried and their performance may be compared with their designed blades and with the ones obtained in this study.

In this study, the other constraint is the use of the known airfoil types. Apart from these, new airfoil designs may be made by the use of XFOIL program and a method of designing new airfoil shapes which show reasonably high performance may be proposed.

Besides, blade element-momentum (BEM) theory approach has been used to design HAWT blades. There are other approaches to predicting blade performance and to designing blades that may be more applicable in some situations. Vortex wake method, for example, might be used and results of this method can be compared with the results of BLADE DESIGN PROGRAM.

In FEM analysis section the blade treated as a cantilever and a trust load of 75N is applied on it. The resulting displacement, Von Mises and principal stress are examined. The result of blade displacement shows a maximum of 11mm in ANSYS and 7mm in CATIA. The elemental and nodal von misses stresses in ANSYS shows a little bit higher than in CATIA, from this it can be concluded that ANSYS is more conservative.

Structural design of HAWT blades is as important as their aerodynamic design. The dynamic structural loads which a rotor will experience play the major role in determining the lifetime of the rotor. Obviously, aerodynamic loads are a major source of loading and must be well understood before the structural response can be accurately determined and also the blade geometry parameters are required for dynamic load analysis of wind turbine rotors. So such a study on the dynamic load analysis of HAWT blades might also use the outputs of BLADE DESIGN PROGRAM.

REFERENCES

1. Spera, D. A., "Wind Turbine Technology", Asme Press, 1998
2. Manwell, J. F., McGowan, J. G., Rogers, A. L., "Wind Energy Explained; Theory, Design and Application", John Wiley & Sons Ltd, 2002
3. Golding, E. W., "The Generation of Electricity by Wind Power", London E. & F. M. Spon Ltd. A Halsted Press Book, 1976
4. Kovarik, T., Pipher C., Hurst, J., "Wind Energy", Prism Press, 1979
5. World wind report 2008
6. Teferi Taye, "wind energy harnessing - Theory and the Ethiopian experience", Journal of the ESME, Vol. II, No. 2, October 1999
7. Hansen, A. C., Butterfield, C. P., "Aerodynamics of Horizontal- Axis Wind Turbines", Annual Review of Fluid Mechanics, Vol.25, 1993
8. Le Gourieres, D., "Wind Power Plants, Theory and Design", Pergamon Press, 1982
9. Duncan, W. J., "An Elementary Treatise on the Mechanics of Fluids", Edward Arnold Ltd, 1962
10. 10- Durand, W. F., "Aerodynamic Theory, Volume 2", Dover Publications, Inc., 1963
11. Rijs, R. P. P., Smulders, P. T., "Blade Element Theory for Performance Analysis of Slow Running Wind Turbines", Wind Engineering, Vol.14 No.2, 1990
12. Lock, C. N. H., "Experiments to Verify the Independence of the Elements of an Airscrew Blade", Br. A.R.C.R and M.953, 1924
13. Wilson, R. E., Lissaman, P. B. S., Walker, S. N., "Aerodynamic Performance of Wind Turbines", Energy Research and Development Administration, 1976
14. Glauert, H., "The Elements of Airfoil and Airscrew Theory", Cambridge Univ. Press, 1983
15. Zhiquan, Y., Zhaoxue, C., Jingyi, C., Shibao, B., "Aerodynamic Optimum Design Procedure and Program for the Rotor of a Horizontal-Axis Wind Turbine", Journal of Wind Engineering and Industrial Aerodynamics, Vol.39, 1992
16. Afjeh, A. A., Keith, T. G., "A Simple Computational Method for Performance Prediction of Tip-Controlled Horizontal Axis Wind Turbines", Journal of Wind Engineering and Industrial Aerodynamics, Vol.32, 1989

17. Gould, J., Fiddes, S. P., "Computational Methods for the Performance Prediction of HAWTs", ", Journal of Wind Engineering and Industrial Aerodynamics, Vol.39, 1992
18. Pandey, M. M., Pandey, K. P., Ojha, T. P., "An Analytical Approach to Optimum Design and Peak Performance Prediction for Horizontal Axis Wind Turbines", ", Journal of Wind Engineering and Industrial Aerodynamics, Vol.32, 1989
19. Nathan, G. K., "A Simplified Design Method and Wind-Tunnel Study of Horizontal-Axis Windmills", ", Journal of Wind Engineering and Industrial Aerodynamics, Vol.6, 1980
20. Vossinis, A., Voutsinas, S., "Computer-Aided Design of Blades: Current Capabilities and ghfgPerspectives",http://www.fluid.mech.ntua.gr/wind/avis/avigotem.html
21. Munduate, X., Coton, F. N., "An Aerodynamic Method for the Preliminary Design of Horizontal Axis Wind Turbines", Journal of Advanced Engineering Design, Vol.40, No.1, 2000
22. De Vries, O., "Fluid Aspects of Wind Energy Conversion", AGARD Report 243, 1979
23. Timmer, W. A., van Rooy, R. P. J. O. M., "Thick Airfoils for HAWTs", Journal of Wind Engineering and Industrial Aerodynamics, Vol.39, 1992
24. Drela, M., "XFOIL Subsonic Airfoil Development System", http://raphael.mit.edu/xfoil , 2001
25. Abbott, I. H., von Doenhoff, A. E., "Theory of Wing Sections, including a summary of airfoil data", Dover Publications, 1959
26. Riegels, F. W., "Aerofoil Sections; results from wind-tunnel investigations, theoretical foundations", Butterworths, 1961
27. Tony Burto, " WIND ENERGY HAND BOOK", Jhon Wiley sons, Ltd, 2001
28. S a Kale and S N Sapali, "Functional and strength Design of one MW Wind Turbine Blade", ENVIROENERGY 2009